Solar Energy Materials & Solar Cells 255 (2023) 112289

Contents lists available at ScienceDirect

Solar Energy Materials and Solar Cells

journal homepage: www.elsevier.com/locate/solmat

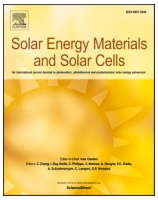

# CdTe-based thin film photovoltaics: Recent advances, current challenges and future prospects

Michael A. Scarpulla [a,*], Brian McCandless [b], Adam B. Phillips [c], Yanfa Yan [c], Michael J. Heben [c], Colin Wolden [d], Gang Xiong [e], Wyatt K. Metzger [e], Dan Mao [e], Dmitry Krasikov [e], Igor Sankin [e], Sachit Grover [e], Amit Munshi [f], Walajabad Sampath [f], James R. Sites [f], Alexandra Bothwell [f,g], David Albin [g], Matthew O. Reese [g], Alessandro Romeo [h], Marco Nardone [i], Robert Klie [j], J. Michael Walls [k], Thomas Fiducia [k], Ali Abbas [k], Sarah M. Hayes [l]

[a] MSE & ECE Departments, University of Utah, Salt Lake City, UT, 84112, USA
[b] Institute of Energy Conversion (retired), University of Delaware, Newark, DE, 19716, USA
[c] Wright Center for Photovoltaics Innovation and Commercialization, University of Toledo, Toledo, OH, 43606, USA
[d] Department of Chemical Engineering, Colorado School of Mines, Golden, CO, 80401, USA
[e] First Solar Inc, 1035 Walsh Ave, Santa Clara, CA, 95050, USA
[f] Colorado State University, Ft. Collins, CO, 80523, USA
[g] National Renewable Energy Laboratory (NREL), Golden, CO, 80401, USA
[h] Universita' di Verona, Department of Computer Science, Ca' Vignal 2- Strada Le Grazie 15, 37134, Verona, Italy
[i] Department of Physics and Astronomy, Bowling Green State University, Bowling Green, OH, 43403, USA
[j] Department of Physics, University of Illinois Chicago, Chicago, IL, USA
[k] CREST, Wolfson School of Mechanical, Electrical and Manufacturing Engineering, Loughborough University, Loughborough, LE11 3TU, UK
[l] U.S. Geological Survey, Geology, Energy & Minerals Science Center, 12201 Sunrise Valley Dr, Reston, VA, 20192, United States

A B S T R A C T

Cadmium telluride (CdTe)-based cells have emerged as the leading commercialized thin film photovoltaic technology and has intrinsically better temperature coefficients, energy yield, and degradation rates than Si technologies. More than 30 GW peak ($GW_p$) of CdTe-based modules are installed worldwide, multiple companies are in production, modules are shipping at up to 18.6% efficiency, and lab cell efficiency is above 22%. We review developments in the science and technology that have occurred over approximately the past decade. These achievements were enabled by manufacturing innovations and scaling module production, as well as maximizing photocurrent through window layer optimization and alloyed $CdSe_xTe_{1-x}$ (CST) absorbers. Improved chlorine passivation processes, film microstructure, and serendipitous Se defect passivation significantly increased minority carrier lifetime. Efficiencies >22% have been realized for both Cu and As doped CST-based cells. The path to further efficiency gains hinges primarily on increasing open circuit voltage ($V_{oc}$) and fill factor (FF) through innovations in materials, fabrication methods, and device stacks. Replacing the longstanding Cu doping with As doping is resulting in better module stability and is being translated to large-scale production. To realize 25% efficiency and >1 V $V_{oc}$, research and development is needed to increase the minority carrier lifetime beyond 100 ns, reduce grain boundary and interface recombination, and tailor band diagrams at the front and back interfaces. Many of these goals have been realized separately however combining them together using scalable manufacturing approaches has been elusive to date. We review these achievements and outstanding opportunities for this remarkable photovoltaic technology.

## 1. Introduction

Thin film photovoltaic (PV) technologies often utilize monolithic integration to combine cells into modules. This is an approach whereby thin, electronically-active layers are deposited onto inexpensive substrates (e.g. glass) and then interconnected cells are formed by subsequent back contact processes and scribing. This differs from wafer-based (e.g. Si) technologies wherein wafers are individually processed into cells, soldered together, and packaged into modules. Cadmium telluride (CdTe) thin-film PV modules are the primary thin film product on the global market, with more than 30 GW peak ($GW_p$) generating capacity representing many millions of modules installed worldwide, primarily in utility-scale power plants in the US. The U.S.-based company First Solar has progressed from a 25 $MW_p$/year manufacturing line in 2005 to a

* Corresponding author.
*E-mail address:* mike.scarpulla@utah.edu (M.A. Scarpulla).

https://doi.org/10.1016/j.solmat.2023.112289
Received 17 August 2022; Received in revised form 6 March 2023; Accepted 9 March 2023
Available online 28 March 2023

target of 21 $GW_p$ annual production by 2024. This remarkable progress reflects a more than doubling in module power conversion efficiency (PCE) from ~9% to just over 19% over this period as well as the inherent economics of the technology [1]. Thanks the advancements in conversion efficiency and production scaling, the cost has steadily declined by more than 10 times. CdTe technology crossing the $1/$W_p$ barrier helped spur massive investments in photovoltaics manufacturing, which in turn has brought the cost of PV electrical generation below that of many fossil fuels (the two are at least temporally correlated) [2]. Meanwhile, the efficiency of research-scale record cells progressed from 16.5% in 2001 [3] to >22% by 2015 [4]. When looking beyond the traditional metric of efficiency, CdTe technology has demonstrated embodied carbon, embodied energy, and energy payback time that are more than a factor of two lower than Si [5]. For comparison, it is estimated that producing Si modules requires approximately 67 kg $CO_2$ per MWh electricity produced while for CdTe modules the figure is near 11 kg $CO_2$/MWh; a large part of the difference stems from the ~100x lower volume of active semiconductor in CdTe modules (which drives the energy use in all purification and growth/deposition steps). CdTe modules are most-widely deployed in utility-scale power plants built by First Solar; Fig. 1 shows an ariel view of the 550 MW Topaz project in the USA, while Fig. 2 shows schematic views of a modern module and a photo of many modules installed on a 1-axis tracker.

Current CdTe-based module technology relies on a p-type doped CdTe or graded $CdSe_{1-x}Te_x$ (CdSeTe) [6–8] polycrystalline thin film absorber layer with minimum bandgap 1.5 eV–~1.4 eV (respectively) fabricated in a superstrate configuration on glass meaning that light enters through the glass. In most commercial modules, in order to achieve long-term reliability with minimized degradation, a second piece of glass and edge seals hermetically encapsulate the module, presenting a large opportunity for bifacial modules with transparent back electrodes [9–12]. The absorber layer is deposited, most commonly using physical vapor deposition processes, onto a stack of n-type transparent conducting oxide (TCO) window layer and (historically) a buffer layer, as shown in Fig. 3. In thin film technologies, buffer layers were introduced to attempt to make lower-recombination interfaces with the absorber. CdTe-based solar cells have been made on other substrates such as steel or polymers in laboratories, but these approaches have yet to be commercialized.

To deposit the absorber, the largest-scale manufacturer (First Solar) implements vapor-transport deposition (VTD), in which sublimed CdTe vapor is transported by an inert carrier gas to the substrate. Their manufacturing process takes less than 4.5 h to go from TCO-coated glass to a finished modules ready for shipping. Fig. 4 shows a schematic of the VTD system developed by First Solar and the US National Renewable Energy Laboratory that won a 2003 R&D100 award [13]. Other approaches including close-space sublimation, sputtering, and electrodeposition have also been attempted commercially [14]. Absorber deposition is almost universally followed by annealing of the absorber layer in the presence of chlorine (Cl) – a unique processing step involving annealing in the presence of usually (but not always [15,16]) $CdCl_2$ which variously removes intragrain structural defects, induces grain growth or recrystallization, and passivates grain boundaries. Historically, this has been followed by Cu doping and the formation of a p-type back contact (Cu-free cells are a current thrust in R&D). The formation of Ohmic contacts to p-type CdTe has historically been challenging and providing access to the surface to allow surface treatment is one reason for the superstrate architecture, as opposed to substrate architecture used for other thin film chalcogenide technologies e.g. Cu(In, Ga)$Se_2$ (CIGSe). P-type ZnTe deposited by sputtering is currently utilized as a back contact in leading production.

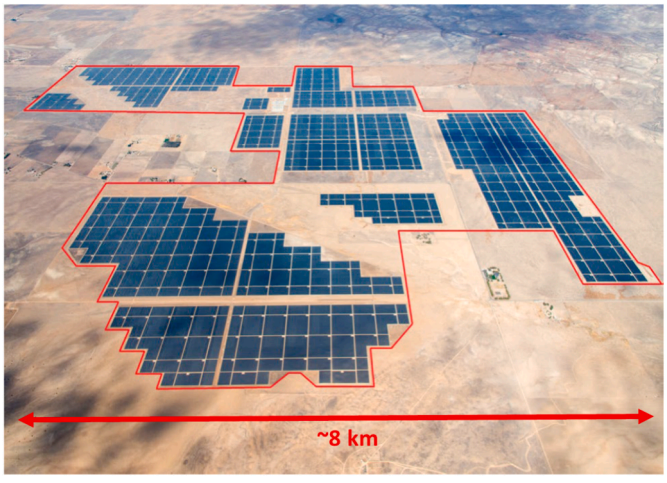


**Fig. 1.** Ariel view of the Topaz solar farm, San Louis Obispo County, CA, USA. It was completed in 2014 using >9 million First Solar CdTe modules for an AC generating capacity of 550 MW. It is currently owned by Berkshire Hathaway Energy and produces an average of nearly 1.3 million megawatt-hours (MW·h) annually. Image courtesy of First Solar.

The device physics of film photovoltaic devices follow those for p-n heterojunctions, however especially in capacitance, cells having buffer layers also share features with (very leaky) metal-insulator-semiconductor (MIS) structures [17]. To date photocarrier collection from the TCO and buffer layers has been negligible, thus both photocurrent and photovoltage are developed in the absorber layer. Prior to approximately 2014, minority carrier lifetimes were low (~1–10 ns at best) with correspondingly short minority carrier diffusion lengths. However, lifetimes of many hundreds of ns have been measured from recent absorber layers implying diffusion lengths greatly exceeding the cell thickness. A recent report on CdTe single crystals demonstrated lifetime exceeding 30 ms and diffusion lengths of 100 μm [18]. As bulk lifetime has increased, the TCO/CdSeTe interface and similarly, hole-selective, low-resistance, passivated Ohmic back contacts have become critical topics of current R&D. Efficiency is assessed at the max power point (MPP), which is very close in voltage to the open-circuit voltage ($V_{oc}$) and thus also flatband voltage in the absorber. The band diagram of Fig. 5 is thus shown at $V_{oc}$ rather than the conventional short circuit current ($J_{sc}$) or V = 0 point because remediating the outstanding voltage and efficiency losses at the maximum power point (which is close to $V_{OC}$) must be the goal. FF is close to its maximum given typical diode ideality factors. Similarly, hole-selective, low-resistance, passivated Ohmic back contacts are critical topics of current R&D. Conceptualization of the cell as a long-lifetime absorber with low-resistance, thermodynamically-reversible (Ohmic), carrier-selective contacts is critical for properly identifying paths to higher $V_{oc}$ and efficiency. For all PV cells approaching the detailed balance SQ limit, carrier collection is thus necessarily by diffusion rather than drift and the device should be recognized as a short diode, which implies that that even the back contact recombination velocity are important to eliminate.

$J_{SC}$ as well as FF have now been optimized by advancements in device architecture, materials, and processing which has progressed to a stage where the cell operating principles have evolved to that of other high-efficiency (>20%) single-junction PV technologies utilizing long minority carrier diffusion lengths for collection from the whole of the absorber by diffusion (as opposed to collection from only a portion via drift in the case of short diffusion lengths) [19]. Further, parasitic optical and resistive losses associated with the historical CdS/CdTe solar cell architecture have been largely overcome by replacement of the CdS with wider-gap buffer alternatives [20,21] and/or fully consuming the buffer layer to form an alloyed region in the front of the absorber [6].

Despite these remarkable achievements, CdTe thin film technology has not yet overcome obstacles limiting its $V_{OC}$. Within the detailed balance limit, ignoring Auger recombination and assuming mandated emission into 2π str, the optical band gap $E_G$ of 1.48 eV for CdTe (~1.4 eV for alloyed CdSeTe) should enable AM1.5G $V_{oc}$ of 1.214 V (1.140 V) [23], yet $V_{oc}$ remains stubbornly at or below 850–900 mV for all but a

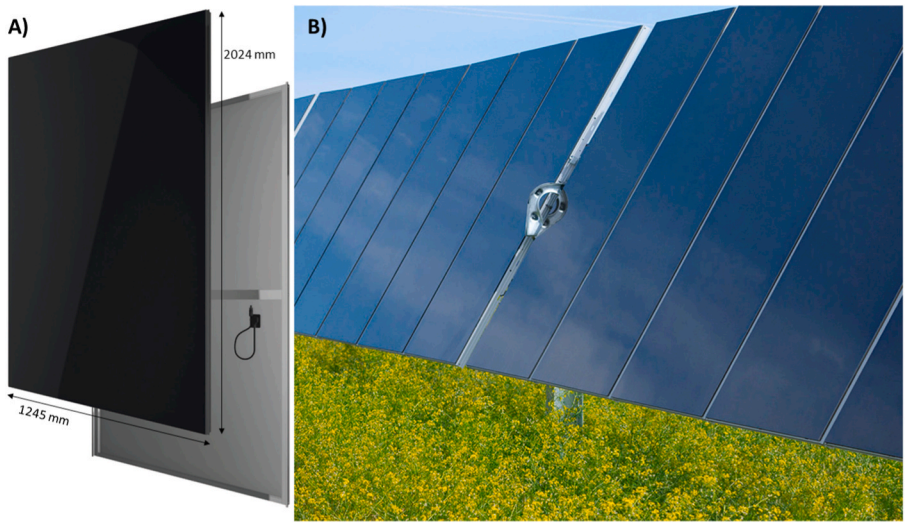


**Fig. 2.** A) Illustrations of the front and back of a modern production CdTe-based module – First Solar Series 6 in this case. These production modules have integrated frames attached on the backside, dual junction boxes to reduce cabling lengths, and are rated at 420–485 Watts peak at 18.2–19.2% AM1.5 efficiency. B) Image of CdTe modules installed on a 1-axis tracker. Images courtesy of First Solar.

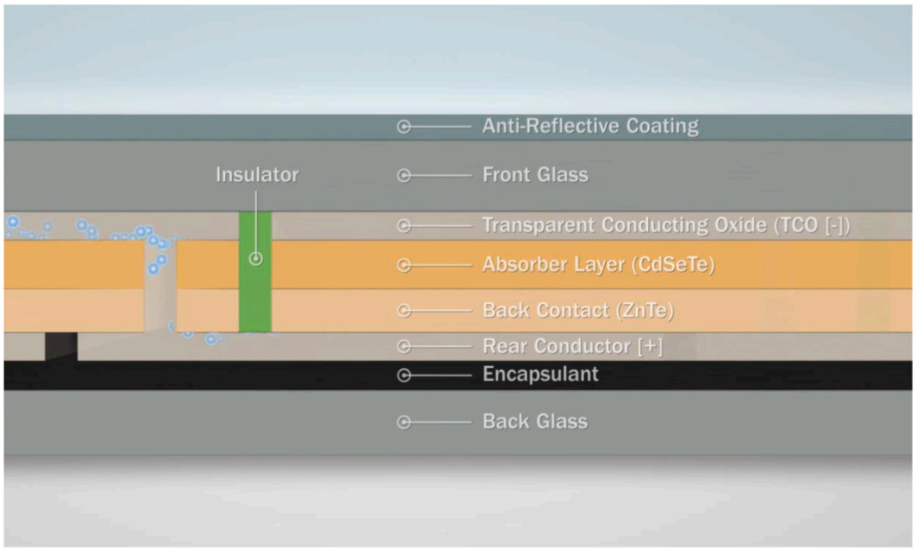


**Fig. 3.** Cross-sectional schematic of a state-of-the-art bifacial CdTe PV module, showing schematic flow of blue electrons from a cell on the left, through the interconnect region, into the cell on the right. The monolithic interconnection of two cells on the left edge and right consists of the black encapsulant used to divide the rear conductor, the vertical current TCO path from the front of the left cell to back of the right cell, and the green insulating layer separating the ZnTe, CdSeTe, and TCO layers between the cells. Image courtesy of First Solar.

very few state-of-the-art polycrystalline thin film cells. Further increasing $V_{oc}$ in large part defines the research avenues for advancing the remaining technical issues needed to achieve PCE >25% [24,25]. The priorities for $V_{OC}$ improvements are *maximizing photocarrier lifetime by eliminating all non-radiative recombination* (1) in the bulk of grains, including from alloy fluctuations causing bandgap variation [26]; (2) at the front buffer/absorber interface; (3) along grain boundaries; and (4) at the back contact. As long as photocarrier lifetimes are still far below the radiative limit, and assuming that at the radiative limit $V_{oc}$ is independent of absorber doping, gains in $V_{oc}$ may also be realized by (5) increasing doping. With the increase of absorber doping, voltage fluctuations (6) from poor dopant activation that may exhibit as sub-bandgap absorption starts to limit voltage [27,28]. Additional increases in cell $V_{oc}$ will result from front and back contact optimization towards carrier-selective, low-resistance, energy-level-matched Ohmic contacts [29]. Ohmic implies no energy level offset from absorber to contact, thus thermodynamically-reversible and inducing no loss of voltage. These attributes will allow photocarriers to be extracted $V_{oc}$ equal to the internal quasi-Fermi level splitting which measures the dynamically-stored electrical potential energy in the form of excess carrier concentration(s), and thus exactly at the respective quasi-Fermi levels without losses (7) of photocurrent $J_{sc}$; or voltage in the forms of (8) energy level offsets or (9) resistance losses through the contact layers. After these lowest-hanging but critical device physics goals are realized, the last logarithmic increments in $V_{oc}$ related to photon recycling and external quantum efficiency (EQE) can be fruitfully pursued [30]. It is emphasized that the next generations of CdTe-based cell technology must resembles high-efficiency cells in which carrier-selective contacts extract carriers and voltage via diffusive transport from an absorber with bulk lifetime approaching the radiative limit; many discussions in older literature were apt for low-lifetime devices relying primarily on carrier collection by drift.

There have been a number of other notable overview and review articles [19,31–35] and books/book chapters [7,17,36–43] on CdTe photovoltaics in addition to the specialized literature. Very rapid progress has occurred and been reported in detail in the open literature in recent years, as well as disclosures by companies (First Solar and GE/Primestar primarily) as to the details of how previously-reported cell

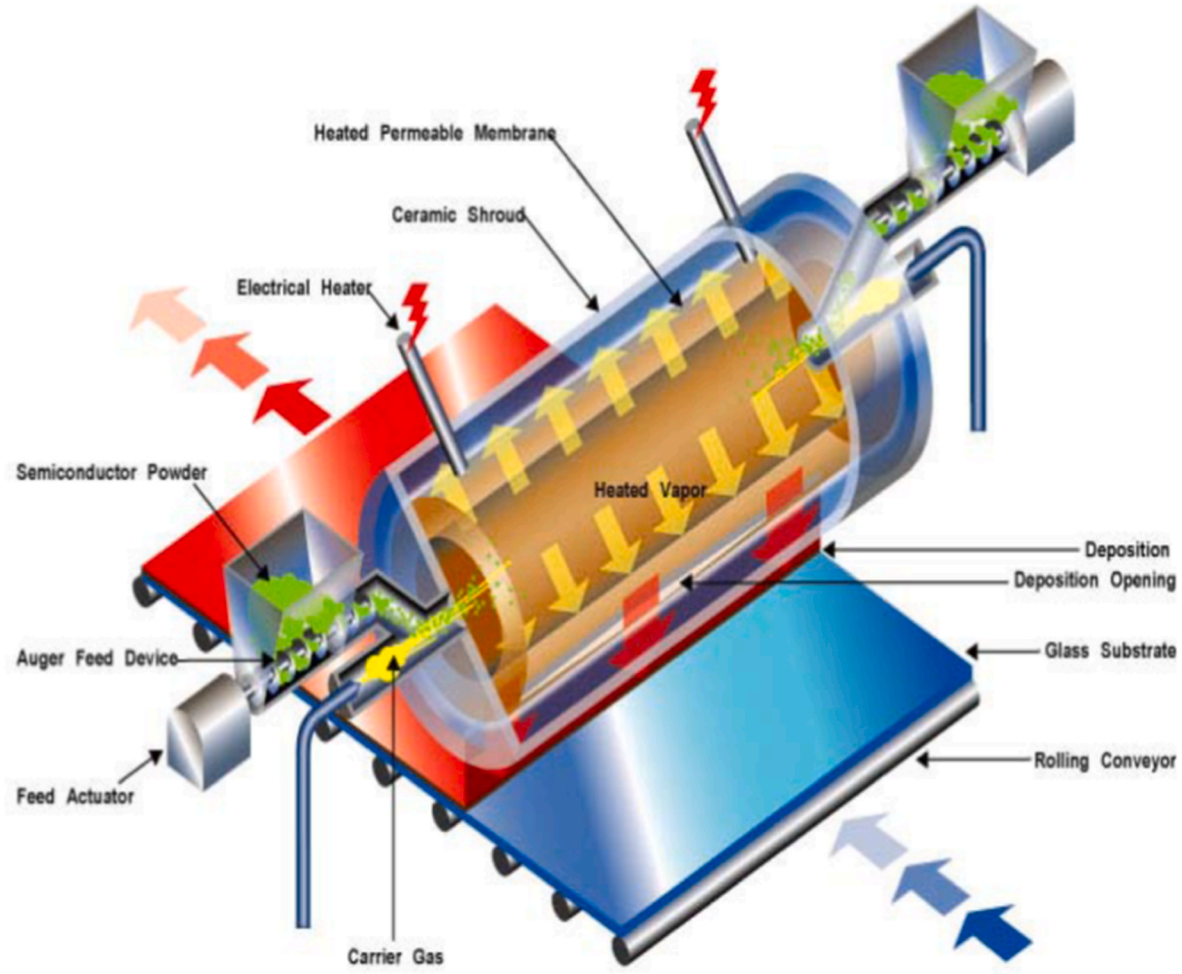


**Fig. 4.** Artist's conception of high-rate VTD system for large scale CdTe PV module manufacturing, showing glass to be coated moving under the apparatus from lower right to upper left, while the CdTe feedstock (shown in green) is continually fed from hoppers into the hot zone of the deposition apparatus which spans the entire width of the glass. Image from US government report in public domain [13].

and module performance records were achieved [19,44,45]. We chose 2014 as a transition year for this paper, as multiple reviews were published near this time covering developments in CdS/CdTe based cells with Cu doping up to that point and it approximates the transition of the technology to the current high-efficiency designs. After 2014, widespread replacement of CdS with wide-gap MgZnO (MZO) buffer layers (as opposed to CdS) or eliminating the buffer layer entirely, and the introduction of Se alloying in the CdTe absorbers have resulted in rapid gains primarily through increases in $J_{sc}$, but also in minority carrier lifetime [19]. Recognizing that intragrain Te-rich native defect chemistry may result in lower minority carrier lifetime and that group-V doping (also facilitated by Cd-rich conditions) might offer higher doping and carrier lifetime set new directions in absorber research [46,47]. Pathways towards the Shockley-Queisser detailed-balance limits for $V_{oc}$ and efficiency have been laid out [25], based first on increasing the absorber effective minority carrier lifetime (determined by intragrain lifetime as well as grain boundary and interface recombination) and hole concentrations (at the radiative limit in low-injection, doping will not matter but while non-radiative recombination is significant, increased doping offers $V_{oc}$ gains). The absorber optimization pathway is widely thought to combine Cd-rich final absorber stoichiometry, substitutional group-V doping replacing Cu, and refinement of film deposition and Cl treatment leading to optimized absorber microstructure free from horizontal grain boundaries and having maximized lateral grain sizes to reduce vertical grain boundary density [48]. The final optimizations are predicted to be related to optimizing contacts, or in other words optimizing interface recombination and heterointerface energy level alignments, band bending, and contact resistance. At the time of writing, many of these concepts have been individually demonstrated in combinations of single-crystalline and polycrystalline embodiments, but integration of all these features together into thin film devices essentially defines the critical path for R&D towards thin film cells approaching the detailed-balance performance limits.

## 2. Brief history to approximately 2014

The photovoltaic effect in II-VI compounds with 6% efficiency was first observed in what were later recognized to be CdS/$Cu_{2-x}S$ heterojunctions in 1954 (interestingly, this is the same year Bell Labs announced 6% crystalline Si cells as "solar batteries") [49,50]. The first all-thin film solar cells were developed based on evaporated CdS films in the former USSR [50]. Through the 1960's to 70's, devices were formed by the Clevite wet process which consisted of immersing polycrystalline CdS films in a Cu-containing aqueous solution causing ion exchange and topotaxial conversion of the surface to $Cu_{2-x}S$, or by the Phillips dry process which involved evaporation of CuCl followed by heat treatment [51]. CdTe thin film solar cells grew out of these II-VI semiconductor beginnings, in-parallel with CdS efforts at General Electric and the US Air Force, as Loferski [52] had realized that the CdTe bandgap was well-matched to the solar spectrum. Also, CdTe could be doped both n-

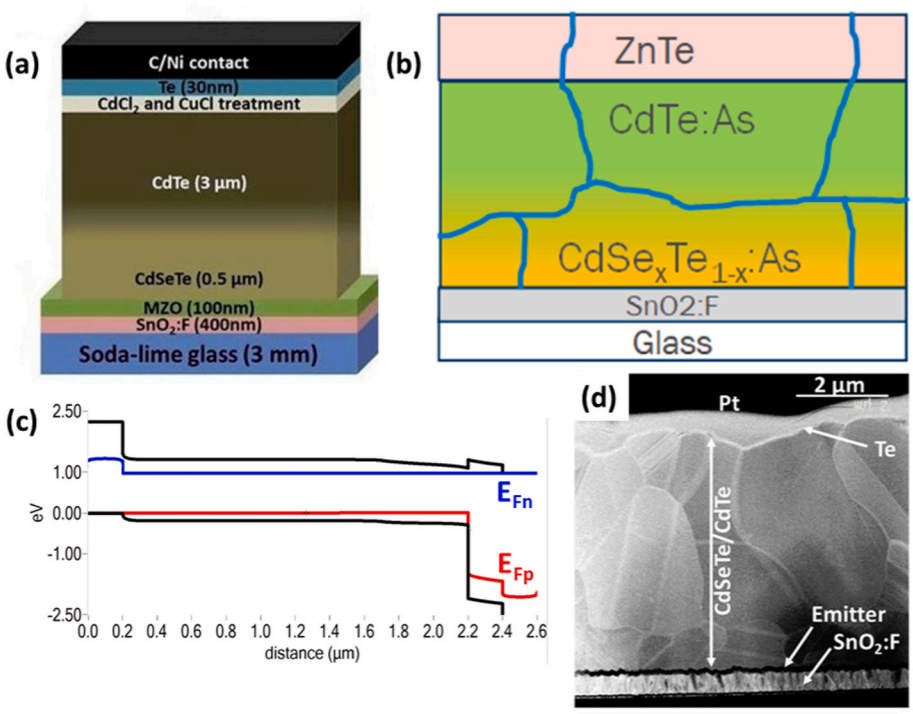


**Fig. 5.** (a) Schematic diagram of Colorado State University (CSU) research cells using MZO buffer, Se-alloyed absorber, Cu doping, and Te back contact layers. (b) Schematic diagram of current First Solar cells with Se-alloyed and As-doped absorber, and using p-type ZnTe back contact. (c) SCAPS [22] band diagram at AM1.5 $V_{oc}$ conditions for a representative FTO/MZO/graded CdSeTe/CdTe/ZnTe cell built on an absorber layer with >100 ns photoelectron lifetime (and thus minority diffusion length ≫ thickness). (d) Cross-sectional SEM micrograph of a representative CSU cell showing large absorber grains.

and p-type – a factor that has not received as much attention in the PV context.

Development of CdTe cells began in the 1960's with single crystal CdTe, evolving from diffusion-doped p-n homojunctions to hybrid thin film/single crystal structures in first homojunction and later heterojunction configurations [7]. Cell development using polycrystalline thin film CdTe deposited in the superstrate configuration on transparent conductive tin oxide coated glass, as still used today, began in 1969 in the USSR but rapidly expanded worldwide to commercial labs such as Kodak (USA) and Matsushita (Japan) and numerous university research labs using different CdTe deposition methods. Cell PCEs exceeded 10% by the late-1980's once a post-deposition anneal of the stack in the presence of $CdCl_2$ (or inclusion of Cl in spray pyrolysis or electrodeposition) was added to the cell fabrication process and found to be compatible with Cu doping. In parallel, annealing with $CdCl_2$ became known in the radiation detector community to improve material properties and device performance. Early work on Cl treatment of TCO/CdS/CdTe cells occurred from 1987 to 1993 by Meyers, Leng, and Frey at Ametek, McCandless and Birkmire at IEC. Finally, Britt and Ferekides at USF produced a world record cell of 15.8% in 1993 [53]. The next innovations resulting in slow increased cell efficiency came from work on front window layers and back contacting processes, leading to a 16.5% cell record from NREL that was not eclipsed for another decade [21]. Throughout the approximately 20-year period from approximately 1994 to 2014, a rather small community of dedicated researchers tried many material and fabrication variations, developing a large body of understanding that underpins the current state of the art.

Several fabrication methodologies reached commercial-scale development during the 1990's, most notably at Monosolar (later to become BP Solar), Photon Incorporated (later to become Golden Photon), Solar Cells Inc (later to become First Solar), and Antec (later to become CTF Solar). Collaborations between corporate, university and national laboratories in this decade fostered much in-depth probing of cell-level operation and potential cell-based instability mechanisms which could affect module lifetime. By the mid-2000's First Solar and BP Solar were the largest commercial entities going into the ~2005–2020 period of accelerating growth of the worldwide solar energy sector. By 2009, CdTe manufacturing costs at First Solar dropped below $1/$W_p$ (~2 years prior to Si doing so and with an order of magnitude lower capacity [54]) a metric previously identified as necessary to reach grid parity for utility scale installations [32]. At the end of 2011, however, as BP Solar ceased CdTe operations, General Electric entered the field, ultimately achieving a then-record cell PCE >18% in 2013 (as GE Primestar); in the same year, they ceased operations and their IP portfolio was acquired by First Solar. In 2012, First Solar achieved a world record 17.3% cell efficiency associated with introduction of the ZnTe contact [55]. Several other companies had CdTe development projects in the 2000–2014 timeframe including Bloo Solar, Canrom, Corning, Solexant, Lucintech, Solar Fields, and Willard & Kelsey Solar Group. Solar Fields' technology was acquired by Calyxo, a subsidiary of Q-Cells, in 2007 and had production in Germany until early 2020. Willard & Kelsey's assets were acquired by Toledo Solar in 2019. For First Solar, 2014 was a benchmark year in thin film CdTe cell efficiency gains and module production. During this time period, these gains in performance were driven primarily by optimizing $J_{sc}$ through reducing parasitic absorption in the TCO and buffer layers by changing and optimizing materials and fabrication, optimization of optical design such as varying layer thicknesses, and through reducing the absorber's minimum bandgap. This last innovation was eventually disclosed [44] after a few years to have been achieved by introducing a $CdSe_{1-x}Te_x$ (CST) layer at the front of the absorber. Through cell-level design changes, cell PCE = 22%, module PCE = 17.5% and module manufacturing cost below USD $0.46/Watt have been achieved [1,56]. In the past decade, a few other commercial ventures have also become active including Toledo Solar, and in China, ASP and CNBM. While First Solar focuses on the utility-scale market and has the majority of today's multi-GW CdTe manufacturing capacity, Toledo Solar, CTF Solar (CNBM), and ASP all have 100 $MW_p$/yr capacities with at least some focus on roof-top and building-integrated (BIPV) markets. Lucintech is another US-based company that is addressing transportation-integrated PV. A more extensive history of PV focusing on CdTe has appeared recently [57]. Fig. 6 displays estimated PV learning curves for c-Si, a-Si, and CdTe up to 2013 showing the cost and price per watt advantage for CdTe and its earlier crossing of the $1/Wp line. These data were compiled from sources outside First Solar and do not represent the official views of the company.

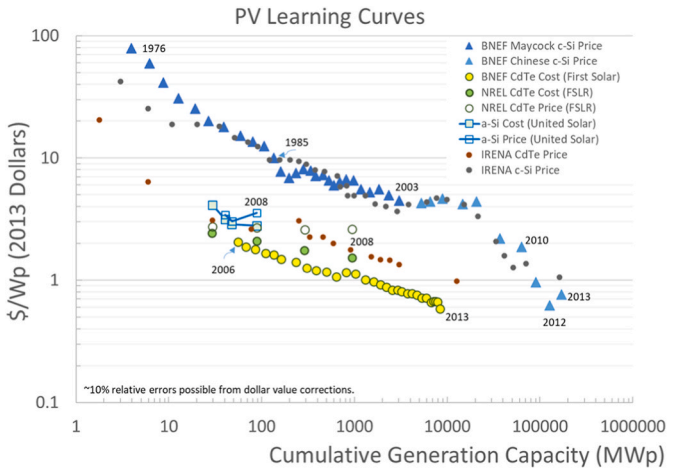


**Fig. 6.** Compiled PV learning curves for Si and CdTe up to 2013. Data compiled by M.A. Scarpulla from various sources as indicated. Special thanks to Tim Gessert for the a-Si data and CdTe data marked as NREL and to Jenny Chase & Paul Maycock for data marked as BNEF. These data were collected from available sources outside of First Solar and do not represent its views or its internal data.

## 3. Modules and industrial trends

In 2019, First Solar reached a milestone of 25 $GW_p$ modules shipped for the utility scale market. The module AM1.5 aperture efficiency exceeded 19% for Series 6 and by the time of writing has reached 19.5% [58]. By 2020, First Solar has largely transformed to Series 6 product (approximately 2 m × 1.25 m) with 5.7 $GW_p$/yr capacity, while retiring the S4 (0.6 m × 1.2 m) production. The current Series 6 module wattage is 420–485 $W_p$ depending on performance binning. 21 $GW_p$ production capacity is expected by the end of 2024 from factories in the US, Malaysia, Vietnam and India like the one pictured in Fig. 7. Toledo Solar has targeted the residential rooftop market with 115 W modules with 0.6 m by 1.2 m form factor. Toledo Solar is also developing semi-transparent products for BIPV. Reel Solar demonstrated 17.2% (aperture) efficiency at 98 $cm^2$ with electroplating of graded CdSeTe absorber. The company also invested in semi-transparent modules with ultrathin absorber layers and in bifacial modules. However, Reel Solar ceased operating in 2020. Advanced Solar Power (ASP) reported 19.7% cell efficiency ($V_{oc}$ = 856 mV, $J_{sc}$ = 28.92 mA/$cm^2$, and FF = 79.63%). ASP's S2 and S3 modules are 0.6 m by 1.2 m in form factor, with name plate wattage 100–105 W. In addition, ASP also developed productions and applications for building-integrated PV (BIPV), such as solar shingles, transparent solar modules, solar facades. In 2019, CNBM ramped up 100 $MW_p$/yr CdTe production in Chengdu, with efficiency 13% and 96% yield. The company also expected to ramp up another 100 $MW_p$ production line in 2020, and additional production capacity planned. CTF, CNBM's research center in Germany, has reported 19.3% CdTe cell efficiency. While other CdTe companies have generally used a business model where they make their own factories and modules, Reel and CTF have attempted a different approach in which they develop the process and build factories for other entities. Similar to ASP and Toledo Solar, CNBM is also developing products for BIPV applications. In 2019, Ruike demonstrated 14.6–15.3% efficiency modules (105–110 W for the 0.6 m × 1.2 m form factor). Ruike currently has 100 MW pilot production and its products also include BIPV applications.

## 4. Recent performance advances

Fig. 8 shows schematic cell material stacks for historical, present, and future CdTe-based cells. According to the Shockley-Queisser detailed-balance framework, a step function absorptivity with optical band gap ($E_G$) = 1.48 eV for pure CdTe can deliver $J_{sc}$ of 29.68 mA/$cm^2$, $V_{OC}$ of 1.214 V, FF of 89.9%, and efficiency of 32.39% for a flat-plate cell operating at 25 °C under AM1.5G illumination and emitting into 2π str ($V_{oc}$, FF, and efficiency drop slightly for radiation into 4π str). The corresponding numbers for the bandgap of 1.4 eV corresponding to an absorber incorporating CST are $J_{sc}$ = 32.88 mA/$cm^2$, $V_{oc}$ = 1.140 V, FF = 89.4%, and PCE = 33.49% [23,59]. Today's benchmarks for CdTe thin film solar cell and module performance are defined by First Solar, with *certified* record cell PCE = 22.1 ± 0.5% and module aperture area PCE = 19.5% [1,58]. The 22.1% record cell device parameters are $V_{OC}$ = 0.887 V, $J_{SC}$ = 31.69 mA/$cm^2$, and FF = 78.5% [4]. By 2014, the IQE curves for record CdTe cells indicated minimum bandgap close to 1.39 eV (QE derivative method), consistent with the use of CST or CST/CdTe absorbers [4]. The EQE and AM1.5 J-V curves for selected record cells are collected in Fig. 9, while AM1.5 performance metrics are tabulated in Table 1.

Comparisons to SQ detailed balance theory for AM1.5G predictions are useful to identify the most important factors for further optimization. Assuming a 1.39 eV minimum bandgap for the 22.1% cell, its $J_{sc}$ is only 1.6 mA/$cm^2$ lower than or 95% of the maximum $J_{sc}$ possible. However, its $V_{oc}$ of 0.887 V indicates an absolute $V_{oc}$ loss ($E_g$/q-$V_{oc}$) of 503 mV. The $V_{oc}$ irreversible losses are $V_{oc,SQ}$ -$V_{oc}$ = 226 mV, corresponding to $V_{oc}$/$V_{oc,SQ}$ = 80% of the maximum possible $V_{oc,SQ}$ = 1.113 V


**Fig. 7.** View of a First Solar manufacturing line. A grey rectangular Series 6 module is visible in the foreground on the conveyance system between the two walkover paths with yellow railings and two workers are present to the left for scale. Hundreds of other nearly-finished modules are visible in the blue metal racks to either side. It is remarkable to note that high-efficiency CdTe modules are produced in factories in which they are transported in open air between process steps rather than e.g. in a cleanroom. Image courtesy of First Solar.

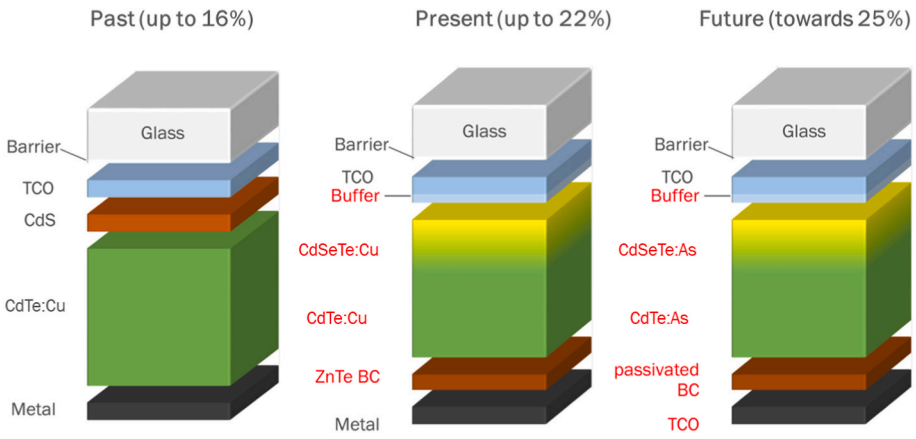


**Fig. 8.** Comparisons of past, present, and future material stacks comprising CdTe-based solar cells. Efficiency figures are approximate, and a move to bifacial modules is underway at the time of writing. TCO = transparent conductive oxide, CdTe:X (X = Cu or As) indicates Cu or As doped semiconductor layers. BC = back contact. Other materials and terms defined in the text. Image courtesy of First Solar.

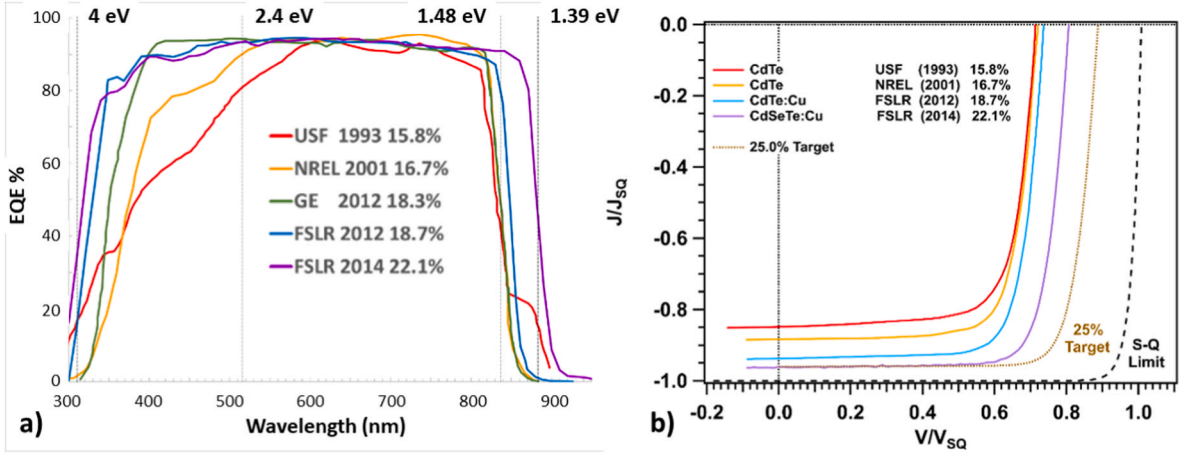


**Fig. 9.** a) Representative EQE spectra and b) AM1.5 J-V curves from world-record CdTe cells spanning 1993-present. The approximate locations of the spectral cutoffs for FTO (4 eV), CdS (2.4 eV), CdTe (1.48 eV), and CdSeTe (1.39 eV) are indicated. QE data were obtained from the original authors or digitized from the publications cited in the text (thus small errors may be introduced). The curious bump at 850–900 nm for the USF 1993 cell is believed to be an experimental artifact by the original authors (personal communication), although CdSTe alloys could in principle yield bandgaps <1.48 eV. Because of the lower effective bandgap in modern cells, the J-V curves are presented relative to the limiting $J_{sc}$ and $V_{oc}$ for their respective bandgaps. Descriptive JV performance parameters are presented in Table 1.

for that bandgap (we note that $V_{oc}$ losses are better considered as additive rather than fractional). The fill factor (FF), which is known to scale with $V_{oc}$, is 88% of the SQ limit. Thus, only small improvements remain to be made for $J_{sc}$ (unless even lower bandgaps are employed) while the 226 mV of $V_{oc}$ deficit beyond thermodynamically-mandated emission indicates that the ratio of sub-gap recombination to total recombination in the cell is still >12,000 ($V_{oc}$-$V_{oc,SQ}$ = $k_BT$ ln($R_{sub-gap}$/$R_{tot}$). Here, we are grouping together both non-radiative recombination as well as radiative recombination that occurs through band tail, defect, and lower-bandgap states separated by less than the transport and optical absorption bandgaps, as all of these forms lower the possible $V_{oc}$ [60]. Thus, the most important and high-payoff tasks for improving CdTe-based cell technology are further reductions of all forms of non-radiative recombination as well as disorder and defects.

Demonstrations of $V_{OC}$>1 V have been made using single crystalline CdTe absorber layers or wafers as noted in Table 1 [61,62], yet $V_{OC}$ remains typically <900 mV in polycrystalline thin film cells with a few scattered reports of devices reaching 900 mV or slightly higher [63–68]. Cells with $V_{OC}$ >850 mV are part of the state of the art. The band-to-band or radiative recombination coefficient $\beta_{rad}$ for CdTe was recently determined from double heterostructures grown by molecular beam epitaxy (MBE) to be ~1 × $10^{-10}$ $cm^3$/s [69,70], which would yield radiative lifetimes of 100 μs and 100 ns for $10^{14}$ and $10^{17}$/$cm^3$ shallow doping respectively (whether n or p type). If effective absorber lifetimes (including interface and grain boundary recombination because these draw photocarriers from the absorber reservoir) fall below these values, gains in quasi-Fermi level (QFL) splitting in the absorber can continue to be made by increasing the absorber doping until lifetime becomes limited by Auger recombination. Additionally, higher absorber doping can help to solve practical challenges such as the formation of a hole-selective, low-resistance Ohmic contact at the back of the cell which would allow the internal QFL splitting to be realized as external $V_{oc}$. However, it should be noted that doping (like band offsets) should be considered a practical tool for device construction. Minority carrier lifetime approaching the radiative limit fundamentally matters for approaching the SQ limit.

The elimination of CdS, which has $E_g$ = 2.4 eV, higher melting point and slight cliff-like band alignment to CdTe, as a buffer resulted in $J_{sc}$ gains by reduction of parasitic absorption at short wavelengths [20,21]. Probably for most fabrication processes, the elimination of CdS which tended to be deposited as nanosized zinc blende grains isostructural with CdTe also helped to minimize or eliminate the fine-grained region

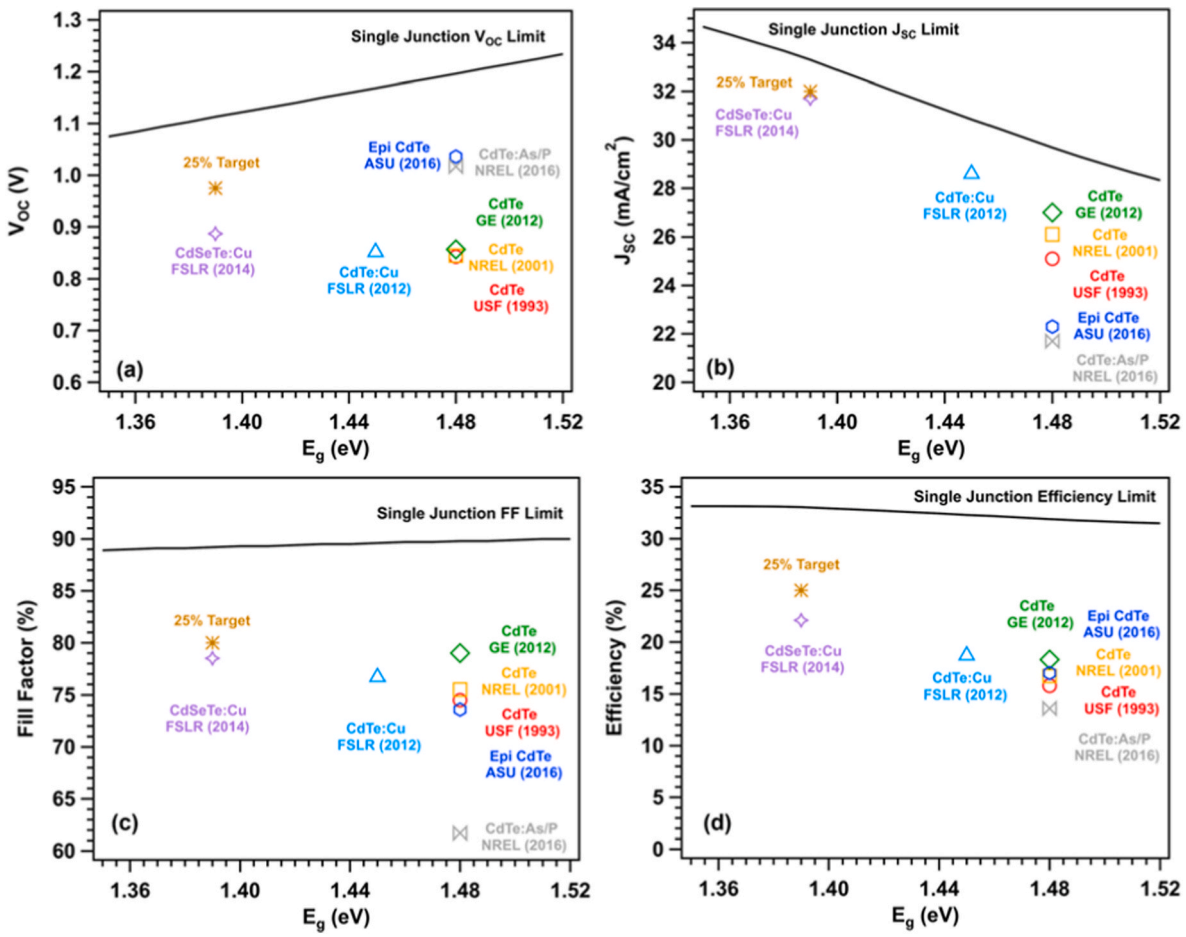


**Fig. 10.** (a–d) Respectively, $V_{oc}$, $J_{sc}$, FF, and efficiency of record CdTe-based cells from Fig. 9 and Table 1 vs. their effective bandgaps. The most significant losses are seen to come from $V_{oc}$ and FF.

**Table 1**
AM1.5G performance parameters of various landmark cells including those from Fig. 10. These values are a mixture of self-reported and certified values. The parameters for the hypothetical 25% cell shown in Figs. 9 and 10 are in bold text.

| Record/ Notable Cell | AM1.5 Efficiency (%) | $J_{sc}$ (mA/cm$^2$) | $V_{oc}$ (V) | FF (%) | Effective $E_g$ from IQE (eV) | $V_{oc,SQ}$ (V) Ref. [23] | $V_{oc}$ Deficit ($V_{oc,SQ}$ -$V_{oc}$) (V)[a] | Notes |
|---|---|---|---|---|---|---|---|---|
| USF 1993 | 15.8 | 25.1 | 0.843 | 74.5 | 1.48 | 1.214 | 0.371 | CdS/CdTe |
| NREL 2001 | 16.7 | 25.9 | 0.845 | 75.5 | 1.48 | 1.214 | 0.369 | $Cd_2SnO_4/Zn_2SnO_4$/CdTe |
| GE 2012 | 18.3 | 27.0 | 0.857 | 79.0 | 1.48 | 1.214 | 0.357 | CdTe absorber |
| FSLR 2012 | 18.7 | 28.6 | 0.853 | 76.7 | 1.45 | 1.186 | 0.333 | CdTe absorber |
| FSLR 2014 | 22.1 | 31.7 | 0.887 | 78.5 | 1.39 | 1.130 | 0.243 | CdSeTe absorber |
| ASU 2016 | 17 | 22.3 | 1.036 | 73.6 | 1.48 | 1.214 | 0.178 | Epitaxial CdTe double heterojunction absorber |
| NREL 2016 | 13.6 | 21.7 | 1.017 | 61.7 | 1.48 | 1.214 | 0.197 | Poly CdS/P-doped CdTe single crystal wafers |
| 25% Targets | 25.0 | **32.0** | **0.975** | **80.0** | **1.39** | 1.130 | **0.155** | Multiple combinations of bandgap and JV |
| | | 31.7 … | 0.956 … | 82.5 … | 1.39 … | 1.130 … | 0.174 … | parameters can achieve 25% |

[a] Note that different authors/groups compute different values of "the" AM1.5G Schockley-Quiesser $V_{oc}$ (and thus $V_{oc}$ deficit) depending on values of inputs (temperature of 25.

containing high densities of grain boundaries at the location of maximum photocarrier generation. Thus, eliminating CdS may also have had a (probably unanticipated) benefit of increasing the effective photocarrier lifetime in the polycrystalline absorber compared to the prior state of the art of tuning the cell fabrication to interdiffuse and consume the CdS as a $CdS_{1-x}Te_x$ graded layer. Higher deposition temperatures and or higher Cl treatment temperatures and $CdCl_2$ overpressures also are known to result in microstructure consisting of large lateral grains spanning the layer thickness [71–75]. While not typical of films used in state of the art devices, it is possible to generate microstructures with grain lateral dimensions far exceeding the film thickness – for example 30 μm wide grains from thermally-evaporated films only a few μm thick [71,72]. In these works, such large grain growth was promoted on MZO but hindered by CdS buffer layers; effects of alloying and interface energies were suspected. Such microstructure optimizations are important because, while it is true that Cl treatment reduces the recombination

velocity of grain boundaries, it is estimated that even the best-passivated boundaries still have effective recombination velocities on the order of $10^4$–$10^5$ cm/s. Especially as bulk minority carrier diffusion length continues to be improved, reducing the total grain boundary area and further passivation strategies are important research directions for maximizing $V_{oc}$. Many research laboratories have moved to $SnO_2$:F/$Mg_xZn_{1-x}O$ as the window/buffer combination although the use of other alternative materials such as i-$SnO_2$, $Zn_2SnO_4$, $Cd_2SnO_4$ and $(In_xGa_{1-x})_2O_3$ have also been reported [20,21,76,77]. Recent disclosures from First Solar do not note the presence of a buffer layer, however it seems unlikely that high-performance cells can be deposited directly on TCO layers. While the importance of columnar, large-grained absorber microstructure in promoting long effective minority carrier lifetime by reducing grain boundary recombination is appreciated, the interplay of using non-isostructural buffer layers, absorber deposition temperature, and absorber post deposition treatments on the microstructure and grain boundary and interface passivation has not been fully elucidated.

The quantum efficiency of recent record CdTe-based devices (e.g. the 22.1% cell shown in Fig. 9) indicates an effective absorber bandgap of $E_G = 1.39$ eV, narrower than pure CdTe. This was obtained via production of a $CdTe_{1-x}Se_x$ alloy in the front portion of the absorber layer to further increase the photocurrent. Whether intentional or not, adding Se dramatically increased both grain and grain boundary lifetimes; so although the band gap is locally reduced, the $V_{OC}$ can be maintained or increased [78]. Commonly today, leading cells incorporate approximately 20–40% Se at the front interface which, because of the bandgap bowing, results in minimum bandgap of 1.4 eV and maximum detailed balance $V_{oc}$ near 1.140 V. The bandgap bowing parameter in $CdSe_{1-x}Te_x$ alloys is near 0.9 with the CdSe endpoint bandgap of 1.7 eV [7]. Additionally, the bandgap narrowing has both conduction band and valence band components, with a small valence band offset between $CdSe_{0.3}Te_{0.7}$ and CdTe [79].

$^{o}$C vs 300 K, round off error in solid angle of solar disc, etc.) and numerical treatment of the model (methods of numerical integration of spectrum, numerical precision of conversion from power to particle flux, etc.). Some uncertainty also exists in terms of the effective absorber bandgap for polycrystalline absorbers. The combined variations can lead to discrepancies in $V_{oc}$ deficit when comparing values computed by different authors/groups that is estimated herein to be as large as approximately $k_BT/q = 0.026$ V. In this table, the values of $V_{oc,SQ}$ were taken from Ref. [23].

Other on-going contributions that are paving the way for future progress and greater cell design flexibility involve raising acceptor density through extrinsic Group V (gr-V = N, P, As, Sb) substitutional doping [27,80–84], and altering the defect landscape to reduce intrinsic defect complexes contributing to recombination centers and compensating defects [46,85–87]. Confidence for doping research on thin film CdTe cells has been bolstered by demonstration of $V_{OC}$>1 V obtained using epitaxially grown As-doped CdTe single crystals [61]. The distribution and role of Cl species in the polycrystalline stacks after the $CdCl_2$ treatments is being evaluated with respect to its accumulation at grain boundaries and at the CdTe-emitter interface [88,89]. Further, Cu doping which, although once shown to be essential for quasi-Ohmic back contact formation [36,43], is now known to contribute to lifetime reduction and operational instabilities [55,63,90,91]. In fact, in the past year, As-doped CdSeTe modules have entered the marketplace (First Solar Series 6 CuRe Modules) partly due to the enhanced stability from the shift to a group-V defect chemistry. These on-going research areas are being guided by integrating first-principles defect calculations with device modeling and laboratory validation through detailed materials characterization. The driving R&D philosophy at present combines defect management in the CdTe-based absorber and at surfaces and interfaces, recognizing that improving various parts of the device can affect others and how they work together, especially, the front contact, the absorber deposition and post deposition processing, and the back contact. Finally, especially as cells become thinner and minority carrier lifetimes approach the radiative limit, the importance of carrier-selective, low-resistance Ohmic back contacts that reflect rather than absorb bandgap luminescence will continue to increase in importance.

## 5. Analysis of outstanding performance losses

Fig. 10 summarizes and puts into perspective the various losses relative to the thermodynamic detailed balance upper limit (i.e. Shockley-Queisser limit) [23,59] as a function of the effective bandgaps of the several different kinds of CdTe-based devices representing recent advancements in the state of the art. Points for each of the cells from Fig. 9 and Table 1 are plotted in terms of their $V_{oc}$, FF, $J_{sc}$, and PCE compared to the SQ limits. It is clear that the largest opportunities for improvement are in $V_{oc}$ and FF; the. We analyze the current, FF, and voltage losses in the following.

Examining the EQE and IV curves in Fig. 9, it can be seen that the $J_{sc}$ of record cells prior to 2012 were being increased primarily from reducing short wavelength parasitic absorption in the TCO and buffer layers. In the case of the 16.7% NREL record cell, the chemical bath deposited CdS buffer was replaced with a sputtered oxygenated CdS, on top of $Cd_2SnO_4$/$ZnSnO_x$ (CTO/ZTO). The sputtered CdS:O allowed a thinner CdS from thickness control of the interdiffusion and was probably the main advance. CTO is a higher quality transparent conducting oxide (TCO) than $SnO_2$:F (FTO), allowing lower sheet resistance at the same transparency. ZTO had improved etch resistance compared to CTO and served as a highly resistant transparent (HRT) layer [20]. While GE and FSLR have not disclosed exactly what window and buffer layers have been used, it is clear that the parasitic absorption onset is being moved toward the limit set by the TCO bandgap (FTO is used in the TEC series coated glasses, CTO has a very similar bandgap). The major jump in efficiency in 2012 occurred primarily due to an increase in current and may be attributed to the introduction of selenium to enable CdSeTe emitters [6] with photoactivity in place of the more traditional CdS emitter. Examining Table 1, it can be seen that the $V_{oc}$ was staying nearly constant and FF fluctuating from 1993 until 2012–2014, thus in those two decades improvements in record efficiencies was driven largely by $J_{sc}$ increases. This is not to say that scattered reports of higher FF and $V_{oc}$ were never achieved during this time, just that these were not paired with other improvements to result in record cells.

It is often useful to analyze the difference between the performance parameters of a solar cell and the ideal ones for its band gap in terms of individual loss mechanisms. In the following example we analyze a relatively-thin FTO/MZO/CdTe cell with 15% efficiency and 835 mV voltage which represents the older generation of typical research lab cells (without Se addition to the absorber) [92]. The measured EQE spectrum in the left panel is shown in blue. When it is multiplied by the standard photon spectrum and integrated, it corresponds to a current density of $J_{SC} = 24.6$ mA/cm$^2$. The maximum current for the bandgap was deduced from the EQE cutoff to be 28.8 mA/cm$^2$, and the individual losses can be determined by spectral reflection and absorption measurements of the layers in front. The losses here in mA/cm$^2$ are 2.3 for reflection, 1.0 for glass absorption, 0.3 for TCO absorption, and 0.6 for incomplete absorption, with small losses from the MZO buffer layer and recombination prior to collection. If it were a cell with a bilayer CdSeTe/CdTe absorber, the EQE region would be divided between CdSeTe and CdTe absorption with most of the current generated in the CdSeTe even when its thickness is the order of 0.5 μm [92]. While there is still some room for improvement, all-in-all the current generation is very close to the *internal* SQ limit – i.e., nearly all the above bandgap light that makes it into the device is converted into current that is collected at short circuit. Nevertheless, as shown in Fig. 10, approximately 10% further improvement in $J_{SC}$ remains possible.

Turning to the FF, we see that losses can also be broken down into components, as shown on the right side of Fig. 11. Bothwell et al. [92] used the approach put forth by Green [93] to determine a FF loss

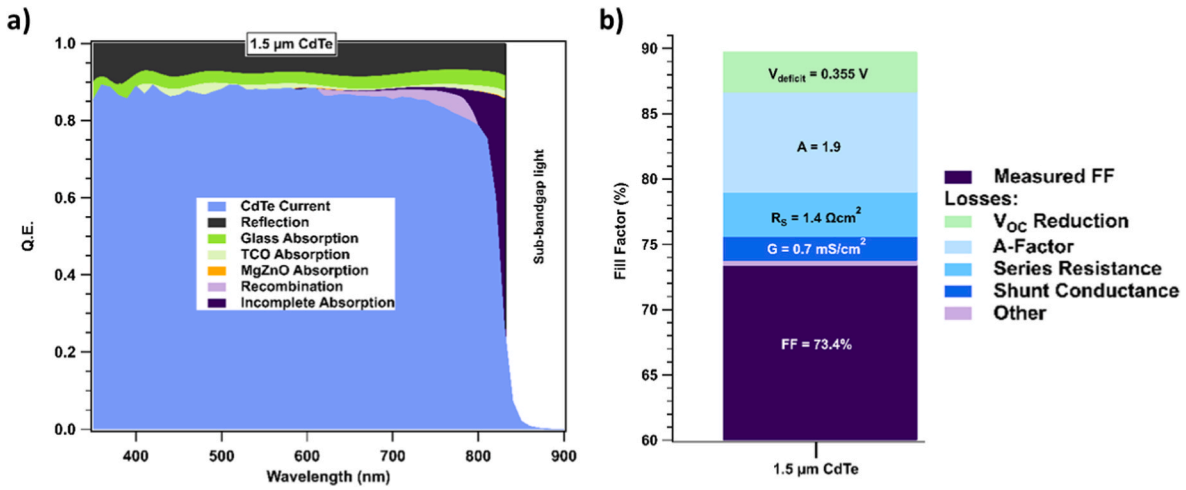


**Fig. 11.** a) Breakdown of current losses and b) fill-factor losses. Images reused with permission by the original authors from Ref. [92].

component due to the loss in $V_{OC}$ relative to $V_{OC,SQ}$. This loss component is due to the fact that the voltage range for diode turn-on is a fixed amount relative to $V_{OC}$, and thus the ideal value of the FF increases as $V_{OC}$ increases. If the device is otherwise operating near the SQ limit, and behaving ideally, this FF loss mechanism would not be found. Thus, this fairly large FF loss mechanism which is ascribed to voltage deficit is connected with the intrinsic operation of the absorber and the extraction of carriers through the contacts.

The other three FF losses shown are derived from the diode equation

$$J = J_o \exp\left[\frac{q(V - JR_s)}{Ak_BT}\right] + GV - J_{SC} \quad \text{Eq. 1}$$

using the procedures described in Ref. [94]. In the example cells above, the diode quality factor A is relatively large, and the series resistance $R_S$ and conductance G are somewhat larger than desirable. The small "other" region is simply the remaining unidentified loss. The diode quality factor, A, which characterizes how the diode turns-on with voltage, gives rise to the largest FF loss component. Many CdTe diodes have A factors approaching 2 and this deviation from ideal behavior is typically attributed to carrier recombination in the depletion region. This FF loss mechanism is also associated with the properties of the interfaces that form the contacts to the absorber layer. As the diode is turning on near the "knee" in the J-V curve, the bands begin to flatten and the internal electric field is reduced. Thus, the carrier transport mechanism transitions from being drift-to diffusion-controlled, particularly in high efficiency devices. Without low-defect interfacial regions, interfacial recombination currents can begin to dominate. The $V_{OC}$ deficit and A-factor loss mechanisms amount, together, to ~10% loss in FF. Although voltage loss is often considered to be the largest single loss in efficiency, the loss in FF in comparison to the SQ-limited FF values is similar in magnitude. The remaining two FF loss mechanism due to series resistance $R_S$ and parallel conductance G are substantially smaller. The loss due to $R_S$ can be ameliorated through cell and module design.

The breakdown of voltage losses, at least at present, is less quantifiable than that of current and fill factor. The voltage deficit between actual and ideal voltage, even with the best CdTe cells, is over 240 mV. The primary factors responsible are the absorber carrier density, recombination at the front and back interfaces, bulk absorber recombination, band tails and bandgap fluctuations, and back-contact band bending. The relative magnitudes of these voltage losses can vary considerably among different cell structures and fabrication details, and definitive measurement and quantification are still works in progress.

For an illustrative set of As-doped Se-alloyed cells, the breakdown of $V_{oc}$ losses has been estimated by Grover as is shown in Fig. 12. For an effective bandgap of 1.4 eV and assuming a step-function in absorptivity

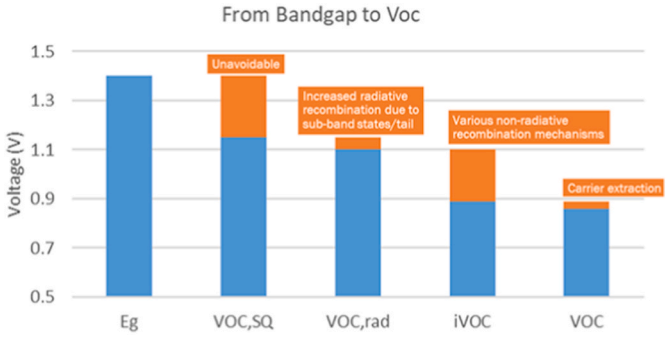


**Fig. 12.** Estimated breakdown of $V_{oc}$ losses in state of the art As-doped, Se-alloyed cells. Proceeding from left to right, the SQ-mandated losses, sub-gap radiative losses, non-radiative losses, and energy-level-alignment losses are successively subtracted to move from the cell effective bandgap near 1.4 eV to measured $V_{oc}$ below 900 mV.

at $E_g$ detailed balance for a flat plate cell radiating into 2π str is 1.140 V as shown as the blue $V_{oc,SQ}$ bar. In the case of As doping, it has been seen that both band tail states and some unidentified deeper defect states emit radiatively [60]. These lower-energy states, which are more-easily observable in luminescence experiments because of carrier "energy funneling", reduce the $V_{oc}$ to approximately 1 V by providing another channel for photocarrier recombination, which is indeed radiative but occurs at a voltage below the bandgap [95–97]. In the detailed balance framework, these states are assumed to emit and absorb reversibly; especially in the case of emission from deep states with multiple levels or involving lattice relaxations, reciprocity between absorption and emission may not be obeyed. These radiative losses can be quantified by converting luminescence spectra into emissivity (and assuming reversibility, further into absorptivity) using the generalized Planck law and then carrying out the detailed balance calculation. The bandgap and fluctuating potential contributions from compensated As doping have been modeled, and shown to be not completely separable (e.g. potential fluctuations can lead to bandgap fluctuations) [28,60]. We note that the losses caused by radiative recombination below the absorption bandgap are currently far smaller than those due to non-radiative recombination. Finally, by comparing calibrated, quantitative luminescence to predictions for total luminescence yield from detailed balance, the internal or implied $V_{oc}$ ($iV_{oc}$) can be determined. The difference between this implied $V_{oc}$ and the radiative limit given the absorption/emission spectrum yields the non-radiative losses. Finally, the difference between the $iV_{oc}$ and measured $V_{oc}$ yields the losses incurred by carrier

extraction, for example mismatch between contact energy levels and the quasi-Fermi levels [68]. This analysis, as briefly discussed previously, clearly points to reductions in non-radiative recombination as the highest-priority R&D tasks for state-of-the-art cells. The "tyranny of the Boltzmann distribution" applies to this endeavor; each increase in $V_{oc}$ by 60 mV requires reducing the non-radiative recombination by a factor of 10 (assuming ideality factor = 1).

As the materials and processing of CdTe devices has improved, the understanding of the devices has also grown. Today's high efficiency devices are short diodes, with three primary competing recombination mechanisms: front interface, back interface, and in the bulk of the absorber [98–101]. This is shown schematically in Fig. 13. Within this framework, FF is a measure of how quickly (as a function of bias) the recombination at each location turns on. A small fill-factor strongly suggests that mechanisms other than and perhaps in addition to Shockley-Read-Hall recombination are operative over a relatively wide voltage range over which the current turns-on.

Considering fill-factor through the recombination framework is critically important to understand the "S-kink" sometimes observed in devices that use wide-bandgap MZO emitters [64,102]. In these cases a barrier exists that prevents the carriers from exiting the absorber layer [103], leading to a build-up of carriers resulting in recombination in the bulk of the absorber and current density loss at low forward bias [104]. This bulk recombination saturates at slightly higher bias, leading to a change in slope in the J-V curve in the power quadrant. At higher bias, another recombination mechanism turns on, and the total recombination current equals the photogenerated current. While series resistance and conductance can indeed be an issue in these devices, it is likely that fill-factor is more strongly affected by the varying recombination mechanisms. Still, tricks to tease out the effect of series resistance, such as varying light intensity, can still be used to generate a breakdown of fill-factor loss as shown above.

Numerical simulations of both the front and back interface show that the band alignment between the absorber and emitter at the front and back buffer layer at the back is critical to eliminating the voltage losses due to the carrier extraction [103,105]. Discussions about the requirements for the front interface tend to center around the conduction band offset between the emitter and absorber [103], but the doping density and Fermi level in the emitter need to be considered [106–108]. To limit voltage loss and recombination at the front interface, the conduction band of the emitter should be higher in energy than the conduction band of the absorber, often called a spike. With proper doping density in the emitter, this leads to a Fermi level that is also above the conduction band of the absorber, leading to a high built-in potential and large band bending at the front interface which repels holes and forms an electron selective contact. The trap-assisted recombination current density at the interface is

$$J_{int} = q \cdot mc_{int} \cdot S_{int} \quad \text{Eq. 2}$$

in which q is the elementary charge, $mc_{int}$ is the density of minority carriers at the interface (holes for the front interface), and $S_{int}$ is the interface recombination velocity. Therefore, fewer holes at the emitter/absorber interface leads to reduced recombination and voltage loss. However, too large of a conduction band offset can lead to a large barrier for electron extraction at this interface, leading to an "s-kink" [103,109]. In addition to the conduction band offset, it is often assumed the valence band position of the emitter is below that of the absorber. While this may provide hole reflection from the back interface, it is more important to develop the wide bandgap emitter to allow transmission of all the light into the absorber. This transition from long diodes, in which minority photocarriers recombine before reaching the back interface, to short diodes in which they don't recombine before reaching it is dramatically changing the requirements for the back contact. The most obvious change is the necessity to passivate interface trap mediated recombination at the back contact. Less obvious, but just as important in future generations of devices, is to avoid the use of materials with smaller bandgaps than the absorber such as Te. This is because, even if photocarriers recombine radiatively they do so across a smaller bandgap which thus reduces the quasi-Fermi level splitting and $V_{OC}$. Additionally in the very highest efficiency designs, such layers or inclusions can induce parasitic absorption of luminescence from the absorber layer. These effects will only become more and more important in thinner cells that approach the detailed balance limit more closely [110–117].

Simulations of the back interface show similar requirements are necessary to limit recombination and voltage loss [105]. At the back interface, electrons are the minority carriers, so reducing recombination and achieving the highest voltages requires upward band banding at the back interface to form a hole selective contact. This upward bending can be achieved when the Fermi level of the back buffer was deeper than the Fermi level of the absorber. In the literature this has been referred to as a positive initial Fermi level offsets (IFLO); we note that in the absence of extra charges the IFLO will equal the built-in potential of the material junction [105]. In practice this may be difficult to accomplish due to deep valence position of CdTe and the potential for Fermi pinning and dipole formation, though the dipoles may form in either direction [118]. While a conduction band offset which impedes electron flow out of the absorber (often called an electron reflector) is thought to be beneficial under certain circumstances, specifically fully-depleted devices [119,119,120,120], it is primarily the band bending, not the offset, that provides the electric field induced electron repulsion [105]. It should also be noted that both a large valence band offset at the back interface and a large conduction band offset at the front interface can impede hole flow out of the device and result in an S-kink in IV measurements [64,109]. Much like the front interface, this S-kink will be exacerbated by low doping levels in the back buffer.

In addition to the band bending, developing passivated interface by reducing interface recombination velocity ($S_{int}$) can reduce recombination and voltage loss. A number of simulation papers show how the combination of band bending (selective contacts) and interface recombination (passivated contacts) can affect the voltage losses for the devices [11,24,107]. At the front of the device, passivation appears to be achieved during the $CdCl_2$ process [89]. At the back interface, developing a passivated back contact may be more important due to the difficulty achieving proper band alignment. As a result, oxides,

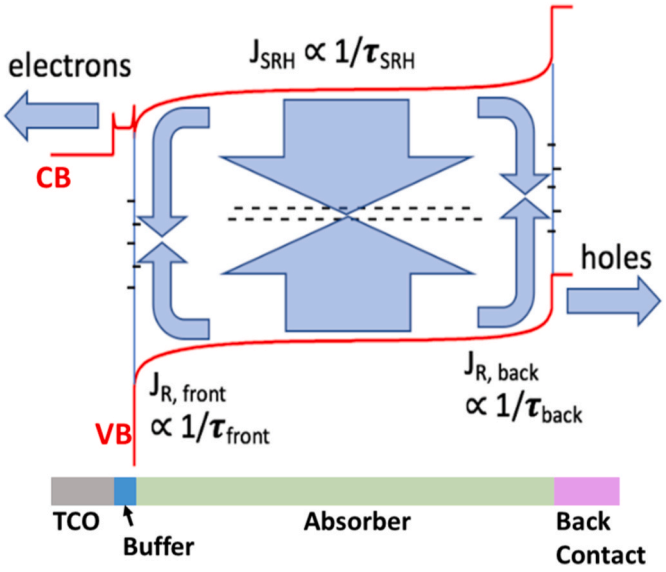


**Fig. 13.** Schematic CdTe cell band diagram (red lines) showing conduction band (CB) and valence band (VB) and recombination processes at the electron contact, in the absorber layer, and at the hole contact. The schematic cell layer structure is shown below. Comparing to Fig. 5c), the "spikes" in the buffer layer here indicate high doping such that the Debeye length is smaller than the thickness.

specifically $AlO_x$ [121,122], are being investigated as a way to decrease recombination and voltage loss due to the back interface [123,124]. Interestingly, this approach still depends on $CdCl_2$ accumulation at the CdTe interface [125], with little to no passivation benefit realized from the $AlO_x$ deposition unless paired with a post-deposition $CdCl_2$ treatment. A general rule has been observed that for any benefit of field effect passivation to be realized there must first be a chemically passivated surface [89]. In CdTe, this has largely been accomplished to date with $CdCl_2$.

## 6. Alloyed $CdSe_xTe_{1-x}$ absorbers

Alloying CdTe with both group II (especially Zn, Mg, and Mn) and group VI elements (especially S and Se) is widely used for bandgap engineering in single crystal bulk and epitaxial growth [126]. The application in polycrystalline thin film devices similarly has a long history, especially $Cd_{1-x}Zn_xTe$ for either wider-gap absorbers or attempting to form an electron minority carrier mirror at the back contact. It is worth mentioning the special role played by O, S, and Se in diffusing along and passivating grain boundaries. A first example is the interaction of $O_2$ with the $CdCl_2$ heat treatment step which has been found in some processes to be beneficial. Later, it was found that S from the CdS buffer layer diffused over quite long distances during deposition and $CdCl_2$ treatment and acted to help passivate grain boundary defects [127]. Simultaneously, $CdS_xTe_{1-x}$ alloying occurred within grains to varying extents depending on the fabrication details. The atomic radius mismatch between S and Te is somewhat larger than that of Se and Te, leading to more propensity for phase segregation. In both of these alloy systems $CdS_xTe_{1-x}$ and $CdSe_xTe_{1-x}$ the large difference in anion electronegativities causes large bandgap bowing parameters thus starting from CdTe the bandgap first decreases with increasing x until a minimum is reached at 1.3–1.4 eV for both alloys at x∼0.25 for S and x∼0.4–0.5 for Se and then increases [7,128–130]. More recently, intense focus has been applied to the effects of Se and in fact it is one of the critical changes that helped to push cell efficiency beyond 20%. We note a recent development utilizing the entirety of the chalcogenide column in the periodic table; cells with Cd(O,S,Se,Te) absorbers achieving greater than 20% efficiency [131].

In the recent past, it could be recognized from QE curves of record cells that bandgap reduction was being implemented but exactly how was not widely known outside GE/Primestar and First Solar [44]. This has meant that academic researchers recently have been working to explain the effects of Se alloying in absorbers that has been empirically known within industry to produce higher efficiency cells since the early 2010's. In the open literature, perhaps the first clear demonstration that CdSeTe alloying by interdiffusing CdSe and CdTe could increase $J_{sc}$ contributions at long wavelength by reducing the effective absorber bandgap was from Paudel and Yan [6].

Most academic research groups working on CdTe cell fabrication have attempted methods of incorporating Se and grading the bandgap near the front of the cell. We use here the example of efforts from CSU as illustration; similar results have been found by many groups by this time. In 2017, Swanson et al. demonstrated that Se could be alloyed into polycrystalline CdTe thin-film during deposition to lower the band-gap of the absorber film [132]. This study used a novel co-sublimation method to introduce depth-varying but controlled amounts of Se into CdTe. Transmission measurements indicated minimum bandgaps of 1.42 eV for $CdSe_xTe_{1-x}$, accompanied by increased $J_{sc}$ and EQE measurements but increases in efficiency were not realized. Next, ∼100 nm of CdSe was deposited on $Mg_xZn_{1-x}O$ (MZO) buffer film on TCO glass followed by ∼500 nm of CdTe and then aggressive $CdCl_2$ treatment to achieve intermixing by solid state diffusion. Following this, a thicker CdTe layer was deposited and second $CdCl_2$ treatment was performed to passivate the newly-deposited CdTe layer. The process was tedious with limited control over the bandgap of the deposited films. Also, cross-sectional microscopy revealed the presence of Kirkendall voiding induced by the differences in Se and Te diffusion. Next, pre-alloyed $CdSe_{0.2}Te_{0.8}$ was acquired from 5 N Plus Inc. and that was utilized for further experimentation. Cross-sectional transmission electron microscopy (TEM) and energy-dispersive x-ray spectroscopy (EDS) maps confirmed that $CdCl_2$ treatment led to interdiffusion of $CdSe_xTe_{1-x}$ and CdTe layers with reduced voiding [133]. By depositing a bilayer with this material along with CdTe to form a graded band-gap device, Munshi et al. demonstrated device efficiency of 19.1% with short-circuit current density of 28.4 mA/cm$^2$ without the use of anti-reflection coating [134]. Using a thicker CdTe layer following the $CdSe_xTe_{1-x}$ layer along with more aggressive CuCl treatment at the back surface can yield cells with $V_{oc}$ >850 mV. By varying the thickness of the front $CdSe_xTe_{1-x}$ layer, it was also determined that 500–900 nm of $CdSe_xTe_{1-x}$ was optimum for improvement in performance in this structure while thicker films led to low $V_{oc}$ and a barrier to charge collection apparent from the 'kink' in the J-V curve.

These studies were aimed at optimizing bandgap grading to increase $J_{sc}$ and increase efficiency. Se was demonstrated to diffuse along grain boundaries (and to a lesser extent within grains) by Fiducia et al. using nano-SIMS. Further, correlated cathodoluminescence (CL) mapping shown in Fig. 14 showed that, both in grains and grain boundaries, with increased Se the CL yield was higher. A telling observation was that the CL was brighter in grain boundaries with Se than in grains for a sample without Se, demonstrating the remarkable passivation of both intra grain and grain boundary non-radiative defects [78]. A follow-up study quantified the Se effect at grain boundaries, demonstrating that while the intragrain diffusion length stayed nearly constant, GBs with higher Se content in the same absorber with graded Se demonstrated, on-average, about an order of magnitude lower recombination velocity [135]. Kephart et al. used sputtered $Al_2O_3$ to passivate both sides of Se-containing $CdSe_xTe_{1-x}$ layers thus forming double heterojunctions. Scanning transmission electron microscopy (STEM) and electron energy-loss spectroscopy (EELS) combined with density functional theory calculations demonstrated that Se and Cl segregate and co-passivate grain boundaries, which leads to a significant increase it the carrier lifetimes [136]. In these structures, time resolved photoluminescence lifetimes up to 430 ns were demonstrated [121,122]. Such long lifetimes demonstrated that Se-alloyed absorbers are capable of reducing recombination by more than an order of magnitude relative to Se-free absorbers. An interesting observation is that $V_{OC}$ is generally about the same as cells with CdTe despite a 100 meV bandgap reduction, which is in part due substantially to these larger minority carrier lifetimes. Detailed analyses of Se-alloyed cells are emerging at the present time [27,68,137]. It is not presently understood why to date no successful Se-alloyed devices have been made without a Se-free absorber layer at the back. Identifying loss mechanisms and strategies for mitigating them are the subjects of ongoing cutting-edge research.

## 7. Interfaces and contacts

Contacts for CdTe devices have been a recurring theme throughout the history of the technology. As discussed above, CdS/CdTe devices struggled with realizing current, due to parasitic absorption. This made thinning the CdS and pairing it with high quality transparent conducting oxides (TCOs) and a highly resistant transparent (HRT) layer (this acronym was originally used to connote i-SnO2, or high resistance tin oxide). The stability of these front oxide layers to high temperature processing and reactive ambients (e.g., $O_2$ and $CdCl_2$) limits the choices. The most common TCOs that have been used include $SnO_2$:F (FTO), $In_2O_3$:$SnO_2$ (ITO – which is typically ∼90% $In_2O_3$ by weight), ZnO:Al (AZO), and $Cd_2SnO_4$ (CTO). FTO has been the most widespread TCO of choice due to its chemical and temperature stability as well as low cost (it can be deposited by the glass manufacturer through an atmospheric pressure chemical vapor deposition process) and ready availability. All of these TCOs, except for FTO, are most commonly sputter-deposited, although solution-deposition routes have been and continued to be

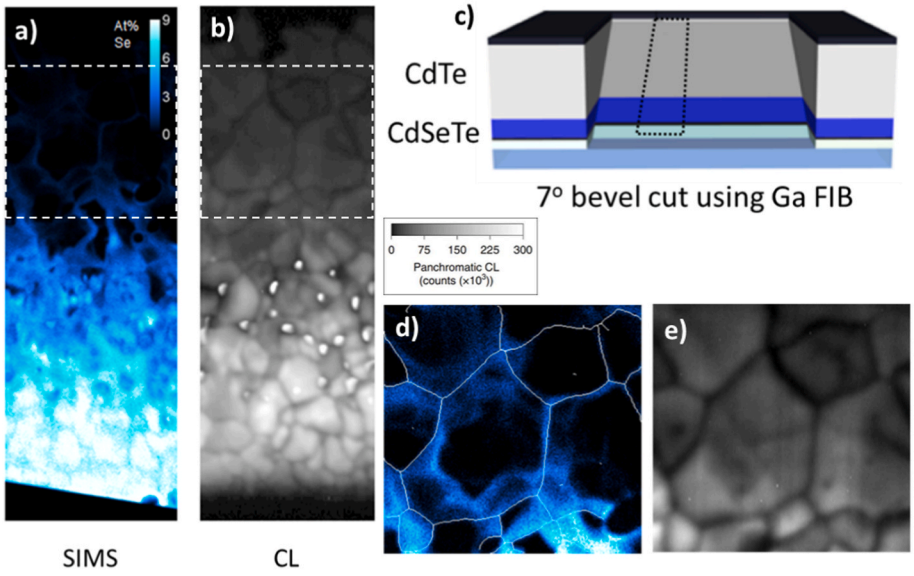


**Fig. 14.** a) nanoSIMS of Se and b) Cathodoluminescence (CL) from the beveled cross-sections of a bilayer CdSeTe/CdTe absorber stack along as indicated by the dashed rectangle shown in the schematic of c). The cross-section was exposed by milling a shallow 7° bevel through a CdSeTe/CdTe device using a focused ion beam. The Se distribution in a) is more concentrated in the front of the device although it has clearly diffused into the CdTe layer especially (but not only) along grain boundaries. The panchromatic CL image of the same area shows much higher luminescence in the Se-rich region (note the CL greyscale is sqrt(intensity)). The higher magnification images d) of Se nanoSIMS and e) CL, which were taken from the dashed areas shown in a) and b), indicate higher CL yield around the fringes of grains where Se has in-diffused from the grain boundaries. The white gain boundaries in d) were defined by a skeletonized nanoSIMS chlorine map (not shown).

explored for some. In the early 2000's there was a focus on eking out more current through the use of TCOs with a higher figure of merit [138], which captures the relative transparency to sheet resistance. This led to the investigation of ITO and CTO. While ITO has some scarcity/cost concerns due to In incorporation, another challenge is the technical one that its performance can degrade at the high temperatures common to CdTe processing. As mentioned above, CTO was one of the innovations that was a part of the NREL world record that lasted from 2001 to 2011 [21]. Advantages of CTO included its lower roughness relative to APCVD-FTO, higher mobility, and overall better figure of merit [139]. High-performance lab-scale CTO typically require a high temperature Ar anneal (~600+ °C) sometimes in the presence of CdS. This may be one of the obstacles to having implemented it at-scale.

A series of materials have been investigated to transition between the TCO and the absorber layer. These have variously been described as buffers, window layers, emitters, and transport layers. In CdS/CdTe devices this transition was generally a two layer stack consisting of an oxide such as i-$SnO_2$, $TiO_2$, i-ZnO, or zinc tin oxide (ZTO) that was then capped with CdS. The second oxide would help reduce the effect of "weak diodes" from pinholes in the CdS that led to shunting as the CdS layer was thinned [140,141]. As higher doping levels are attained with group V defect chemistries, the space charge region collapses such that samples are more sensitive to recombination near the front interface [24,142]. The community is presently searching for alternate front interface couples. Ideally, the properties would include band offset tunability such that a 0.1–0.3 eV spike in the conduction bands could be established, high emitter doping relative to the absorber, low catalytic activity to minimize group V pileup, good carrier selectivity, and low interface recombination velocity, together with good temperature and chemical stability. There are number of candidates that have been considered, including MZO, MZO:Ga, IGO, and i-$SnO_2$. None has yet been demonstrated to combine all properties. Recent investigations have used a thermo-mechanical delamination to reveal the buried front interface (oxide/non-oxide) and study its chemistry, evolution, and stability [88,89,143,144].

Historically, making an Ohmic hole-collecting contact to *p*-CdTe has been challenging due to its low doping efficiency and high ionization potential (5.7–5.9 eV [145,146]); no metal by itself has a sufficiently high work function (Au is 5.1 eV, Pt is 5.65 eV [147]). Those interested in reviewing some of the foundational work on Ohmic and rectifying contacts to CdTe are advised to read Ponpon [148] as well as a recent review by Hall et al. [146]. Ideally, this contact would be well-matched energetically such that it is carrier selective (i.e., electron reflective), passivating, stable, and transparent to enable bifacial systems. Historically, getting even a low barrier at this interface with stability has been a challenge, with "rollover" in current-voltage a common signature of a high back barrier [119], much less all occurring simultaneously. With Se alloying, devices have shifted from the long diode to short diode regime, where interface recombination at the back interface has become more critical to advance efficiency. Passivation would also enable thinning of the absorber layer to reduce Te usage in the next generation devices.

Historically, copper has been critical in lowering the barrier height at the back of devices. Before the more recent shift to group-V dopants, Cu was introduced as a dopant, but post-situ due to its high diffusivity. In some cases, Cu has been introduced through a treatment to the absorber (e.g. $CuCl_2$ [77]), but in many cases it was introduced as part of the back contact. Examples include copper-doped sometimes mercury-containing graphite paste (e.g., DAG or aqua-dag [53]), Cu-doped ZnTe (ZnTe:Cu [149]), copper telluride [150], and a thin (0.1–3 nm) metallic Cu layer followed by metal (e.g. Au, Ni) [151]. Generally, these contacts/Cu-doping require an anneal temperature in the range of 200–250 °C to diffuse and/or activate the Cu. It is important to note that this temperature range is also the same range at which CdTe surfaces can be thermally reconstructed [152] as well as a temperature at which oxidation states at the front interface transition [144].

Prior to making this contact, the surface state of the CdTe has long been recognized as a critical component of the contacting process. The most prevalent approach in the literature has been to establish a Te-rich layer. This can be done through a subtractive process using an oxidative etch such as nitric-phosphoric acid, $Br_2$:methanol, ethylene diamine, potassium dichromate, or even more novel approaches such as methylammonium iodide [110,111,148,150,153] or in an additive process like evaporating ~20 nm of Te [92,134]. If a Te-rich surface is subsequently doped with Cu it can lead to a more highly doped p-type region through the formation of $Cu_xTe$, at least partially explaining the strong historical preference of the community for Te-rich contacts. It has been demonstrated that Te-rich CdTe surfaces have higher recombination than stoichiometric or somewhat Cd-rich surfaces [152], which has led to some pre-contact surface preparations to favor stoichiometric to Cd-rich conditions to achieve better passivation [154,155]. Historically, the low minority lifetime of the absorber made interface recombination at the back contact less important than a reduced barrier height, which modeling indicates a pure Te layer at the back interface can lower [156]. That being said, when another highly doped semiconductor such as ZnTe is used to create a hole transport at the back, a stoichiometric rather than Te-rich surface has been observed to be preferred [154].

More recent modeling suggests these different observations may be related to surface termination of the CdTe. When a Te layer is used to contact a CdTe surface, if the CdTe is terminated with Te instead of Cd it can lead to notably lower efficiency [118]. To date, ZnTe has one of the lowest observed barrier heights of the various contacts surveyed by the community at 0.3–0.5 eV (although Te is similar, or possibly even lower) [157,158] and has also been adopted commercially with improved stability [55].

As the community looks towards group V doped absorber layers with high doping and long minority carrier lifetime, there has been discussion regarding if a Cu-free back contact should (must?) be used and thereby avoid any concerns related to compensating defects and stability. A variety of nominally Cu-free devices and/or back contacts have been examined including using metal oxides (e.g., $MoO_x$ [159] $AlGaO_x$ [160], pnictides (e.g., $Ni_xP$ [161]), tellurides (e.g., Te, ZnTe, PbTe, $Sb_2Te_3$) [68,162], and a host of other miscellaneous other materials (e.g., Au, PTAA, MXenes) [146,155,163]. A caution should be mentioned for any literature that reports Cu-free devices. Cu is a particularly persistent actor, where if it has been introduced previously in a deposition chamber deep-cleans are necessary to remove it. It is also a common impurity in materials used in CdTe processing (e.g., $CdCl_2$). The only way to be sure a device is Cu-free is through dynamic SIMS analysis such that the Cu impurity level can be evaluated relative to the absorber's carrier concentration [164].

As bulk lifetimes have significantly improved past a few ns, recombination at the back interface has become more of a concern. Addressing this would be enabling in both reducing the Te intensity of devices, since CdTe devices do not require 3 μm of absorber from an optics standpoint, as well as facilitating improved bifaciality, which would also require a high quality transparent contact. One proposed approach to address this is an electron reflector material such as ZnTe or CdMgTe [165]. Using point contacts with an electric field passivating material, such as $Al_2O_3$, has been considered as well at both the front and back interfaces [121]. Chemical passivation appears to be a required element to reap the benefits of electric field passivation. A "2D/3D termination" strategy, where a 2D material (e.g., $CdCl_2$) terminates the 3D surface (i.e., CdSeTe) has been one of the primary ways chemical passivation has been achieved [89]. New materials and processes to achieve passivation as well as reducing Fermi level pinning at CdTe surfaces are both ripe for more research.

## 8. Doping and point defects

### 8.1. Native defects and Cu doping in CdTe

Shallow doping in II-VI compound semiconductors is in general not as simple as for Si, Ge, and III-V compounds, especially in polycrystalline thin films. Some II-VI's such as ZnSe and CdTe tend to compensate at least one doping polarity with native defects, and some dopants such as Cu may exhibit limited substitutional stability and tendencies for self-compensation. Both effects can be understood by observing that the formation enthalpy of a charged defect depends linearly on the Fermi energy, thus compensating defects (whether native or incorporating the dopant itself) become more favorable as the Fermi energy moves closer to a band edge. At extremely-high dopant concentrations or chemical potentials, substitutional doping becomes unstable to the formation of secondary phases. The generic term collecting these behaviors is that a "doping limit" is reached. CdTe in polycrystalline form tends to compensate especially p-type doping, and Cu appears to self-compensate more than As or P under many deposition and growth conditions. The native defect properties in CdTe have recently been reevaluated with density functional theory (DFT) using the Heyd–Scuseria–Ernzerhof (HSE06) hybrid functional, which enabled new insights [46,166–172].

Recent DFT calculations have provided insights into why undoped CdTe films can only be made weakly p-type. Also, carrier lifetime is expected to be low when CdTe is synthesized under Cd-poor conditions. It was found that among all possible native defects, that $V_{Cd}$ creates the shallowest accept level. Te-rich (Cd-poor) growth conditions favor the formation of $V_{Cd}$, responsible for the p-type conductivity. Only low p-type conductivity can be achieved in unintentionally-doped CdTe in equilibrium because of two limiting factors of native defects. First, the $V_{Cd}$ accept levels are too deep at approximately 360 meV to be fully ionized. Second, during growth of CdTe films, other native donor-like defects such as Te vacancy ($V_{Te}$), Cd interstitial ($Cd_i$), Cd on Te anti-site ($Cd_{Te}$), etc. also form. However, as the growth temperature increases, more defects are created and since rapid quenching can freeze-in these high temperature concentrations. The doubly-charged Te on Cd anti-site ($Te_{Cd}^{2+}$) has been believed to be the most active non-radiative recombination center, which is undesirable for solar cell applications [46,173,174]. The recombination behavior of the $V_{Cd}$ has been experimentally characterized [91,173] and very recent advanced computations have predicted that trap-assisted recombination from $V_{Cd}$ under equilibrium conditions would result in a loss of 5% in efficiency [175]. Experimentally, Cd-rich conditions have been shown to promote longer minority electron lifetimes [47].

### 8.2. P-type doping

Most monovalent elements like Li, Na, Ag, etc. can act as acceptors on the Cd site, however over many decades Cu has been the most widely adopted, although in the current era it has been recognized that Cu itself had become a limiting factor on efficiency and stability of cells, as discussed in later sections in more detail. Cu forms both substitutional acceptors ($Cu_{Cd}$) and self-compensating donor-like interstitial ($Cu_i$). The $Cu_{Cd}$ (0/−) acceptor level is about 150 meV above the VBM, which while shallower than $V_{Cd}$, is still too deep for full ionization at room temperature. $Cu_i$ donors do not strongly compensate holes generated by $Cu_{Cd}$ acceptors. As a result, Cu doping in CdTe should be able to improve the p-type conductivity in CdTe, as observed experimentally. However, Cu doping causes device instability and degradation due to the high diffusivity of Cu ions, as described more completely in later sections.

Group V pnictides (N, P, As, Sb) substitutional on Te sites have long been known to be effective acceptors. The first DFT calculations using hybrid functionals reevaluated the formation enthalpies and ionization energies of P and As [46,87,90,168,170,175,176]. P and As interstitials are predicted to have rather high formation energies, especially under Cd-rich condition. However, substitutional P and As may form AX centers, converting them from acceptors to donors. When an AX center is formed, the P (or As) atom will move toward its neighboring Te atom and form a P–Te (or As–Te) bond by breaking their two bonds with Cd. The formation of AX centers is predicted to pin $E_F$ under equilibrium growth conditions thus setting a doping limit. These calculated results, so far do not contradicted by experiments in polycrystalline films [83,168,177], suggest that rapid quenching can enhance the hole density, at least temporarily. The very most recent calculations improve upon this work by using very large supercells and including spin-orbit coupling (which affects the valence band edge and thus acceptor ionization energies) suggest that many of these predictions, especially regarding AX behavior, must be re-assessed [178]. Thin film deposition under non-equilibrium conditions at the vapor-solid growth interface may be exploited to optimize the relative concentrations of desired defects. It is noted that direct experimental identification of compensating defects causing low doping efficiency for group-V doping has been sparse at best; further work is necessary to distinguish between compensating native or extrinsic defects, complexes including the dopants, and or AX centers.

In terms of experimental doping results, multiple single crystal growth results using the Bridgman and travelling heater methods have found doping limits with hole density in the low $10^{17}/cm^3$ range. Up to that level, the activation ratio (hole density/dopant density) has been shown to be as high as 50% especially under the Cd-rich conditions from Cd-solvent THM [82–84,177,179–181]. At extremely high doping

concentrations, 2nd phase precipitates such as $Cd_3As_2$ or $Cd_3P_2$ form in all known single crystal growth methods (e.g. THM and Bridgeman [61,85,182]), but it is clear that a point defect compensation mechanism operates at lower doping. Increased doping with quenching and persistent photoconductivity have been observed. Self-compensation by AX centers is suspected, however no direct structural evidence has eliminated other possibilities such as defect complexes that may dissociate and re-associate. Minority carrier lifetimes of 10's to 100's of ns have been observed in As-doped single crystals grown by Cd-rich THM demonstrating that the combination of high p-type doping and long electron lifetimes are possible with group-V doping and Cd-rich conditions. In polycrystalline device structures, especially when passivated at the back surface, lifetimes exceeding 1000 ns have been measured and doping measured from capacitance-voltage (CV) can reach into the $10^{17}/cm^3$ range. Understanding and optimizing the interactions of Gr-V p-type doping, Cl, Se, and grain boundary passivation are still topics of intense research. Recently it has been reported that As can pile up near the front n-type contact interface and compensate p-type doping which lowers cell efficiency [183]. As doping has recently been implemented in production modules (First Solar Series 6 CuRe) and has been found to produce modules with better long-term stability than ones with Cu doping. It is important to note that the body of literature on degradation of cells and modules, including most of what is summarized later in this paper, focuses on Cu-doped cells. Group-V doped cells and modules have simply not been studied long enough for a large body of literature to be built up, however the early indications are that As-doped cells are significantly more stable and reliable than Cu-doped predecessor technologies [90].

## 9. Roles of post deposition $CdCl_2$ treatment

The discovery of the cadmium chloride ($CdCl_2$) activation process was the key innovation responsible for elevating device performance above 15% and attracting commercial interest in the early 1990's [184]. After CdTe deposition the absorber is typically exposed to $CdCl_2$ either by immersion, evaporation, or sublimation coupled with annealing at ~400 °C at time scales on the order of minutes. Activation with alternative Cl sources, notably $Cl_2$ and $MgCl_2$ [15,16,104,185,186] but including many others, is also effective but cells never quite reach the same performance levels as for $CdCl_2$. Especially in the case of close space sublimation (CSS) and other deposition techniques resulting in slightly Te-rich stoichiometry (which can be beneficial for promoting larger grains thus reducing grain boundary recombination), it is suspected that the Cd pushes the overall stoichiometry to Cd-rich thus reducing intragrain defect mediated recombination. This interplay of microstructure and defect evolution during film growth and $CdCl_2$ treatment may help to explain seemingly contradictory results obtained by different groups [187]. Also, alternative heating schemes such as rapid thermal processing (RTP) and laser annealing may be used [188–191]. The $CdCl_2$ activation process has a number of significant benefits including: i) promoting II-VI interdiffusion, ii) grain growth, recrystallization and randomization of grain orientation, iii) removal of structural defects such as stacking faults, and iv) passivation of grain boundaries and interfaces [192]. In CdS/CdTe devices with Cu doping, $CdCl_2$ facilitates interdiffusion of these layers and the formation of a high quality heterojunction [193] and it was generally agreed that the presence of oxygen in the annealing environment had a positive role in promoting this process. The second impact of $CdCl_2$ activation is increasing the size and quality of CdTe gains [194–196]. Regardless of deposition method, the quality of as-deposited CdTe is generally quite poor, with high densities of defects and stacking faults present as shown in Figs. 15 and 16. The SEM and TEM images in Fig. 15 display the dramatic improvements realized at the grain and atomic level, respectively [195]. Twin boundaries remain after treatment, but these features are generally thought to be benign in terms of recombination. The stacking faults terminate at grain boundaries or free surfaces as shown in Fig. 15 and are also benign [196,197]. However, their removal after the $CdCl_2$ activation treatment strongly correlates with a dramatic increase in device efficiency. The removal of stacking faults is caused by sufficient chlorine segregating into the adjacent grain boundaries [198–201]. It is believed that dislocations are effective recombination centers, although their density is generally small in high-quality films. It is the passivation effect of the chlorine that is responsible for the increased efficiency. Interestingly, if the chlorine is removed by

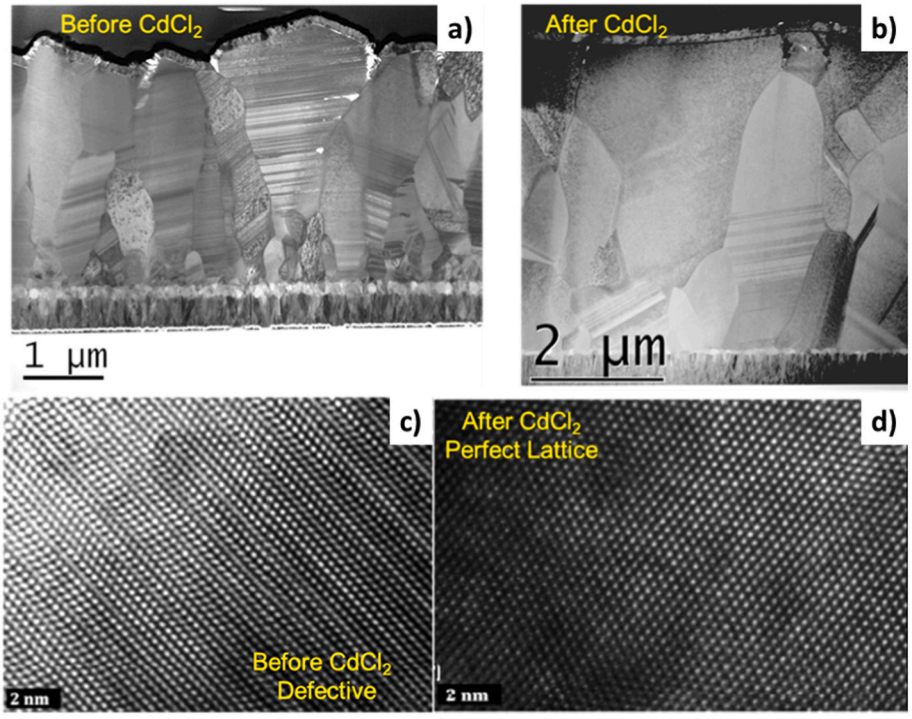


**Fig. 15.** Cross-sectional TEM images of representative cell microstructures before and after $CdCl_2$ treatment, at low resolution a)-b) and at atomic resolution c)-d). As shown in a), before $CdCl_2$ treatment, a fine-grained layer is visible in the CdTe layer in contact with the buffer layer and many stacking faults and twinned regions are present within grains as the parallel bands of contrast as shown in c). After treatment, as shown in b), the densities of both the small grains (and their associated grain boundaries) and the planar intragrain defects as shown in d) are significantly reduced.

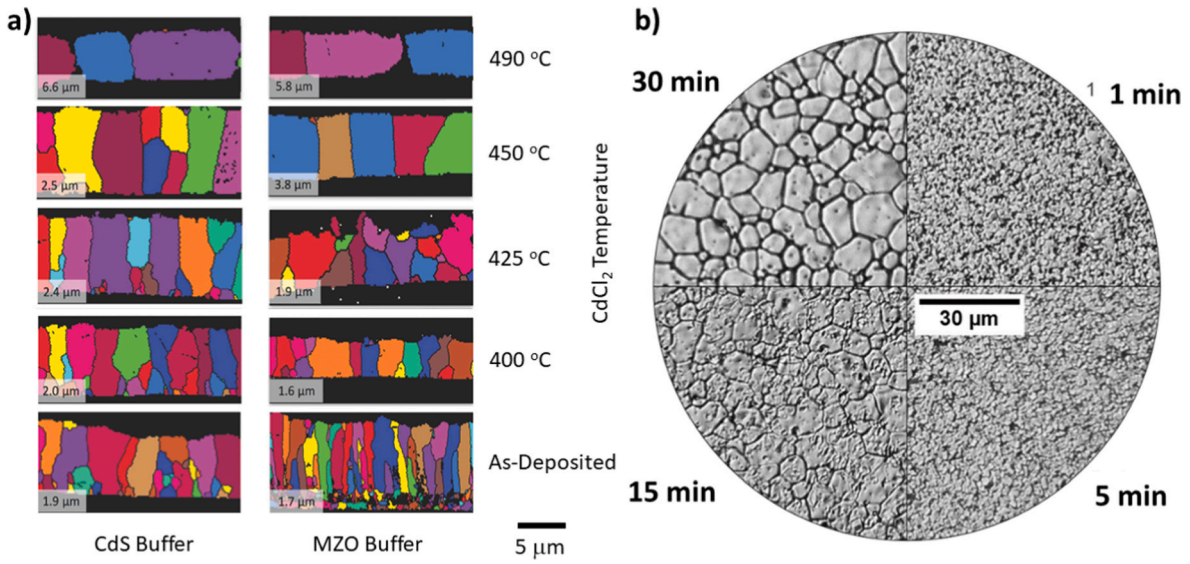


**Fig. 16.** a) EBSD images of microstructure changes during $CdCl_2$ treatment at temperatures from 400 to 490 °C. The scale bar of 5 μm applies to all of the EBSD images. Figure redrawn from elements in Ref. [73] b) Composite top view optical micrographs of ~4 μm thick thin films deposited by thermally evaporating CdTe at 150 nm/min and 475 °C substrate temperature then annealed in a closed graphite vessel containing $CdCl_2$ for different times [71]. The image b) is copyright IEEE and reused by the original author with permission.

annealing, the stacking faults return and the device efficiency declines dramatically [202]. The grain growth during $CdCl_2$ and its temperature dependence is shown eloquently in the electron backscatter detection (EBSD) images shown in Fig. 16. Although the CdTe morphology improves with temperature other issues such as film delamination can occur with excessive time or temperature.

Finally, it is known than Cl segregates to grain boundaries [198–200] and interfaces [88], and its presence has been credited with passivation. Many observations of increased electron beam-induced current (EBIC) signals from grain boundaries have been made leading to the suggestion that grain boundaries might actually help polycrystalline solar cell performance at least near $J_{sc}$, however this concept has been firmly debunked when the excess recombination (or dark current $J_o$) is taken into account [203–205]. The $CdCl_2$ activation step is capex intensive, with early practitioners describing it as the "the most intricate process in manufacturing" [206]. Due to these complications and environmental concerns related to its high solubility in water, there has been a long history of exploring alternatives to $CdCl_2$, including HCl [207], $Cl_2$ [16], chlorofluorocarbons [208,209], and non-toxic salts such as $MgCl_2$ [15, 185]. Chlorine is associated with removal of extended defects, both intragrain and in some cases facilitating recrystallization and grain growth thus removing grain boundaries. Its main role common across many types of film deposition is to passivate grain boundary states. Resulting device efficiencies using these alternative chlorine sources has at times approached, but never surpassed, the performance with $CdCl_2$. So while chlorine is primarily responsible for the observed benefits, the impact of cadmium is non-negligible suggesting that it decreases the concentrations of Te-rich defects. The formation of Cd and Cl-related 2D layers at the absorber/window interface during Cl treatment may play a role in reducing interface recombination [88,89].

Recent advances, including the replacement of CdS with higher-bandgap emitters, the use of selenium alloys, and increased p-type doping have not diminished the importance of the $CdCl_2$ activation step. The $CdCl_2$ treatment retains its role with respect to II-VI interdiffusion, now facilitating selenium compositional grading in CST devices [78, 136]. Alloying appears to proceed in a two-step process where Se first diffuses relatively quickly through the absorber along grain boundaries, followed by a slower alloying reaction with CdTe grains, similar to the diffusion observed in CdS/CdTe diffusion couples. The elimination of CdS has altered the constraints on process conditions employed for $CdCl_2$ activation. In CdS devices using isothermal processing of CdTe coated with $CdCl_2$, treatment temperature was limited to approximately 430 °C because higher temperatures in many cases resulted in complete interdiffusion with the CdS (which was and problems device delamination. Alternative emitters such as MZO experience negligible interdiffusion and enable the use of higher temperature, creating much larger CdTe grains which may contribute to improved performance [73–75]. The presence of $O_2$ in the ambient was considered beneficial in CdS/CdTe devices [210], as oxygen modifies the Cd/Te equilibrium, producing surface $CdTeO_3$ and CdO oxides on the surface. $CdCl_2$ and $O_2$ concentrations each control the resulting oxide content and the CdS diffusivity. In devices using MZO it has been found to be detrimental [64,106]. In this architecture $CdCl_2$ is typically conducted in the absence of oxygen as its presence is thought to eliminate beneficial oxygen vacancies or alter the MZO conduction band alignment. In CST absorbers recrystallization still occurs, but the degree of grain growth is significantly less than in binary CdTe. This is attributed to the higher activation energy for recrystallization for CdSe [211], and thus higher activation temperatures are often used [212]. Chlorine as well as selenium decorate grain boundaries in alloyed devices [78,136]. Chlorine retains its role passivating grain boundaries, while the role of Se at grain boundaries is less clear.

A $CdCl_2$ thermal annealing process has been long established as a critical step for making CdTe devices [213]. It is commonly accepted that the grain boundary passivation by chlorine during $CdCl_2$ annealing step plays an important role in optimizing polycrystalline CdTe solar cells [7,194,214–219]. The $CdCl_2$ acts as a flux, lowering the temperature at which Cd–Te bonds can be broken and modifies the defect landscape within grains and grain boundaries; reports suggest the eutectic point is further lowered with the introduction of oxygen [17, 220]. As seen in Fig. 16, aggressive $CdCl_2$ treatments at temperatures approximately 450–500 °C, high overpressures of $CdCl_2$ and optimized times can completely transform the microstructure to eliminate horizontal grain boundaries and minimize the number of vertical ones [71–75]. For as-deposited microstructure consisting of narrow columnar grains and thus copious grain boundaries, dramatic recrystallization occurs with the degree of change increasing strongly with increasing temperature to near equiaxed grains with lateral and through-thickness dimensions nearly equal near 450 °C. At temperatures near 490 °C, recrystallization results in grains wider laterally than the film thickness.

It is noted that if the as-deposited microstructure has less grain boundary area per volume, the driving force for recrystallization is smaller so recrystallization may not be observed. In the 1990's, vapor phase $CdCl_2$ treatments were developed in order to decouple the $CdCl_2$ chemical activity from annealing temperature. The amount of the chlorine needed to passivate the grain boundaries was largely quantified by dynamic secondary ion mass spectrometry (D-SIMS). However, the reported values often varied in a large range [221,222]. More recently, the discovery of chlorine segregation at grain boundaries in polycrystalline CdTe filled the understanding gap of various reported chlorine values. When chlorine was largely segregated at grain boundaries, the varying densities of grain boundaries in different samples led to different levels of detected chlorine [200,201,223]. Chlorine was identified to replace roughly 25% of Te at grain boundaries by transmission electron microscopy (TEM) [223] and later confirmed by time-of-flight-SIMS (ToF-SIMS) results [199]. It was reported that devices with different chlorine levels due to different grain size actually had similar concentration of chlorine at grain boundaries, reaching saturation level, as demonstrated by the proportionality of Cl to grain boundary length as shown in Fig. 17. This provided convincing evidence that overall chlorine concentration is regulated by the grain boundary density and is stable across different devices. Keeping chlorine saturated at grain boundaries was critical to maintain device performance [199].

## 10. Cu doping in chlorinated absorbers

Historically, Cu has played an important role in the formation of the device back contact as well as in formation of p-doping in CdTe absorber. Formation of p-doping with Cu dopant generally consists of three steps [86,224,225]. The first step is the incorporation of Cu atoms in the form of Cui + interstitial defects from a Cu source deposited on the back side of the absorber (the Cui + diffusion barrier is close to 0.5 eV [46,225]). The second step is a knock-out reaction, i.e. exchange of $Cu_i$ with Cd lattice atom with formation of $Cu_{Cd}^{-}$ acceptor and $Cd_i^{+2}$ byproduct (reaction energy is 1.0 eV [176]). The third step is out-diffusion of the $Cd_i^{+2}$ byproduct to the back contact, GBs or extended defects ($Cd_i^{+2}$ diffusion barrier is 0.4 eV [225]). Since the incorporation of $Cu_i^{+}$ is slowed down by the forming built-in field and the knock-out reaction energy is 1 eV, annealing at T > 200 °C is required for efficient activation of Cu [86]. Importantly, simulations of Cu activation in a realistic TCO/CdSeTe stack predict a non-uniform doping profile with the accumulation of acceptor doping in the regions with high electrostatic potential, i.e. near the absorber front interface [86]. Such nonuniform doping may influence device operation and must be taken into account in device modeling of realistic solar cells.

The resulting doping level (hole density) depends on the efficiency of Cui + conversion into $Cu_{Cd}^{-}$ as well as on the density of compensating donors and defects in CdTe. The efficiency of $Cu_i^{+}$ conversion is defined primarily by the efficient outdiffusion of $Cd_i^{+2}$ byproduct outside CdTe grains after activation [86,226]. In thermodynamic grand canonical formalism, conditions of efficient Cd outdiffusion are defined by a low Cd chemical potential [46]. Theoretically, in an uncontaminated CdTe lattice under low Cd chemical potential, one may achieve fully activated Cu with hole density above $10^{16}$ $cm^{-3}$ for Cu density of $10^{17}$ $cm^{-3}$. However, in the actual devices, the density of free holes ($10^{14}$-$10^{15}$ $cm^{-3}$) is usually much lower than the density of incorporated Cu in CdTe absorber ($10^{17}$-$10^{18}$) [151], [227], [228]. The reason for such low hole density is a strong compensation of $Cu_{Cd}^{-}$ acceptors by donor-like defects and complexes. According to atomistic simulations, in CdTe with Cu and Cl, point defects and complexes mostly tend to behave as donors with just a few defects acting as acceptors [46,176]. Therefore, formation of $Cu_{Cd}^{-}$ acceptors is accompanied by formation of donor defects and complexes, which leads to partial compensation of Cu doping. Importantly, Cu doping anneals are always performed after the chlorination stage required to improve the minority carrier lifetime. The mechanisms behind lifetime improvement in CdTe deposited using vapor transport deposition method are recrystallization of the grains with increase of the average grain size, passivation of interfaces and grain boundaries, mitigation of extended defects, and passivation of $Te_{Cd}$ recombination centers inside the grains [201,229]. As discussed previously, during chlorination, Cl is introduced into the CdTe absorber in concentrations of at least $10^{18}$ $cm^{-3}$. As opposed to Cu that does not segregate at grain boundaries [198], chlorine primarily resides at grain boundaries [199, 200], with some residual amount remaining inside the grain interiors following the chloride treatment that promotes secondary recrystallization (grain regrowth). Inside the grains, Cl may interact with freshly formed $Cu_{Cd}$ acceptors. As a result, $(Cl_iCu_{Cd})^{+2}$ double donor complexes are formed [176], being one of the key reasons of highly compensated Cu doping and long-term degradation (Fig. 18).

An important limitation of Cu doping is a non-shallow ionization level of 0.15–0.20 eV of $Cu_{Cd}$ acceptor based on calculations [46,176]. Such a non-shallow acceptor generates less free holes than a shallow acceptor, especially at low temperatures, worsening separation of electrons and holes. Consequently, CdTe absorbers with typical (1–5)•$10^{14}$ $cm^{-3}$ hole density from Cu doping have lower performance than if the acceptors were shallow.

Another consequence of the non-shallow acceptor ionization level of $Cu_{Cd}$ is reduced carrier lifetime when Cu doping is high and

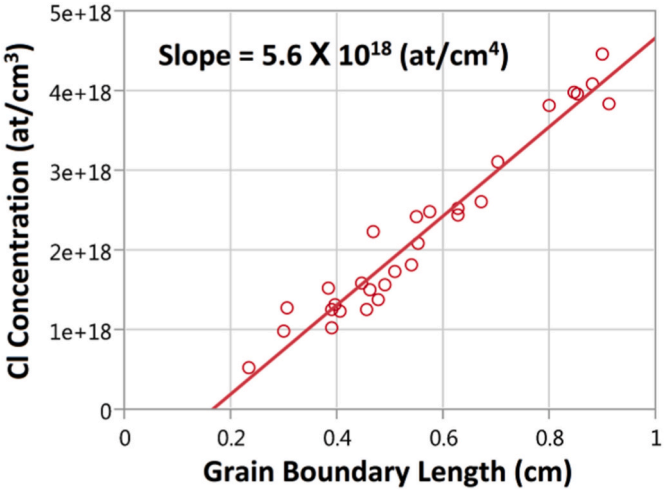


**Fig. 17.** Total chlorine concentration (atoms/$cm^3$) measured by ToF-SIMS shows a linear relationship with the grain boundary length (cm) measured by EBSD within a fixed 2D fixed field of view. Image from Ref. [199] copyright IEEE and reused by the original author with permission.

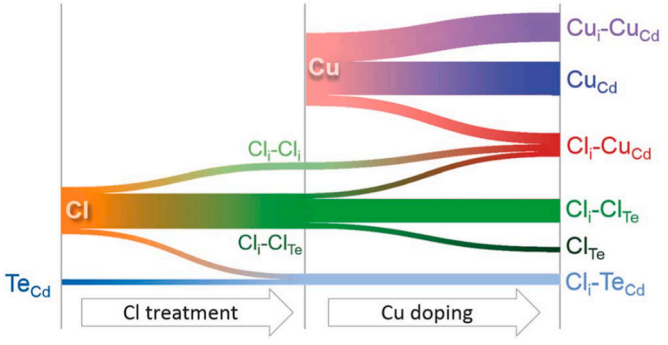


**Fig. 18.** Sankey diagram qualitatively showing the defect evolution during Cl treatment and Cu doping stages. Exact concentrations and flows of defects depend on experimental conditions. This particular diagram with arbitrary thicknesses of flows may or may not correspond to real conditions. Figure from Ref. [176] Copyright Royal Society of Chemistry and reused by the original authors with permission.

uncompensated. While the Cu level is not near mid gap, still the electron lifetime may become limited by recombination a $Cu_{Cd}$ acceptors [230]. When doping is high, $Cu_{Cd}$ acceptors are only partially ionized and neutral $Cu^0_{Cd}$ defects can capture free electrons fast, despite the relatively low calculated electron capture cross-section of $2.5 \times 10^{-17}$ $cm^2$ [230]. The subsequent capture of a hole finalizing the Schockley-Reed-Hall (SRH) recombination cycle is fast due to the abundance of holes in p-type material. If high, uncompensated Cu doping were to be achieved, such limitation of lifetime could become a bottleneck for efficiency improvement. This, however, is not the case in typical CdTe-based absorbers with highly-compensated Cu doping.

Alloying CdTe with Se reduces the band gap, thus increasing photogeneration and short-circuit current. Simultaneously, alloying introduces a number of additional negative and positive effects that influence cell performance. Among negative effects are the reduced energy gap for bulk recombination and the lower *p*-dopability of high-Se region of absorber. It was found based on first-principles calculations that acceptor defects have slightly higher formation energy and deeper levels in $CdSe_{0.25}Te_{0.75}$ than in binary CdTe, while donors have lower formation energies. Simulation of Cu doping in CdSeTe graded alloy predicts stronger compensation of Cu doping in high-Se region of graded absorber [86]. These results are in agreement with experimental observations of worse dopability of CdSeTe alloys [231] as well as with the principles of *p*-dopability established by Zunger [232]. At the same time, a reduction of $Cu_{Cd}$ formation energy in $CdSe_{0.25}Te_{0.75}$ alloy was predicted based on modeling in Ref. [233] which does not seem to be fully in line with other data.

Two positive effects of graded CdSeTe alloy films are the grading of electron affinity towards the main junction creating a pseudo-electric field as well as the change in band offset at the front interface [79,233]. These effects facilitate carrier separation in the bulk and reduce the recombination at the front interface. Another reported effect of Se alloying is an increased intensity of hyperspectral cathodoluminescence inside CdSeTe grains [78]. This result suggests that the activity of primary SRH recombination centers, such as $Te_{Cd}$, are suppressed in Se alloys by either lower densities of such centers or due to a reduced capture rate of free carriers [234].

Besides low doping values, another important limitation of Cu doping is its long-term stability. The gradients of electrochemical potential of free carrier depend on absorber doping [235], therefore degradation of doping with time worsens separation of photogenerated charge carriers, thus, reducing cell efficiency. . In chlorine-free Cu-doped single crystals, the literature has had mixed reports of doping stability, with some indicating stability at room temperature [236] and others indicating degradation over the course of 1–2 months or when annealed to 200–250 °C [47]. In chlorine-free polycrystalline films with supersaturated Cu ($\sim 10^{19}$ $cm^{-3}$) introduced at high temperature, doping degradation was explained by a dissolution of the Cu atoms from precipitates or extended defects at low temperature with formation of neutral $(Cu_iCu_{Cd})^0$ complexes [224].

In chlorinated CdTe absorber with an optimal amount of Cu ($\sim 10^{17}$ $cm^{-3}$), degradation of doping with time is always observed [237,238]. This doping degradation is not accompanied by long-range redistribution of Cu within the absorber. A correlation between the chlorination conditions and performance stability of Cu-doped devices has also been reported. While the precipitation and dissolution of $Cu_i$ may still contribute to doping instability in a chlorinated CdTe absorber with optimal Cu concentration, another plausible hypothesis of doping instability is the interaction of Cu acceptors with Cl atoms [90]. The process of slow doping compensation may happen after cells are cooled down after fabrication. After cool down, Cl is slowly released from a neutral $(Cl_i\text{-}Cl_{Te})$ complex in grain interiors and from grain boundaries and then binds with $Cu^-_{Cd}$ acceptor to form the compensating $(Cl_i\text{-}Cu_{Cd})^{+2}$ donor complex, which leads to slow doping reduction [90,176].

Both described mechanisms of doping instability are driven by temperature and rely on the injection of interstitial donor species ($Cl_i$ or $Cu_i$) from a source to CdTe grain bulk. However, only the Cl-related mechanism allows to explain the absence of doping degradation in Cl-free devices and doping degradation in chlorinated devices observed in work [90]. The atomistic mechanism of Cl-related doping degradation together with the experimental and theoretical impact of doping degradation on device performance as well as the reversibility of doping degradation were studied in Ref. [90]. The temperature-driven doping compensation of Cu doping agrees qualitatively with the slow performance decay as well as with downwards/upwards efficiency stabilization of Cu-doped modules during winter/summer in the field [239] and at colder/higher stress temperature in laboratory tests [240]. The described mechanisms of doping compensation are inherent to Cu dopant and should be absent in Group-V-doped acceptor. This might explain excellent doping stability in accelerated life tests of As-doped CdTe cells observed in Refs. [27,90].

## 11. Degradation and ageing of devices with Cu and Cl

The majority of fielded power-production CdTe modules at this time are glass-glass construction with desiccated polyisobutylene edge seals. On the other hand, most laboratory cells are not encapsulated. In some cases, e.g. cells with MZO buffer layers, lab-scale cells are known to change over time and exhibit instabilities possibly as a result of uptake of water vapor from air. Thus we first remark that some effects found in stress or degradation studies on lab cells are not always relevant to actual module behaviors. Others such as the migration of Cu do translate to modules.

The degradation mechanisms have been only strongly connected with the possible diffusion of impurities in the bulk, discussed somewhat in the previous section, and in the junction. In a CdTe solar cell, impurities might come typically from the following cases (i) impurity elements from raw material, (ii) impurities including chlorine from $CdCl_2$ and similar activation treatments, and (iii) elements released from substrate and from front and back contacts. The main driving forces for migration of impurities in the device are temperature and bias, both generated by the irradiation of light. Migration strongly depends on the type of impurity; particular impurities of note include Na, Cl, and Cu. If the CdTe is doped with other dopants, these might also contribute to the degradation of the device.

The effects of chlorine have been extensively studied. Chlorine does not contribute to the metastability of the device although it can have an important role in doping the bulk [241] and in passivating the grain boundaries [214]. However, only high temperature can lead to movement of chlorine atoms [202]. Sodium can diffuse from the glass into the device structure [242]. Also, some diffusion of species from the front contact might occur [243] such as indium diffusion from ITO when CdTe is deposited at high temperature. However the introduction of high stability TCOs, such as (but not only) $SnO_2$:F [244] together with a barrier layer for Na, typically $SiO_2$ [245], has scaled back the problem. For these reasons, Cu happens to be the main impurity responsible for degradation effects. As already mentioned, Cu has been used for improving the back contact of the devices by delivering a higher work function, and, at the same time, its diffusion enhances CdTe doping.

So, Cu can be crucial for high efficiency devices but, at the same time, can represent the main reason of CdTe solar cell degradation. To manage the Cu insertion, we have to separate the two effects and control them in a different manner. In particular we have to analyze separately the effects of Cu in the two following areas (i) Cu at the back contact and (ii) Cu in the CdTe bulk. Elemental Cu at the back contact is known to be strongly detrimental for the stability of the device, in particular Cu ions tend to diffuse into the CdTe bulk and, even if they can fill cadmium vacancies, they are not stable in their positions and may diffuse towards the junction slowly shunting the device. The depth of understanding relating to the role of Cu has come from CdS/CdTe device structures, though findings similar to those discussed below have recently been

reported for CdSe/CdTe devices, with a noted dependence on the initial CdSe thickness [246].

Typical accelerated stability tests are done under light at a temperature of 80 °C in two different conditions: at open circuit (OC) or at short circuit (SC). Limited degradation in SC conditions has been observed [247] and is explained by the fact that Cu diffuses as a positive ion inside the CdTe/CdS structure. In the absence of external bias, as in open circuit condition, $Cu^+$ ions migrate toward the CdS. This is particularly evident when no treatment on the surface is provided [228]. In this case $Cu^+$ diffuses into the bulk with reduction of shallow defects and consequentially of carrier concentration.

Instead, if a compound is generated at the surface, Cu is not in its elemental form and shows a different behavior. Forming a compound that incorporates Cu is the strategy to reduce or eliminate Cu diffusion and consequentially deliver high stability solar cells. One of the first and very important work that has revealed the effect of Cu based compounds is the work from Wu et al. which demonstrated that $Cu_xTe_{1-x}$ with x£1.4 forms as a very stable compound [248]. $Cu_xTe_{1-x}$ compounds have been prepared by deposition and growth on the CdTe surface by etching of CdTe and consequential formation of Te-rich surface and reaction with Cu at high temperature [228]. Cu can also be sequestered in stable compounds such as ZnTe [149], $As_2Te_3$ or $Bi_2Te_3$ [249].

On the other hand, once Cu is stabilized at the back contact the need for Cu inclusion into CdTe for doping has to be engineered, otherwise CdTe would require an alternative doping. Regarding this, it has to be considered that Cu has a very low solubility in CdTe. Once the amount of Cu exceeds the solubility limit it segregates, possibly especially at the grain boundaries, giving a place for degradation [164,250]. According to first principle calculations, it can be expected that Cu atoms at CdTe grain boundaries are energetically favored compared to CdTe bulk [251]. The solubility of Cu in CdTe single crystals has been measured at higher temperatures. From this an extrapolation presented by Perrenoud et al. [164], suggests a Cu solubility between $3 \times 10^{13}$ and $3 \times 10^{14}$ $Cu/cm^3$ at room temperature. Driving in a 0.1 nm thick Cu layer on a 5 μm thick CdTe layer results in a Cu concentration of $8 \times 10^{13}$ $Cu/cm^3$ [250]. This would exceed the solubility limit but in this case a quenching of the stack by fast cooling would improve stability.

Another successful process for including Cu, by controlling accurately its quantity in order not to exceed the solubility of the element in CdTe, is to convey Cu by chlorine and more specifically by $CuCl_2$ deposition and subsequent annealing. Beach et al. suggest that the defects induced by $CdCl_2$, probably Cl-induced donors, increase the solubility of $Cu_{Cd}$ acceptors [252]. The $CuCl_2$ is applied after the standard $CdCl_2$ activation treatment since combining activation treatment and Cu doping in a single step is not possible: $CdCl_2$ activation treatment is applied at a temperature which would cause significant Cu diffusion if inserted in its elemental form. On the other hand via chlorine it is able to solute into the CdTe limiting segregation [133,253].

The benefits and drawbacks of Cu in CdTe devices are evident in Fig. 19 [254]. Cells with Cu in the back contact and in the bulk CdTe exhibit a higher initial efficiency but degrade rapidly to a level at or below devices without Cu. This was the commonly observed trend for devices prior to 2016. Fabrication of the cells used for Fig. 19 was typical at NREL [255] with CdS grown by chemical bath deposition, CdTe deposited by close space sublimation, $CdCl_2$ anneal, and nitric-phosphoric acid back contact etch followed by graphite paste (with or without $Cu_{1.4}Te$) then Ag-paste. Cells were stressed under AM1.5G, 1-sun light intensity, and open-circuit conditions at 65 °C. Performance changes were determined by periodically removing the cells to measure JV and CV [256]. The rate at which CdTe devices containing Cu degrade is a function of the amount of Cu present [246,254]. Fig. 19 (b) shows the comparison of the degradation rates of two sets of devices made with the deposition of 2 nm and 0.1 nm Cu thick layer at the back contact, after bromine-methanol etching. In this case solar cells have been made by vacuum evaporation at the University of Verona. The devices were put in a special metal box, kept at 80 °C and, by a dedicated rack of lamps, under an irradiation of one sun. Looking at Fig. 19 (b) it can be clearly observed that, for the 2 nm Cu case, the degradation is prominent in the first 200 h when Cu has the strongest diffusion. Instead, for the 0.1 nm case, the degradation is milder and much slower (in Ref. [151] a different degradation mechanism has been identified), also the stabilized efficiencies are higher).

Although there was a clear correlation between Cu content and degradation, kinetic models were developed to better understand the mechanisms. Viable models should account for common observations, such as (i) degradation modes with strong FF loss, followed by $V_{oc}$, and insignificant $J_{sc}$ loss (sometimes increasing), (ii) increasing rollover of the JV-curve in forward bias [254,256–258], (iii) replacing the back contact after stress tests can partially eliminate FF loss and rollover without $V_{oc}$ improvement [258], (iv) thermally activated degradation rate with activation energy of approximately 1 eV [259], (v) similar degradation modes observed by exposure to light, electron beam [260], and dark forward bias, (vi) increasing apparent doping and decreasing depletion width with stress [254,261], and (vii) stress at $V_{oc}$ bias is more detrimental than stress at $J_{sc}$ (V = 0) bias [257,259,262,263].

While diffusion of Cu is certainly a factor during degradation, ion

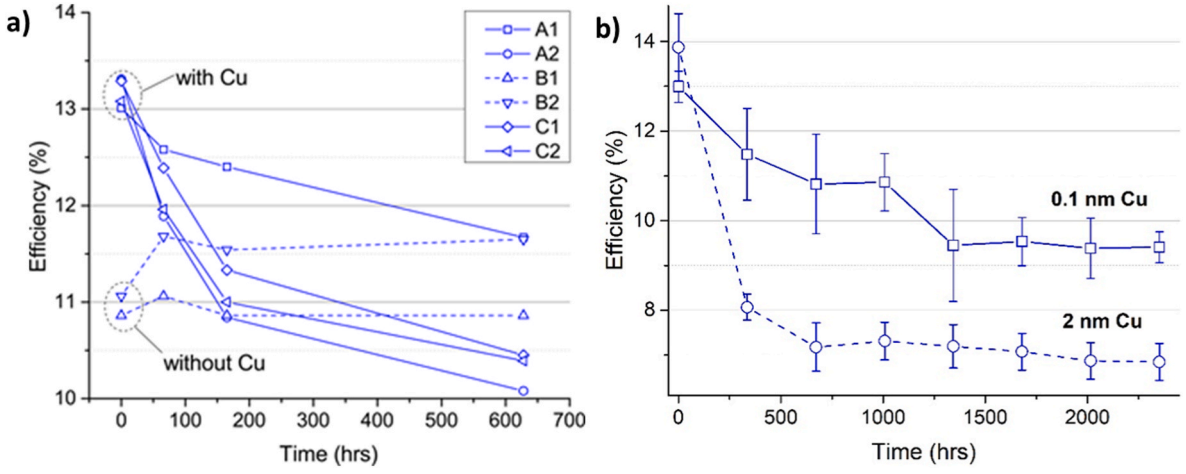


**Fig. 19.** a) Efficiency versus stress time for four CdTe cells with Cu in the back contact (solid lines) and two without Cu (dashed lines). Stress conditions were AM1.5G, 1-sun light intensity, open-circuit, and T = 65 °C. Image from Ref. [254] copyright IEEE and reused by the original authors with permission. b) Efficiency versus stress time for two sets of differently contacted all-evaporated CdTe cells: the 2 nm Cu contacted devices strongly degrade in the first 200 h reaching a lower stabilized efficiency compared to the 0.1 nm Cu contacted cells. Image from Ref. [151] copyright Elsevier and reused with permission by the original authors.

transport alone cannot account for the range of observations described above [261,263,264]. The following two mechanisms were tested by comparing numerical simulations to stress data: (1) large lattice relaxation (defect transformations) driven by charge injection in the absorber, and (2) back contact deterioration (possibly due to Cu out-diffusion) resulting in an increasing Schottky barrier with stress [254,265]. In the lattice relaxation mechanism [266], charge injected by light, e-beam, or voltage bias drives a defect transformation reaction. The numerical device models showed reasonable correspondence with the stress data under various conditions if the reaction was assumed to generate deep recombination defects and shallow acceptor donors concurrently, as may occur from the dissociation of a defect complex. This type of model does not specify the defect species involved, but it does allow for simulation of stress over a wide range of conditions and the extraction of an activation energy from temperature dependent data [267]. An activation energy close to 1 eV was determined to be appropriate for CdTe cells. The back-contact deterioration mechanism was found to affect FF and JV curve rollover without modification of other metrics. Simultaneously applying back contact deterioration and lattice relaxation mechanisms accounted for the observed changes in performance metrics, JV roll-over, and CV data [254]. It is worth noting that when First Solar first introduced ZnTe as part of the back contact stack, which should serve to bind Cu tightly, they observed a reduction in degradation during 300 day accelerated light soak tests from 17% using their previous metal contact to <10% with ZnTe [55].

Recently, devices with MZO buffer exhibited significant loss of FF under light/heat stress, without the marked $V_{OC}$ loss observed in CdS-buffer devices [268]. An increase in the electric field near the Cd(Se,Te)/MZO interface identified by KPFM electric potential profiling along with device simulations determined that the degradation was associated with the presence of charged defects at the interface along with a decrease in MZO doping during stress. An increase in the conduction band spike at the Cd(Se,Te)/MZO interface likely also played a role. A slight increase in the back contact barrier was also detected by KPFM. Cell stability improved by using a back contact that was less permeable to moisture [269]. Doping the MZO layer with Ga is another proposed approach for stabilizing these devices. The degradation mode described above was *irreversible*, but it is important to note that *reversible* performance variations were also observed. In the latter case, Cd(Se,Te)/MZO devices that were in the dark for an extended period of time had an average efficiency of 12%, which increased to 16.7% after 1–2 h of light soaking at room temperature. The underlying defect kinetics is an open question.

This section has described laterally *uniform* degradation mechanisms that cause temporal variations of device parameters due to dopant/defect concentrations and contact barriers. These are simplified 1D models for processes that may be occurring preferentially at grain boundaries, extended defects, and interfaces. Such *nonuniform* mechanisms are prevalent in any polycrystalline material. They are 3D by nature and give rise to shunting and weak micro-diodes (regions of low $V_{oc}$, but not shunted) [270–272]. Such nonuniformities are unavoidable in high-throughput, large-area, thin-film technology and can have dominant impacts on device degradation by robbing current from a large area of the cell or creating hot spot (runaway) instabilities [273].

Lastly, one of the main drivers for adoption of As doping in production modules by First Solar in the past few years is the greater stability and slower degradation in cells using this new doping scheme. In a recent work, Krasikov et al. [90] lay out arguments that the long-term degradation of Cu-doped CdSeTe solar cells is driven by the formation of compensating $(Cl_i\text{-}Cu_{Cd})^{+2}$ compensating donor complexes under the bias conditions of operating cells and modules. This mechanism is not present in As-doped cells because of the inefficiency of the Cl-acceptor complex with As acceptors. The absence of such a long-term degradation mechanism coupled with the ability (under the right processing conditions) to achieve doping concentrations in the $10^{16}$-$10^{17}/cm^3$ range, which will help with cell performance including $V_{OC}$ as long as lifetime is below the radiative limit, make arsenic the current best dopant for high-efficiency and reliable modules.

## 12. Environmental and health

Concerns regarding the environmental impact of large-scale deployment of CdTe-based photovoltaics have been raised since Cd is listed among the 126 priority pollutants [274] and Te can also be toxic [275]. However, a recent review indicated that several lifecycle analyses have suggested CdTe has advantages across all environmental impact categories (e.g. energy required to produce a module, global warming potential, and others) relative to other PV technologies ([5,276] and references therein). Several works have argued that CdTe-based solar panels effectively encapsulate Cd and Te, which are produced as byproducts of Cu and Zn mining and refining, between two hermetically-sealed glass sheets, thereby reducing the overall environmental impacts and exposure hazards [276–278]. This is especially true since any Cd or Te not recovered during mining, smelting, and refining would be released to the environment.

The Cd release to the surficial environment and worker exposure have also been evaluated during the manufacture of CdTe-based modules, as well as risks associated with total module lifecycle [276,279,280]. An evaluation of the manufacturing process at First Solar reveals low environmental releases of Cd and low worker exposures during routine manufacturing process, both far below regulatory limits [276,277,281,282]. Results from experiments attempting to mimic panel field breakage are mixed, due to variable experimental design, but typical results do not exceed screening values [282]. Further evaluation of unusual events, such as fire and severe weather suggested that these events would likely not be significant routes of Cd to the surficial environment. In contrast, disposal in landfills or incineration could result in environmental releases, necessitating careful PV end-of-life management [276–278,283,284]. In terms of carcinogenic risks, Cd is most bioavailable in the form of highly-water-soluble salts such as $CdCl_2$ which allow easy uptake into organisms. The bioavailability of Cd from CdTe has been quantified to be approximately 100 times lower than from $CdCl_2$ in acidic gastric fluids mimicking an ingestion route of exposure [285].

It is important to note that the total amount of CdTe used in a PV module is very small compared to the total mass of the module and balance of systems components like racking. The volume of active semiconductor in $cm^3$ per module area in $m^2$ is numerically the same as its thickness in μm (so a module with 3 μm-thick CdTe absorber uses 3 $cm^3/m^2$ while Si-based modules with 300 μm-thick cells use 300 $cm^3/m^2$ of Si). In glass-glass CdTe modules the volume of glass is 4000 $cm^3/m^2$ for 2 mm-thick and 6000 $cm^3/m^2$ for 3-mm-thick glass. For reference, the rated PV generating capacity for per $m^2$ is the AM1.5 spectral power of 1 $kW_p/m^2$ times the module efficiency which can be roughly estimated as 18–20% (so 180–200 $W_p/m^2$). The mass of other components like cabling, plastic junction box, elastomeric sealant, metal racking, and other installation components are likewise very large. Thus, even if the production of these components on a per mass or per volume basis uses or emits smaller amounts of harmful substances as byproducts or has lower embodied energy or $CO_2$ emissions compared to the CdTe, the large utilization ratio in the overall system argues that the material used as the active semiconductor plays a minimal overall role in determining the environmental or health impacts.

Concerns over the potential toxicity of PV modules should be put into context by comparing to other commonly-used materials and scenarios with *de-facto* societally-accepted risks to environment and health. A widely-accepted product with parallels in terms of using a harmful heavy-metal element in a well-encapsulated manner with near-ideal end-of-useful-life reclamation procedures is the use of lead-acid starter batteries in the estimated~1.5 billion motor vehicles worldwide. Each such battery currently in use contains on the order of 10 kg lead (~50 mol Pb atoms) and on the order of 1 L of a Pb-saturated sulfuric acid

electrolyte. For comparison, the mass of Cd in a modern CdTe solar module of 2.5–3 $m^2$ area is approximately 20 g which is 0.2 mol of Cd atoms or about 250 times fewer heavy metal atoms than a car battery. The lifecycle risk of Pb emissions from battery use, which accounts for 88% of global Pb use [286], exists from mining and manufacturing to accidents or fires during use. However, the main route of Pb emission from such batteries comes from improper or inadequately-controlled recycling [287]. Lead-acid batteries have been recycled for nearly 100 years and in the US, the rate of lead-acid battery recycling is higher than for any other single product at 97–99%, which sets an incredibly successful template for closed-loop use of very useful but toxic elements [288]. The CdTe PV industry, chiefly First Solar as the largest-scale manufacturer worldwide to date, has set an example of guaranteed recycling. In the context of utility-scale installations, proper reclamation and recycling of CdTe from end-of-life modules is the norm. If CdTe modules begin to be sold into other, less-centrally-controlled markets like building-integrated, residential or commercial rooftops, care will be needed to ensure proper recovery and recycling of those modules. Fig. 20 shows a recycling plant run by First Solar to recover and recycle its own Cd, Te, glass, and other materials from rejected parts from manufacturing as well as decommissioned modules. As it moved to large-scale manufacturing in the past decade, First Solar established a novel independently-held fund to guarantee recycling of its modules to ensure recovery especially of the CdTe but also the other useful materials.

Another strand of concern regarding CdTe solar modules are the chance of carcinogenic emissions if modules are involved in fires [289]. It is worth remembering that, in the event of a structure fire, common materials such as wood, paint, furniture, synthetic fiber rugs, electronics, adhesives, flooring, vinyl siding, insulation, and even galvanized steel also release carcinogenic, toxic, or otherwise harmful substances as vapors and smoke. Many organic molecules emitted from incomplete combustion of even the most sustainable plant-derived materials like wood are also known carcinogens [290]. The enormous volumes of these materials used in the built environment are similarly subject to fire risks overall are *de-facto* judged as societally-acceptable. The majority of contemporary Si modules utilize polymer/plastic backsheets which can also release toxic and carcinogenic substances under conditions of incomplete combustion. It is important to consider such secondary risks of CdTe photovoltaics not in isolation but in the context of other points of comparison.

**Fig. 20.** View of a First Solar module recycling facility. First Solar has over 10 years of experience in large-scale recovery and recycling its manufacturing rejects and end-of-life fielded modules, with capacity in Malaysia, Germany, Vietnam, and the US for processing >2 million modules per year. To date, more than 230,000 metric tons of modules have been recycled. Image courtesy of First Solar.

Summing up, CdTe photovoltaics relies on potentially toxic elements, Cd and Te. However, Cd and Te are recovered as byproducts of base metal extraction and CdTe PV modules sequester these elements, which would otherwise not be recovered and released to the surficial environment in mine wastes, in a low-bioavailability compound encapsulated inside long-lifetime products. While utilizing these elements in PV has some inherent risk associated with it to human and environmental health, the exposures have proven to be low during device manufacture, during both routine use and under lower probability events (e.g., fire), and recycling. The largest concern is associated with end-of-life recapture and recycling, since this will occur at a larger and larger scales into the future. Further, the risks from using CdTe as the active semiconductor in PV modules should not be judged in isolation, but rather within the context and compared to other alternatives. This suggests an interesting area of study in risk and impact quantification for various PV technologies, as well as comparisons to other technologies in the built environment for context. Comparisons in terms of cradle-to-grave carbon emission is one example in this direction [5].

## 13. Cd and Te mining and refining

Supplies and utilization of the elements Cd and Te have been discussed in depth in Refs. [291–310]. Cadmium and tellurium are both obtained primarily as byproducts of Cu, lead (Pb), bismuth (Bi) and zinc (Zn) mining and refining [291–294], which effectively decouples supply and demand for Cd and Te because of the much larger scales of the production of the primary base metal targets. For example, Cu is produced worldwide on the 10 million tons/yr scale while Te production is measured in hundreds of tons per year (Cd is produced on the order of 10's of thousands of tons/yr). In simple terms, Cd and Te are byproducts of the production of other metals and concentrate in and are recovered from waste products [291,292]. Currently, only small fractions of the Te and Cd contained in ores are recovered [297–301,304–308]. In this sense, the use of Cd and Te as CdTe photovoltaics represents a very good use for these derivatives of primary metal production that would otherwise be released to the environment or require managed sequestration. CdTe photovoltaics currently consumes a significant fraction of global Te production, but Te is also used in thermoelectric devices (e.g. PbTe), metallurgy, vulcanizing rubber, and other uses [292].

Most Cu is currently recovered from sulfide ores using a pyrometallurgical process, although oxidized ores are becoming an important source and are typically recovered using hydrometallurgical leaching techniques [311]. In addition to Cu, these ores contain low concentrations of gold (Au), silver (Ag), platinum (Pt) and other precious metals, as well as Se and Te. In the pyrometallurgical process, Cu minerals in ore are concentrated by flotation and refined to industrial purity by smelting followed by electrolytic refining. In the final electrolytic refining step, less pure copper anodes are dissolved and plated onto cathodes to produce Cu with >99.99% [311]. Elements, including Te, Se, and precious metals are concentrated in the left-behind anode slimes or precipitate out of the bath as tank slimes. In many operations, these slimes are next processed to recover additional Cu and Te, Se, and precious metals [311]. However, it is estimated that less than 5% of Te present in ores is concentrated into the anode slimes from which Te is currently recovered [302–304]. Assessment of the fate of the estimated 95% Te recovered from anode slimes and evaluation of opportunities for its recovery could be a valuable contribution.

Recent studies [298,299] have estimated that globally only about 26% of the Te present in anode slimes (1.3% of that in ores) is currently

recovered. The low overall Te recovery rate is due to two factors. First not all anode slimes are processed in a way that recovers Te. Indeed, recovery processes optimized for precious metals require different chemical conditions than those optimized for Se and Te recovery [312]. Second, although benchtop rates of Te recovery from anode slimes are quite high (greater than 90%, in some cases), industrial-scale processes report recoveries approximately 30–60% [313]. Thus, more widespread recovery of Te from Cu refining operations and increasing recovery rates present opportunities.

Increasing the Te recovery rate from copper refineries could be of great interest to the industry, although different or additional processes may be required. For example, in 2022 Rio Tinto initiated enhanced Te recovery at the Bingham Canyon mine in Utah [296], highlighting that Te can be recovered within the U.S. Anode slimes are a very attractive target since they are often significantly enriched relative to geological sources; approximately a few wt% compared to mg/kg of ore [306]. Additionally, other sources of Te are currently being investigated, such as byproduct Te recovery from operating gold mines [295,301] and historical mine wastes [308]. While indeed representing potential sources enriched in Te, these are on smaller scales than that represented by Cu refining.

After recovery, the Cd, Se, Te, and any dopant elements to be used in high-performance CdTe-based photovoltaics undergo further refining and purification steps by specialty material suppliers. This stems from the fundamental fact that solar cells are minority carrier devices (thermoelectrics, for example, are majority carrier devices and thus can have more impurity tolerance). Although direct-gap semiconductors can in general tolerate higher concentrations of impurities causing non-radiative recombination than indirect materials like Si, it is still it is critical to reduce lifetime-killing impurities to levels where they do not impact the minority carrier lifetime. For example, in CdTe (which has $\sim 2.8 \times 10^{22}$ atoms/cm$^3$) doped p-type to $10^{16}$/cm$^3$ with radiative lifetime ~500 ns, hypothetical mid-gap impurities with electron capture cross sections $10^{-18}$ to $10^{-13}$ cm$^2$ would be expected to begin to affect the intragrain lifetime at concentrations near (respectively) $10^{18}$ to $10^{13}$/cm$^3$. The formation of CdTe occurs by direct reaction at elevated temperatures and for long times in high-purity inert containers, perhaps involving multiple reaction and mixing steps. Typically, a granulated or powder product is used as the source for VTD deposition.

## 14. Conclusions and outlook

Herein we have reviewed the developments in the cell technology that has enabled CdTe solar modules to emerge as the highest-production thin film photovoltaic technology. The primary innovations were scaling manufacturing which is enabled by the intrinsic benefits of thin film technology, coupled with the ability to deposit CdTe with vapor transport deposition. Rapid improvements in short circuit current $J_{SC}$ were achieved through optimization of the buffer and window layers and alloying with Se to reduce the absorber bandgap. Optimization of $CdCl_2$ treatments and the addition of Se have resulted in large increases in minority carrier lifetimes, leading to higher voltages. The path to further increases in efficiency hinges primarily on increasing the $V_{oc}$ and FF through innovations in materials, fabrication methods, and device stacks followed by translation into modules. To reach >25% efficiency, combining $V_{oc}$ above 1 V is the primary goal. The path to these metrics is believed to require further reducing grain boundary and interface recombination, band tailing, and achieving low-resistance, passivated, Ohmic, carrier selective contacts at the front and back interfaces. Many of these goals have been realized separately, and the research and development community is working hard to integrate these innovations together to keep the rapid growth trajectory of CdTe technology moving in order to supply renewable electricity worldwide at the terawatt scale.

## CRediT authorship contribution statement

**Michael A. Scarpulla:** Writing – review & editing, Writing – original draft. **Brian McCandless:** Writing – review & editing, Writing – original draft. **Adam B. Phillips:** Writing – review & editing, Writing – original draft. **Yanfa Yan:** Writing – review & editing, Writing – original draft. **Michael J. Heben:** Writing – review & editing, Writing – original draft. **Colin Wolden:** Writing – review & editing, Writing – original draft. **Gang Xiong:** Writing – review & editing, Writing – original draft. **Wyatt K. Metzger:** Writing – review & editing, Writing – original draft. **Dan Mao:** Writing – review & editing, Writing – original draft. **Dmitry Krasikov:** Writing – review & editing, Writing – original draft. **Igor Sankin:** Writing – review & editing, Writing – original draft. **Sachit Grover:** Writing – review & editing, Writing – original draft. **Amit Munshi:** Writing – review & editing, Writing – original draft. **Walajabad Sampath:** Writing – review & editing, Writing – original draft. **James R. Sites:** Writing – review & editing, Writing – original draft. **Alexandra Bothwell:** Writing – review & editing, Writing – original draft. **David Albin:** Writing – review & editing, Writing – original draft. **Matthew O. Reese:** Writing – review & editing, Writing – original draft, Conceptualization. **Alessandro Romeo:** Writing – review & editing, Writing – original draft. **Marco Nardone:** Writing – review & editing, Writing – original draft. **Robert Klie:** Writing – review & editing, Writing – original draft. **J. Michael Walls:** Writing – review & editing, Writing – original draft. **Thomas Fiducia:** Writing – review & editing, Writing – original draft. **Ali Abbas:** Writing – review & editing, Writing – original draft. **Sarah M. Hayes:** Writing – review & editing, Writing – original draft.

## Declaration of competing interest

The authors declare the following financial interests/personal relationships which may be considered as potential competing interests: This review paper includes authors working in CdTe from academia, national laboratories, and a major manufacturer of CdTe modules (First Solar Inc = FSLR). Most or all of the authors do have patents or patent disclosures related to CdTe PV technology, and obviously some of the authors work for a for-profit. HOWEVER, there are no new findings in this paper since it is a review paper. Therefore we see no conflicts of interest by the authors. The self-interest of the FSLR authors is self-evident from their affiliation.

## Data availability

Data will be made available on request.

## Acknowledgements & Disclaimers

The authors acknowledge and thank the CdTe R&D community past and present without whose work none of the current accomplishments could be possible. Some of the authors thank 5 N Plus for supplying various high-purity materials. Some of the authors acknowledge DOE EERE Solar Energy Technologies Office (SETO) Agreement Number DE-EE0007543. M.A.S. acknowledges support from the NSF EPM under award 1711885 and thanks N.D. Rock for assistance with citations and the manuscript. Special thanks from MAS to Tim Gessert, Jenny Chase & Paul Maycock for sharing PV learning curve data in 2014. A.M. and W.S. acknowledge the US National Science Foundation under the IUCRC for Solar Powered Future (award number 2052735). Some of this material is based upon work supported by the U.S. Department of Energy's Office of Energy Efficiency and Renewable Energy (EERE) under the Solar Energy Technologies Office Award Numbers DE-EE0008557, DE-EE0008552, and DE-EE0008974. Some of this work was authored in part by the National Renewable Energy Laboratory, operated by Alliance for Sustainable Energy, LLC, for the U.S. Department of Energy (DOE) under Contract No. DE-AC36-08GO28308 and Award Number 37989. Funding

provided by the U.S. Department of Energy Office of Energy Efficiency and Renewable Energy Solar Energy Technologies Office. The views expressed in the article do not necessarily represent the views of the DOE or the U.S. Government. The U.S. Government retains and the publisher, by accepting the article for publication, acknowledges that the U.S. Government retains a nonexclusive, paid-up, irrevocable, worldwide license to publish or reproduce the published form of this work, or allow others to do so, for U.S. Government purposes. The views expressed in this article do not necessarily represent the views of any companies mentioned or noted in the affiliations of the authors.

## References

[1] M. Green, E. Dunlop, J. Hohl Ebinger, M. Yoshita, N. Kopidakis, X. Hao, Solar cell efficiency tables (version 57), Prog. Photovoltaics Res. Appl. 29 (1) (2021) 3–15, https://doi.org/10.1002/pip.3371.

[2] First Solar Press Release, "First Solar Passes $1 Per Watt Industry Milestone, Feb. 2009. Accessed: Jan. 03, 2021. [Online]. Available: https://investor.firstsolar.com/news/press-release-details/2009/First-Solar-Passes-1-Per-Watt-Industry-Milestone/default.aspx.

[3] M.A. Green, K. Emery, D.L. King, S. Igari, W. Warta, Solar cell efficiency tables (version 19), Prog. Photovoltaics Res. Appl. 10 (1) (2002) 55–61, https://doi.org/10.1002/pip.428.

[4] M.A. Green, K. Emery, Y. Hishikawa, W. Warta, E.D. Dunlop, Solar cell efficiency tables (version 46), Prog. Photovoltaics Res. Appl. 23 (7) (2015) 805–812, https://doi.org/10.1002/pip.2637.

[5] H.M. Wikoff, S.B. Reese, M.O. Reese, Embodied energy and carbon from the manufacture of cadmium telluride and silicon photovoltaics, Joule 6 (7) (Jul. 2022) 1710–1725, https://doi.org/10.1016/j.joule.2022.06.006.

[6] N.R. Paudel, Y. Yan, Enhancing the photo-currents of CdTe thin-film solar cells in both short and long wavelength regions, Appl. Phys. Lett. 105 (18) (Nov. 2014), https://doi.org/10.1063/1.4901532. Art. no. 18.

[7] B.E. McCandless, J.R. Sites, Cadmium telluride solar cells, in: Handbook of Photovoltaic Science and Engineering, John Wiley & Sons, Ltd, 2003, pp. 617–662, https://doi.org/10.1002/0470014008.ch14.

[8] P.J. Sebastian, The transport and optical properties of CdSe-CdTe pseudobinary thin films, Thin Solid Films 245 (1–2) (1994) 132–140, https://doi.org/10.1016/0040-6090(94)90888-5.

[9] D. Pokhrel, et al., Copper iodide nanoparticles as a hole transport layer to CdTe photovoltaics: 5.5 % efficient back-illuminated bifacial CdTe solar cells, Sol. Energy Mater. Sol. Cells 235 (Jan. 2022) 111451, https://doi.org/10.1016/j.solmat.2021.111451.

[10] S. Marsillac, V.Y. Parikh, A.D. Compaan, Ultra-thin bifacial CdTe solar cell, Sol. Energy Mater. Sol. Cells 91 (15) (2007) 1398–1402, Sep, https://doi.org/10.1016/j.solmat.2007.04.025.

[11] A.B. Phillips, K.K. Subedi, G.K. Liyanage, F.K. Alfadhili, R.J. Ellingson, M. J. Heben, Understanding and advancing bifacial thin film solar cells, ACS Appl. Energy Mater. 3 (7) (2020) 6072–6078, Jul, https://doi.org/10.1021/acsaem.0c00851.

[12] Y. Kwon, J. Seo, Y. Kang, D. Kim, J. Kim, Bifacial CdS/CdTe thin-film solar cells using a transparent silver nanowire/indium tin oxide back contact, Opt Express 26 (2) (Jan. 2018) A30–A38, https://doi.org/10.1364/OE.26.000A30.

[13] R.C. Powell, Research Leading to High-Throughput Manufacturing of Thin-Film CdTe PV Modules, NREL Subcontract Report NREL/SR-520-39669, Apr. 2006. Accessed: Jan. 10, 2023. [Online]. Available: https://www.nrel.gov/docs/fy06osti/39669.pdf.

[14] D. Cunningham, M. Rubcich, D. Skinner, Cadmium telluride PV module manufacturing at BP Solar, Prog. Photovoltaics Res. Appl. 10 (2) (2002) 159–168, https://doi.org/10.1002/pip.417.

[15] J.D. Major, R.E. Treharne, L.J. Phillips, K. Durose, A low-cost non-toxic post-growth activation step for CdTe solar cells, Nature 511 (7509) (Jul. 2014) 7509, https://doi.org/10.1038/nature13435. Art. no.

[16] J. Trevithick, J. Li, T.R. Ohno, C.A. Wolden, Activation of CdTe solar cells using molecular chlorine, IEEE 43rd Photovoltaic Specialists Conference (PVSC) (2016), https://doi.org/10.1109/PVSC.2016.7749648. Jun. 2016, pp. 0518–0523.

[17] Scheer Roland, Hans-Werner Schock, Chalcogenide Photovoltaics: Physics, Technologies, and Thin Film Devices, Wiley-VCH, 2011.

[18] P. Ščajev, et al., Impact of dopant-induced band tails on optical spectra, charge carrier transport, and dynamics in single-crystal CdTe, Sci. Rep. 12 (1) (Jul. 2022) 1, https://doi.org/10.1038/s41598-022-16994-7. Art. no.

[19] M. Gloeckler, I. Sankin, Z. Zhao, CdTe solar cells at the threshold to 20% efficiency, IEEE J. Photovoltaics 3 (4) (2013) 1389–1393, Oct, https://doi.org/10.1109/JPHOTOV.2013.2278661.

[20] X. Wu, High-efficiency polycrystalline CdTe thin-film solar cells, Sol. Energy 77 (6) (Dec. 2004) 803–814, https://doi.org/10.1016/j.solener.2004.06.006.

[21] X. Wu, et al., 16.5%-efficient CdS/CdTe polycrystalline thin-film solar cell, Proc. 17th Eur. Photovoltaic Sol. Energy Conf. (2001) 995–1000.

[22] M. Burgelman, P. Nollet, S. Degrave, Modelling polycrystalline semiconductor solar cells, Thin Solid Films 361 (2000) 527–532, https://doi.org/10.1016/s0040-6090(99)00825-1.

[23] S. Rühle, Tabulated values of the Shockley–Queisser limit for single junction solar cells, Sol. Energy 130 (Jun. 2016) 139–147, https://doi.org/10.1016/j.solener.2016.02.015.

[24] A. Kanevce, M.O. Reese, T.M. Barnes, S.A. Jensen, W.K. Metzger, The roles of carrier concentration and interface, bulk, and grain-boundary recombination for 25% efficient CdTe solar cells, J. Appl. Phys. 121 (21) (Jun. 2017), 214506, https://doi.org/10.1063/1.4984320.

[25] G.M. Wilson, et al., The 2020 photovoltaic technologies roadmap, J. Phys. Appl. Phys. 53 (49) (Sep. 2020), 493001, https://doi.org/10.1088/1361-6463/ab9c6a.

[26] U. Rau, J.H. Werner, Radiative efficiency limits of solar cells with lateral band-gap fluctuations, Appl. Phys. Lett. 84 (19) (May 2004) 3735–3737, https://doi.org/10.1063/1.1737071.

[27] W.K. Metzger, et al., Exceeding 20% efficiency with in situ group V doping in polycrystalline CdTe solar cells, Nat. Energy 4 (10) (Oct. 2019) 10, https://doi.org/10.1038/s41560-019-0446-7.

[28] J. Moseley, et al., Impact of dopant-induced optoelectronic tails on open-circuit voltage in arsenic-doped Cd(Se)Te solar cells, J. Appl. Phys. 128 (10) (Sep. 2020), 103105, https://doi.org/10.1063/5.0018955.

[29] T. Dittrich, Materials Concepts for Solar Cells, WORLD SCIENTIFIC (EUROPE), 2017, https://doi.org/10.1142/q0131.

[30] O.D. Miller, E. Yablonovitch, S.R. Kurtz, Strong internal and external luminescence as solar cells approach the shockley–queisser limit, IEEE J. Photovoltaics 2 (3) (Jul. 2012) 303–311, https://doi.org/10.1109/JPHOTOV.2012.2198434.

[31] CdTe thin film solar cells: device and technology issues, Sol. Energy 77 (6) (Dec. 2004) 823–830, https://doi.org/10.1016/j.solener.2004.05.023.

[32] C.A. Wolden, et al., Photovoltaic manufacturing: present status, future prospects, and research needs, J. Vac. Sci. Technol., A 29 (3) (Mar. 2011), 030801, https://doi.org/10.1116/1.3569757.

[33] D. Bonnet, P. Meyers, Cadmium-telluride—material for thin film solar cells, J. Mater. Res. 13 (10) (1998) 2740–2753, Oct, https://doi.org/10.1557/JMR.1998.0376.

[34] S.H. Demtsu, J.R. Sites, Quantification of losses in thin-film CdS/CdTe solar cells, in: Conference Record of the Thirty-First IEEE Photovoltaic Specialists Conference, 2005, pp. 347–350, https://doi.org/10.1109/PVSC.2005.1488140. Jan. 2005.

[35] T.A. Gessert, et al., Research strategies toward improving thin-film CdTe photovoltaic devices beyond 20% conversion efficiency, Sol. Energy Mater. Sol. Cells 119 (Dec. 2013) 149–155, https://doi.org/10.1016/j.solmat.2013.05.055.

[36] T.A. Gessert, D. Bonnet, Polycrystalline cadmium telluride photovoltaic devices, in: Series on Photoconversion of Solar Energy, second ed., vol. 4, IMPERIAL COLLEGE PRESS, 2014, pp. 209–244, https://doi.org/10.1142/9781848167681_0005.

[37] T.A. Gessert, 1.19 - cadmium telluride photovoltaic thin film: CdTe, in: A. Sayigh (Ed.), Comprehensive Renewable Energy, Elsevier, Oxford, 2012, pp. 423–438, https://doi.org/10.1016/B978-0-08-087872-0.00122-0.

[38] A. Romeo, CdTe and CuInGaSe2 thin-film solar cells, in: A. Shah (Ed.), Solar Cells and Modules, Springer International Publishing, Cham, 2020, pp. 197–217, https://doi.org/10.1007/978-3-030-46487-5_8.

[39] T.D. Lee, A.U. Ebong, A review of thin film solar cell technologies and challenges, Renew. Sustain. Energy Rev. 70 (2017) 1286–1297, Apr, https://doi.org/10.1016/j.rser.2016.12.028.

[40] D. Bonnet, Chapter IC-2 - CdTe thin-film PV modules, in: A. McEvoy, T. Markvart, L. Castañer (Eds.), Practical Handbook of Photovoltaics, second ed., Academic Press, Boston, 2012, pp. 283–322, https://doi.org/10.1016/B978-0-12-385934-1.00009-X.

[41] K. Durose, Patterns in the control of CdTe solar cell performance, Adv. Charact. Thin Film Sol. Cells (Sep. 2020) 7–44, https://doi.org/10.1049/PBPO166E_ch2.

[42] M. Burgelman, Cadmium telluride thin film solar cells: characterization, fabrication and modeling, in: Thin Film Solar Cells, John Wiley & Sons, Ltd, 2006, pp. 277–324, https://doi.org/10.1002/0470091282.ch7.

[43] T. Gessert, B. McCandless, C. Ferekides, CHAPTER 3 thin-film CdTe photovoltaic solar cell devices, in: Advanced Concepts in Photovoltaics, The Royal Society of Chemistry, 2014, pp. 61–86, https://doi.org/10.1039/9781849739955-00061.

[44] M. Gloeckler, The adolescence of cadmium telluride photovoltaics, in: Proceedings of 44th, IEEE PVSC, Washington DC, 2017.

[45] D. Weiss, The Future of 2nd and 3rd-Generation Photovoltaics," Presented at the Gordon Research Conference "Pathways for Solar Energy Conversion and Storage: Electricity, Thermal and Fuel, Hong Kong, Jun. 2018.

[46] J.-H. Yang, W.-J. Yin, J.-S. Park, J. Ma, S.-H. Wei, Review on first-principles study of defect properties of CdTe as a solar cell absorber, Semicond. Sci. Technol. 31 (8) (2016), 083002, https://doi.org/10.1088/0268-1242/31/8/083002.

[47] J.M. Burst, et al., Carrier density and lifetime for different dopants in single-crystal and polycrystalline CdTe, Apl. Mater. 4 (11) (Nov. 2016), 116102, https://doi.org/10.1063/1.4966209.

[48] W.K. Metzger, et al., Resetting the defect chemistry in CdTe, IEEE 42nd Photovoltaic Specialist Conference (PVSC) (2015) 1–3, https://doi.org/10.1109/PVSC.2015.7356444. Jun. 2015.

[49] D.C. Reynolds, G. Leies, L.L. Antes, R.E. Marburger, Photovoltaic effect in cadmium sulfide, Phys. Rev. 96 (2) (Oct. 1954) 533–534, https://doi.org/10.1103/PhysRev.96.533.

[50] Alan L. Fahrenbruch, Richard H. Bube, Fundamentals of Solar Cells, Academic Press, New York, 1983.

[51] H.P. Garg, Advances in Solar Energy Technology, in: Collection and Storage Systems, ume 1, Springer Netherlands, 1987 [Online]. Available: https://books.google.com/books?id=Mp-CRcIEHgwC.

[52] J.J. Loferski, Theoretical considerations governing the choice of the optimum semiconductor for photovoltaic solar energy conversion, J. Appl. Phys. 27 (7) (Jul. 1956) 777–784, https://doi.org/10.1063/1.1722483.

[53] J. Britt, C. Ferekides, Thin-film CdS/CdTe solar cell with 15.8% efficiency, Appl. Phys. Lett. 62 (22) (1993) 2851–2852, https://doi.org/10.1063/1.109629.

[54] M.O. Reese, et al., Increasing markets and decreasing package weight for high-specific-power photovoltaics, Nat. Energy 3 (11) (Nov. 2018) 11, https://doi.org/10.1038/s41560-018-0258-1. Art. no.

[55] N. Strevel, L. Trippel, C. Kotarba, I. Khan, Improvements in CdTe module reliability and long-term degradation through advances in construction and device innovation, Photo Interpret. 22 (Dec. 2013) 1–8.

[56] Dr Simon Philipps, Fraunhofer ISE photovoltaics report 2020, Accessed: Jan. 03, 2021. [Online]. Available: https://www.ise.fraunhofer.de/en/publications/studies/photovoltaics-report.html.

[57] A. Bosio, S. Pasini, N. Romeo, The history of photovoltaics with emphasis on CdTe solar cells and modules, Coatings 10 (4) (Apr. 2020) 4, https://doi.org/10.3390/coatings10040344. Art. no.

[58] M.A. Green, et al., Solar cell efficiency tables (Version 60), Prog. Photovoltaics Res. Appl. 30 (7) (2022) 687–701, https://doi.org/10.1002/pip.3595.

[59] W. Shockley, H.J. Queisser, Detailed balance limit of efficiency of p-n junction solar cells, J. Appl. Phys. 32 (3) (Mar. 1961) 510–519, https://doi.org/10.1063/1.1736034.

[60] A. Onno, et al., Sub-bandgap features in CdSeTe solar cells: parsing the roles of material properties and cell optics, IEEE 48th Photovoltaic Specialists Conference (PVSC) (2021) 1754–1757, https://doi.org/10.1109/PVSC43889.2021.9518829. Jun. 2021.

[61] J.M. Burst, et al., CdTe solar cells with open-circuit voltage breaking the 1 V barrier, Nat. Energy 1 (3) (Mar. 2016) 16015, https://doi.org/10.1038/nenergy.2016.15.

[62] Y. Zhao, et al., Monocrystalline CdTe solar cells with open-circuit voltage over 1 V and efficiency of 17, Nat. Energy 1 (6) (Jun. 2016) 16067, https://doi.org/10.1038/nenergy.2016.67.

[63] D. Kuciauskas, et al., The impact of Cu on recombination in high voltage CdTe solar cells, Appl. Phys. Lett. 107 (24) (Dec. 2015), 243906, https://doi.org/10.1063/1.4938127.

[64] D.-B. Li, et al., Eliminating S-kink to maximize the performance of MgZnO/CdTe solar cells, ACS Appl. Energy Mater. 2 (4) (Apr. 2019) 4, https://doi.org/10.1021/acsaem.9b00233. Art. no.

[65] D.-B. Li, et al., CuSCN as the back contact for efficient ZMO/CdTe solar cells, Materials 13 (8) (Jan. 2020), https://doi.org/10.3390/ma13081991. Art. no. 8.

[66] D.-B. Li, et al., Maximize CdTe solar cell performance through copper activation engineering, Nano Energy 73 (Jul. 2020), 104835, https://doi.org/10.1016/j.nanoen.2020.104835.

[67] S.S. Bista, et al., Effects of Cu precursor on the performance of efficient CdTe solar cells, ACS Appl. Mater. Interfaces 13 (32) (Aug. 2021) 38432–38440, https://doi.org/10.1021/acsami.1c11784.

[68] A. Onno, et al., Understanding what limits the voltage of polycrystalline CdSeTe solar cells, Nat. Energy 7 (5) (May 2022), https://doi.org/10.1038/s41560-022-00985-z. Art. no. 5.

[69] C.H. Swartz, et al., Radiative and interfacial recombination in CdTe heterostructures, Appl. Phys. Lett. 105 (22) (Dec. 2014), 222107, https://doi.org/10.1063/1.4902926.

[70] X.-H. Zhao, M.J. DiNezza, S. Liu, S. Lin, Y. Zhao, Y.-H. Zhang, Time-resolved and excitation-dependent photoluminescence study of CdTe/MgCdTe double heterostructures grown by molecular beam epitaxy, J. Vac. Sci. Technol., B 32 (4) (May 2014), 040601, https://doi.org/10.1116/1.4878317.

[71] J.R. Winger, M.A. Scarpulla, Grain growth in CdTe films during CdCl2 treatment: TeCl4 theory, IEEE 46th Photovolt. Special.Conf.(PVSC) (2019) 1834–1838, https://doi.org/10.1109/PVSC40753.2019.8980923. Jun. 2019.

[72] B.S. Falbaum, J.R. Winger, M.A. Scarpulla, Dramatic Recrystallization during CdCl 2 Treatment of Evaporated CdTe Thin Filmsa," Presented at the 2018 IEEE 7th World Conference on Photovoltaic Energy Conversion, WCPEC 2018 - A Joint Conference of 45th IEEE PVSC, 28th PVSEC and 34th EU PVSEC, 2018, pp. 176–179, https://doi.org/10.1109/PVSC.2018.8547287.

[73] M. Amarasinghe, et al., Obtaining large columnar CdTe grains and long lifetime on nanocrystalline CdSe, MgZnO, or CdS layers, Adv. Energy Mater. 8 (11) (Apr. 2018), https://doi.org/10.1002/aenm.201702666. Art. no. 11.

[74] D. Albin, M. Amarasinghe, M.O. Reese, J. Moseley, H. Moutinho, W.K. Metzger, Colossal grain growth in Cd(Se,Te) thin films and their subsequent use in CdTe epitaxy by close-spaced sublimation, J. Phys. Energy 3 (2021), 024003, https://doi.org/10.1088/2515-7655/abd297.

[75] M. Amarasinghe, et al., Influence of CdTe deposition temperature and window thickness on CdTe grain size and lifetime after CdCl 2 recrystallization, IEEE J. Photovoltaics 8 (2) (Mar. 2018) 600–603, https://doi.org/10.1109/JPHOTOV.2018.2790701.

[76] M.K. Jamarkattel, et al., Indium gallium oxide emitters for high-efficiency CdTe-based solar cells, ACS Appl. Energy Mater. 5 (5) (May 2022) 5484–5489, https://doi.org/10.1021/acsaem.2c00153.

[77] T. Ablekim, et al., Thin-film solar cells with 19% efficiency by thermal evaporation of CdSe and CdTe, ACS Energy Lett. 5 (3) (Mar. 2020) 892–896, https://doi.org/10.1021/acsenergylett.9b02836.

[78] T.A.M. Fiducia, et al., Understanding the role of selenium in defect passivation for highly efficient selenium-alloyed cadmium telluride solar cells, Nat. Energy 4 (6) (2019), https://doi.org/10.1038/s41560-019-0389-z. Art. no. 6, Jun.

[79] E.G. LeBlanc, D. Leinen, M. Edirisooriya, A. Los, T.H. Myers, Valence band offset determination of CdSeTe and CdMgTe alloys with CdTe using X-ray photoemission spectroscopy, Appl. Surf. Sci. 529 (Nov. 2020), 147126, https://doi.org/10.1016/j.apsusc.2020.147126.

[80] B.E. McCandless, et al., Overcoming carrier concentration limits in polycrystalline CdTe thin films with in situ doping, Sci. Rep. 8 (1) (Sep. 2018), https://doi.org/10.1038/s41598-018-32746-y. Art. no. 1.

[81] B. McCandless, et al., Enhanced p-type doping in polycrystalline CdTe films: deposition and activation, IEEE J. Photovoltaics 9 (3) (May 2019) 912–917, https://doi.org/10.1109/JPHOTOV.2019.2902356.

[82] A. Nagaoka, K. Nishioka, K. Yoshino, D. Kuciauskas, M.A. Scarpulla, Arsenic doped Cd-rich CdTe: equilibrium doping limit and long lifetime for high open-circuit voltage solar cells greater than 900 mV, APEX 12 (8) (2019), https://doi.org/10.7567/1882-0786/ab27fb.

[83] A. Nagaoka, et al., Comparison of Sb, As, and P doping in Cd-rich CdTe single crystals: doping properties, persistent photoconductivity, and long-term stability, Appl. Phys. Lett. 116 (13) (2020), https://doi.org/10.1063/5.0004883.

[84] A. Nagaoka, K. Nishioka, K. Yoshino, D. Kuciauskas, M.A. Scarpulla, Growth and characterization of arsenic-doped CdTe1−xSex single crystals grown by the Cd-solvent traveling heater method, J. Electron. Mater. 49 (11) (2020) 6971–6976, https://doi.org/10.1007/s11664-020-08343-z.

[85] T. Ablekim, et al., Self-compensation in arsenic doping of CdTe, Sci. Rep. 7 (1) (Jul. 2017) 4563, https://doi.org/10.1038/s41598-017-04719-0.

[86] I. Sankin, D. Krasikov, Kinetic simulations of Cu doping in chlorinated CdSeTe PV absorbers, Phys. Status Solidi A 216 (15) (2019), 1800887, https://doi.org/10.1002/pssa.201800887.

[87] D. Krasikov, I. Sankin, Beyond thermodynamic defect models: a kinetic simulation of arsenic activation in CdTe, Phys. Rev. Mater. 2 (10) (Oct. 2018), 103803, https://doi.org/10.1103/PhysRevMaterials.2.103803.

[88] C.L. Perkins, C. Beall, M.O. Reese, T.M. Barnes, Two-Dimensional cadmium chloride nanosheets in cadmium telluride solar cells, ACS Appl. Mater. Interfaces 9 (24) (Jun. 2017), https://doi.org/10.1021/acsami.7b03671. Art. no. 24.

[89] D.L. McGott, et al., 3D/2D passivation as a secret to success for polycrystalline thin-film solar cells, Joule 5 (5) (May 2021) 1057–1073, https://doi.org/10.1016/j.joule.2021.03.015.

[90] D. Krasikov, D. Guo, S. Demtsu, I. Sankin, Comparative study of as and Cu doping stability in CdSeTe absorbers, Sol. Energy Mater. Sol. Cells 224 (Jun. 2021), 111012, https://doi.org/10.1016/j.solmat.2021.111012.

[91] D. Kuciauskas, et al., Recombination analysis in cadmium telluride photovoltaic solar cells with photoluminescence spectroscopy, IEEE J. Photovoltaics 6 (1) (Jan. 2016) 313–318, https://doi.org/10.1109/JPHOTOV.2015.2483366.

[92] A.M. Bothwell, J.A. Drayton, P.M. Jundt, J.R. Sites, Characterization of thin CdTe solar cells with a CdSeTe front layer, MRS Adv 4 (37) (2019) 2053–2062, https://doi.org/10.1557/adv.2019.332.

[93] A. Martin, Green, *Solar Cells: Operating Principles, Technology, and System Applications*, Prentice Hall, 1981.

[94] S.S. Hegedus, W.N. Shafarman, Thin-film solar cells: device measurements and analysis, Prog. Photovoltaics Res. Appl. 12 (2–3) (2004) 155–176, https://doi.org/10.1002/pip.518.

[95] U. Rau, Reciprocity relation between photovoltaic quantum efficiency and electroluminescent emission of solar cells, Phys. Rev. B 76 (8) (Aug. 2007), 085303, https://doi.org/10.1103/PhysRevB.76.085303.

[96] X. Wang, M.S. Lundstrom, On the use of rau's reciprocity to deduce external radiative efficiency in solar cells, IEEE J. Photovoltaics 3 (4) (Oct. 2013) 1348–1353, https://doi.org/10.1109/JPHOTOV.2013.2278658.

[97] S. Siebentritt, T.P. Weiss, M. Sood, M.H. Wolter, A. Lomuscio, O. Ramirez, How photoluminescence can predict the efficiency of solar cells, J. Phys. Mater. 4 (4) (Oct. 2021), 042010, https://doi.org/10.1088/2515-7639/ac266e.

[98] A.B. Phillips, G.K. Liyanage, F.K. Alfadhili, M.J. Heben, Understanding CdTe performance with engineered front and back interfaces, IEEE 46th Photovolt. Special.Conf.(PVSC) (2019), https://doi.org/10.1109/PVSC40753.2019.8980683. Jun. 2019, pp. 0777–0782.

[99] S. Paul, et al., Analysis of back-contact interface recombination in thin-film solar cells, IEEE J. Photovoltaics 8 (3) (May 2018) 871–878, https://doi.org/10.1109/JPHOTOV.2018.2819664.

[100] S. Grover, J.V. Li, D.L. Young, P. Stradins, H.M. Branz, Reformulation of solar cell physics to facilitate experimental separation of recombination pathways, Appl. Phys. Lett. 103 (9) (Aug. 2013), 093502, https://doi.org/10.1063/1.4819728.

[101] J.V. Li, S. Grover, M.A. Contreras, K. Ramanathan, D. Kuciauskas, R. Noufi, A recombination analysis of Cu(In,Ga)Se2 solar cells with low and high Ga compositions, Sol. Energy Mater. Sol. Cells 124 (2014) 143–149, https://doi.org/10.1016/j.solmat.2014.01.047.

[102] R. Pandey, et al., Mitigation of J–V distortion in CdTe solar cells by Ga-doping of MgZnO emitter, Sol. Energy Mater. Sol. Cells 232 (Oct. 2021), 111324, https://doi.org/10.1016/j.solmat.2021.111324.

[103] T. Song, A. Kanevce, J.R. Sites, Emitter/absorber interface of CdTe solar cells, J. Appl. Phys. 119 (23) (Jun. 2016), 233104, https://doi.org/10.1063/1.4953820.

[104] G. Yeung, et al., Robust passivation of CdSeTe based solar cells using reactively sputtered magnesium zinc oxide, Sol. Energy Mater. Sol. Cells 233 (Dec. 2021), 111388, https://doi.org/10.1016/j.solmat.2021.111388.

[105] G.K. Liyanage, A.B. Phillips, F.K. Alfadhili, R.J. Ellingson, M.J. Heben, The role of back buffer layers and absorber properties for >25% efficient CdTe solar cells, ACS Appl. Energy Mater. 2 (8) (2019) 5419–5426, Aug, https://doi.org/10.1021/acsaem.9b00367.

[106] T. Ablekim, et al., Tailoring MgZnO/CdSeTe interfaces for photovoltaics, IEEE J. Photovoltaics 9 (3) (May 2019), https://doi.org/10.1109/JPHOTOV.2018.2877982. Art. no. 3.

[107] T. Ablekim, E. Colegrove, W.K. Metzger, Interface engineering for 25% CdTe solar cells, ACS Appl. Energy Mater. 1 (10) (2018) 5135–5139, Oct, https://doi.org/10.1021/acsaem.8b01173.

[108] R. Pandey, T. Shimpi, A. Munshi, J.R. Sites, Impact of carrier concentration and carrier lifetime on MgZnO/CdSeTe/CdTe solar cells, IEEE J. Photovoltaics 10 (6) (Nov. 2020) 1918–1925, https://doi.org/10.1109/JPHOTOV.2020.3017741.

[109] A.O. Pudov, A. Kanevce, H.A. Al-Thani, J.R. Sites, F.S. Hasoon, Secondary barriers in CdS–CuIn1−xGaxSe2 solar cells, J. Appl. Phys. 97 (6) (2005), 064901, https://doi.org/10.1063/1.1850604.

[110] S. Misra, et al., Observation and implications of composition inhomogeneity along grain boundaries in thin film polycrystalline CdTe photovoltaic devices, Adv. Mater. Interfac. 6 (2019) 16, https://doi.org/10.1002/admi.201900152.

[111] S. Misra, et al., Cadmium selective etching in CdTe solar cells produces detrimental narrow-gap Te in grain boundaries, ACS Appl. Energy Mater. 3 (2) (2020) 1749–1758, https://doi.org/10.1021/acsaem.9b02224.

[112] B.J. Simonds, V. Palekis, B. Van Devener, C. Ferekides, M.A. Scarpulla, Surface stoichiometry of pulsed ultraviolet laser treated polycrystalline CdTe, J. Appl. Phys. 116 (1) (2014), https://doi.org/10.1063/1.4887079.

[113] B.J. Simonds, V. Palekis, M.I. Khan, C.S. Ferekides, M.A. Scarpulla, Pulsed UV laser annealing of polycrystalline CdTe, Proc. SPIE-Int. Soc. Opt. Eng. 8826 (2013), https://doi.org/10.1117/12.2024437 presented at the.

[114] B.J. Simonds, V. Palekis, B. Van Devener, C. Ferekides, M.A. Scarpulla, Pulsed laser induced ohmic back contact in CdTe solar cells, Appl. Phys. Lett. 104 (14) (2014), https://doi.org/10.1063/1.4870838.

[115] B.J. Simonds, V. Kheraj, V. Palekis, C. Ferekides, M.A. Scarpulla, Reduction of Fermi level pinning and recombination at polycrystalline CdTe surfaces by laser irradiation, J. Appl. Phys. 117 (22) (Jun. 2015), 225301, https://doi.org/10.1063/1.4921950.

[116] B.J. Simonds, V. Palekis, B. Van Devener, C. Ferekides, M.A. Scarpulla, Te-rich CdTe surface by pulsed UV laser treatment for ohmic back contact formation, presented at the 2014, IEEE 40th Photovolt. Special. Conf. (2014) 2407–2411, https://doi.org/10.1109/PVSC.2014.6925413. PVSC 2014.

[117] B.J. Simonds, V. Palekis, B. Van Devener, C. Ferekides, M.A. Scarpulla, Te-rich CdTe surface by pulsed UV laser treatment for ohmic back contact formation, presented at the 2014, IEEE 40th Photovolt. Special. Conf. (2014) 2407–2411, https://doi.org/10.1109/PVSC.2014.6925413. PVSC 2014.

[118] A.P. Nicholson, A. Shah, R. Pandey, A.H. Munshi, J. Sites, W. Sampath, Te/CdTe and Al/CdTe interfacial energy band alignment by atomistic modeling, *ACS Appl. Mater. Interfaces*, Jun (2022), https://doi.org/10.1021/acsami.2c05244.

[119] J. Pan, M. Gloeckler, J.R. Sites, Hole current impedance and electron current enhancement by back-contact barriers in CdTe thin film solar cells, J. Appl. Phys. 100 (12) (Dec. 2006), 124505, https://doi.org/10.1063/1.2400799.

[120] J. Sites, J. Pan, Strategies to increase CdTe solar-cell voltage, Thin Solid Films 515 (15) (May 2007) 6099–6102, https://doi.org/10.1016/j.tsf.2006.12.147.

[121] J.M. Kephart, et al., Sputter-deposited oxides for interface passivation of CdTe photovoltaics, IEEE J. Photovoltaics 8 (2) (Mar. 2018) 587–593, https://doi.org/10.1109/JPHOTOV.2017.2787021.

[122] D. Kuciauskas, J.M. Kephart, J. Moseley, W.K. Metzger, W.S. Sampath, P. Dippo, Recombination velocity less than 100 cm/s at polycrystalline Al2O3/CdSeTe interfaces, Appl. Phys. Lett. 112 (26) (Jun. 2018), 263901, https://doi.org/10.1063/1.5030870.

[123] K.K. Subedi, et al., Enabling bifacial thin film devices by developing a back surface field using CuxAlOy, Nano Energy 83 (May 2021), 105827, https://doi.org/10.1016/j.nanoen.2021.105827.

[124] F.K. Alfadhili, et al., Back-surface passivation of CdTe solar cells using solution-processed oxidized aluminum, ACS Appl. Mater. Interfaces 12 (46) (Nov. 2020) 51337–51343, https://doi.org/10.1021/acsami.0c12800.

[125] C.L. Perkins, et al., Interfaces between CdTe and ALD Al2O3, IEEE J. Photovoltaics 8 (6) (2018) 1858–1861, Nov, https://doi.org/10.1109/JPHOTOV.2018.2870139.

[126] R. Triboulet, P. Siffert, CdTe and Related Compounds; Physics, Defects, Hetero- and Nano-Structures, Crystal Growth, Surfaces and Applications, Elsevier, 2010, https://doi.org/10.1016/C2009-0-61369-6.

[127] Y. Yan, M.M. Al-Jassim, Transmission electron microscopy of chalcogenide thin-film photovoltaic materials, Curr. Opin. Solid State Mater. Sci. 16 (1) (Feb. 2012) 39–44, https://doi.org/10.1016/j.cossms.2011.10.001.

[128] K. Ohata, J. Saraie, T. Tanaka, Optical energy gap of the mixed crystal CdSxTe1-x, Jpn. J. Appl. Phys. 12 (10) (Oct. 1973) 1641, https://doi.org/10.1143/JJAP.12.1641.

[129] L. Hannachi, N. Bouarissa, Electronic structure and optical properties of CdSexTe1−x mixed crystals, Superlattice. Microst. 44 (6) (Dec. 2008) 794–801, https://doi.org/10.1016/j.spmi.2008.09.013.

[130] N. Muthukumarasamy, S. Jayakumar, M.D. Kannan, R. Balasundaraprabhu, Structural phase change and optical band gap bowing in hot wall deposited CdSexTe1−x thin films, Sol. Energy 83 (4) (Apr. 2009) 522–526, https://doi.org/10.1016/j.solener.2008.10.004.

[131] D.-B. Li, et al., 20%-efficient polycrystalline Cd(Se,Te) thin-film solar cells with compositional gradient near the front junction, Nat. Commun. 13 (1) (Dec. 2022), https://doi.org/10.1038/s41467-022-35442-8. Art. no. 1.

[132] D.E. Swanson, J.R. Sites, W.S. Sampath, Co-sublimation of CdSexTe1−x layers for CdTe solar cells, Sol. Energy Mater. Sol. Cells 159 (Jan. 2017) 389–394, https://doi.org/10.1016/j.solmat.2016.09.025.

[133] A.H. Munshi, et al., Effect of CdCl2 passivation treatment on microstructure and performance of CdSeTe/CdTe thin-film photovoltaic devices, Sol. Energy Mater. Sol. Cells 186 (Nov. 2018) 259–265, https://doi.org/10.1016/j.solmat.2018.06.016.

[134] A.H. Munshi, et al., Polycrystalline CdSeTe/CdTe absorber cells with 28 mA/cm2 short-circuit current, IEEE J. Photovoltaics 8 (1) (Jan. 2018), https://doi.org/10.1109/JPHOTOV.2017.2775139. Art. no. 1.

[135] T. Fiducia, et al., Selenium passivates grain boundaries in alloyed CdTe solar cells, Sol. Energy Mater. Sol. Cells 238 (May 2022), 111595, https://doi.org/10.1016/j.solmat.2022.111595.

[136] J. Guo, et al., Effect of selenium and chlorine co-passivation in polycrystalline CdSeTe devices, Appl. Phys. Lett. 115 (15) (Oct. 2019), https://doi.org/10.1063/1.5123169. Art. no. 15.

[137] X. Zheng, E. Colegrove, J.N. Duenow, J. Moseley, W.K. Metzger, Roles of bandgrading, lifetime, band alignment, and carrier concentration in high-efficiency CdSeTe solar cells, J. Appl. Phys. 128 (5) (Aug. 2020), 053102, https://doi.org/10.1063/5.0013726.

[138] T.M. Barnes, et al., Comparing the fundamental physics and device performance of transparent, conductive nanostructured networks with conventional transparent conducting oxides, Adv. Energy Mater. 2 (3) (2012) 353–360, https://doi.org/10.1002/aenm.201100608.

[139] X. Wu, P. Sheldon, T.J. Coutts, D.H. Rose, W.P. Mulligan, H.R. Moutinho, CdS/CdTe thin-film devices using a Cd2SnO4 transparent conducting oxide, AIP Conf. Proc. 394 (1) (Feb. 1997) 693–702, https://doi.org/10.1063/1.52871.

[140] A. Kanevce, J.R. Sites, Impact of nonuniformities on thin Cu(in,Ga)Se2 solar cell performance, MRS Online Proc. Libr. 1012 (1) (Oct. 2007) 802, https://doi.org/10.1557/PROC-1012-Y08-02.

[141] Y. Roussillon, V.G. Karpov, D. Shvydka, J. Drayton, A.D. Compaan, Back contact and reach-through diode effects in thin-film photovoltaics, J. Appl. Phys. 96 (12) (2004) 7283–7288, Dec, https://doi.org/10.1063/1.1808902.

[142] D.L. McGott, E. Colegrove, J.N. Duenow, C.A. Wolden, M.O. Reese, Revealing the importance of front interface quality in highly doped CdSexTe1−x solar cells, ACS Energy Lett. 6 (12) (2021) 4203–4208, Dec, https://doi.org/10.1021/acsenergylett.1c01846.

[143] D.L. McGott, et al., Thermomechanical lift-off and recontacting of CdTe solar cells, ACS Appl. Mater. Interfaces 10 (51) (Dec. 2018) 44854–44861, https://doi.org/10.1021/acsami.8b16476.

[144] C.L. Perkins, D.L. McGott, M.O. Reese, W.K. Metzger, SnO2-Catalyzed oxidation in high-efficiency CdTe solar cells, ACS Appl. Mater. Interfaces 11 (13) (2019) 13003–13010, https://doi.org/10.1021/acsami.9b00835. Apr.

[145] G. Teeter, X-ray and ultraviolet photoelectron spectroscopy measurements of Cu-doped CdTe(111)-B: observation of temperature-reversible CuxTe precipitation and effect on ionization potential, J. Appl. Phys. 102 (3) (Aug. 2007), 034504, https://doi.org/10.1063/1.2759876.

[146] R.S. Hall, D. Lamb, S.J.C. Irvine, Back contacts materials used in thin film CdTe solar cells—a review, Energy Sci. Eng. 9 (5) (2021) 606–632, https://doi.org/10.1002/ese3.843.

[147] H.B. Michaelson, Relation between an atomic electronegativity scale and the work function, IBM J. Res. Dev. 22 (1) (Jan. 1978) 72–80, https://doi.org/10.1147/rd.221.0072.

[148] J.P. Ponpon, A review of ohmic and rectifying contacts on cadmium telluride, Solid State Electron. 28 (7) (Jul. 1985) 7, https://doi.org/10.1016/0038-1101(85)90019-X.

[149] T.A. Gessert, A.R. Mason, P. Sheldon, A.B. Swartzlander, D. Niles, T.J. Coutts, Development of Cu-doped ZnTe as a back-contact interface layer for thin-film CdS/CdTe solar cells, J. Vac. Sci. Technol. Vac. Surf. Films 14 (3) (May 1996), https://doi.org/10.1116/1.580394. Art. no. 3.

[150] C.S. Ferekides, et al., High efficiency CSS CdTe solar cells, Thin Solid Films 361–362 (Feb. 2000) 520–526, https://doi.org/10.1016/S0040-6090(99)00824-X.

[151] E. Artegiani, J.D. Major, H. Shiel, V. Dhanak, C. Ferrari, A. Romeo, How the amount of copper influences the formation and stability of defects in CdTe solar cells, Sol. Energy Mater. Sol. Cells 204 (Jan. 2020), 110228, https://doi.org/10.1016/j.solmat.2019.110228.

[152] M.O. Reese, et al., Intrinsic surface passivation of CdTe, J. Appl. Phys. 118 (15) (Oct. 2015), https://doi.org/10.1063/1.4933186. Art. no. 15.

[153] S.C. Watthage, et al., Selective Cd removal from CdTe for high-efficiency Te back-contact formation, IEEE J. Photovoltaics 8 (4) (2018) 1125–1131, Jul, https://doi.org/10.1109/JPHOTOV.2018.2830302.

[154] T.A. Gessert, et al., Pathways toward higher performance CdS/CdTe devices: Te exposure of CdTe surface before ZnTe:Cu/Ti contacting, Thin Solid Films 535 (May 2013) 237–240, https://doi.org/10.1016/j.tsf.2012.11.087.

[155] J. Hack, C. Lee, S. Grover, G. Xiong, Hole transport material for passivated back contacts on CdTe solar cells, IEEE 48th Photovoltaic Specialists Conference (PVSC) (2021) 1880–1882, https://doi.org/10.1109/PVSC43889.2021.9519026. Jun. 2021.

[156] T. Song, A. Moore, J.R. Sites, Te layer to reduce the CdTe back-contact barrier, IEEE J. Photovoltaics 8 (1) (Jan. 2018) 293–298, https://doi.org/10.1109/JPHOTOV.2017.2768965.

[157] J.V. Li, et al., Electrical characterization of Cu composition effects in CdS/CdTe thin-film solar cells with a ZnTe:Cu back contact, IEEE 38th Photovoltaic Specialists Conference (PVSC) 2 (2012) 1–5, https://doi.org/10.1109/PVSC-Vol2.2012.6656756. Jun. 2012.

[158] F.K. Alfadhili, A.B. Phillips, G.K. Liyanage, J.M. Gibbs, M.K. Jamarkattel, M. J. Heben, Controlling band alignment at the back interface of cadmium telluride solar cells using ZnTe and Te buffer layers, MRS Adv 4 (16) (Mar. 2019) 913–919, https://doi.org/10.1557/adv.2019.31.

[159] H. Lin, Irfan, W. Xia, H.N. Wu, Y. Gao, C.W. Tang, MoOx back contact for CdS/CdTe thin film solar cells: preparation, device characteristics, and stability, Sol.

Energy Mater. Sol. Cells 99 (Apr. 2012) 349–355, https://doi.org/10.1016/j.solmat.2012.01.001.
[160] Z. Akkuly, et al., Optimization of the solution-based aluminium gallium oxide buffer layer for CdTe solar cells, IEEE 48th Photovoltaic Specialists Conference (PVSC) (2021) 2132–2135, https://doi.org/10.1109/PVSC43889.2021.9519067. Jun. 2021.
[161] B. Ghosh, S. Purakayastha, P.K. Datta, R.W. Miles, M.J. Carter, R. Hill, Formation of a stable ohmic contact to CdTe thin films through the diffusion of P from Ni-P, Semicond. Sci. Technol. 10 (1) (Jan. 1995) 71, https://doi.org/10.1088/0268-1242/10/1/012.
[162] C.H. Swartz, et al., Evaluation of PbTe and SnTe as ohmic contact layers in CdTe solar cell devices, Appl. Surf. Sci. 598 (Oct. 2022), 153656, https://doi.org/10.1016/j.apsusc.2022.153656.
[163] B.E. Sartor, et al., Titanium carbide MXene hole contacts for CdTe photovoltaics, Sol. RRL 6 (11) (2022), 2200366, https://doi.org/10.1002/solr.202200366.
[164] J. Perrenoud, et al., A comprehensive picture of Cu doping in CdTe solar cells, J. Appl. Phys. 114 (17) (Nov. 2013), https://doi.org/10.1063/1.4828484. Art. no. 17.
[165] D.E. Swanson, et al., Incorporation of Cd1-xMgx Te as an electron reflector for cadmium telluride photovoltaic cells, MRS Online Proc. Libr. 1771 (1) (Dec. 2015) 133–138, https://doi.org/10.1557/opl.2015.389.
[166] J. Ma, et al., Dependence of the minority-carrier lifetime on the stoichiometry of CdTe using time-resolved photoluminescence and first-principles calculations, Phys. Rev. Lett. 111 (6) (Aug. 2013), https://doi.org/10.1103/PhysRevLett.111.067402. Art. no. 6.
[167] J. Ma, J. Yang, S.-H. Wei, J.L.F. Da Silva, Correlation between the electronic structures and diffusion paths of interstitial defects in semiconductors: the case of CdTe, Phys. Rev. B 90 (15) (Oct. 2014), https://doi.org/10.1103/PhysRevB.90.155208. Art. no. 15.
[168] J.-H. Yang, et al., Enhanced p-type dopability of P and as in CdTe using non-equilibrium thermal processing, J. Appl. Phys. 118 (2) (Jul. 2015), https://doi.org/10.1063/1.4926748. Art. no. 2.
[169] J.-H. Yang, J.-S. Park, J. Kang, S.-H. Wei, First-principles multiple-barrier diffusion theory: the case study of interstitial diffusion in CdTe, Phys. Rev. B 91 (7) (Feb. 2015), https://doi.org/10.1103/PhysRevB.91.075202. Art. no. 7.
[170] J.-H. Yang, J.-S. Park, J. Kang, W. Metzger, T. Barnes, S.-H. Wei, Tuning the Fermi level beyond the equilibrium doping limit through quenching: the case of CdTe, Phys. Rev. B 90 (24) (Dec. 2014), https://doi.org/10.1103/PhysRevB.90.245202. Art. no. 24.
[171] J.-H. Yang, L. Shi, L.-W. Wang, S.-H. Wei, Non-radiative carrier recombination enhanced by two-level process: a first-principles study, Sci. Rep. 6 (1) (Apr. 2016), https://doi.org/10.1038/srep21712. Art. no. 1.
[172] J.-H. Yang, W.-J. Yin, J.-S. Park, W. Metzger, S.-H. Wei, First-principles study of roles of Cu and Cl in polycrystalline CdTe, J. Appl. Phys. 119 (4) (Jan. 2016), https://doi.org/10.1063/1.4940722. Art. no. 4.
[173] D. Kuciauskas, D. Krasikov, Spectroscopic and microscopic defect and carrier-lifetime analysis in cadmium telluride, IEEE J. Photovoltaics 8 (6) (2018) 1754–1760, Nov, https://doi.org/10.1109/JPHOTOV.2018.2866180.
[174] D.N. Krasikov, A.V. Scherbinin, A.A. Knizhnik, A.N. Vasiliev, B.V. Potapkin, T. J. Sommerer, Theoretical analysis of non-radiative multiphonon recombination activity of intrinsic defects in CdTe, J. Appl. Phys. 119 (8) (Feb. 2016), 085706, https://doi.org/10.1063/1.4942529.
[175] S.R. Kavanagh, A. Walsh, D.O. Scanlon, Rapid recombination by cadmium vacancies in CdTe, ACS Energy Lett. 6 (4) (2021) 1392–1398, Apr, https://doi.org/10.1021/acsenergylett.1c00380.
[176] D. Krasikov, I. Sankin, Defect interactions and the role of complexes in the CdTe solar cell absorber, J. Mater. Chem. 5 (7) (2017) 3503–3513, Feb, https://doi.org/10.1039/C6TA09155E.
[177] A. Nagaoka, D. Kuciauskas, J. McCoy, M.A. Scarpulla, High p-type doping, mobility, and photocarrier lifetime in arsenic-doped CdTe single crystals, Appl. Phys. Lett. 112 (19) (May 2018), 192101, https://doi.org/10.1063/1.5029450.
[178] I. Chatratin, S. Mukherjee, A. Janotti, Hybrid functional calculations for antimony doping in CdTe, in: Proceedings of 49th IEEE PVSC, 2022. Phillidelphia, PA, Jun.
[179] A. Nagaoka, K. Yoshino, Y. Nose, D. Kuciauskas, M.A. Scarpulla, Group-V doping impact on Cd-rich CdTe single crystals grown by traveling-heater method, IEEE 44th Photovolt. Special. Conf. (PVSC) (2017) 1679–1681, https://doi.org/10.1109/PVSC.2017.8366462. Jun. 2017.
[180] A. Nagaoka, D. Kuciauskas, M.A. Scarpulla, Doping properties of cadmium-rich arsenic-doped CdTe single crystals: evidence of metastable AX behavior, Appl. Phys. Lett. 111 (23) (Dec. 2017), 232103, https://doi.org/10.1063/1.4999011.
[181] A. Nagaoka, K.-B. Han, S. Misra, T. Wilenski, T.D. Sparks, M.A. Scarpulla, Growth and characterization of Arsenic doped CdTe single crystals grown by Cd-solvent traveling-heater method, J. Cryst. Growth 467 (Jun. 2017) 6–11, https://doi.org/10.1016/j.jcrysgro.2017.03.002.
[182] T. Ablekim, S.K. Swain, J. McCoy, K.G. Lynn, Defects in undoped p-type CdTe single crystals, IEEE J. Photovoltaics 6 (6) (2016) 1663–1667, https://doi.org/10.1109/jphotov.2016.2609639.
[183] B. Good, E. Colegrove, M.O. Reese, Effects of absorber near-interface compensation on Cd(Se,Te) solar cell performance, Sol. Energy Mater. Sol. Cells 246 (Oct. 2022), 111928, https://doi.org/10.1016/j.solmat.2022.111928.
[184] P.V. Meyers, C.H. Liu, T.J. Frey, Method of Making Photovoltaic Cell with Chloride Dip, 1989, US4873198A.
[185] B.L. Williams, J.D. Major, L. Bowen, W. Keuning, M. Creatore, K. Durose, A comparative study of the effects of nontoxic chloride treatments on CdTe solar cell microstructure and stoichiometry, Adv. Energy Mater. 5 (21) (Nov. 2015), https://doi.org/10.1002/aenm.201500554. Art. no. 21.
[186] J. Li, et al., Controlled activation of ZnTe:Cu contacted CdTe solar cells using rapid thermal processing, Sol. Energy Mater. Sol. Cells 133 (Feb. 2015) 208–215, https://doi.org/10.1016/j.solmat.2014.10.045.
[187] I.S. Khan, V.K. Evani, V. Palekis, C. Ferekides, Effect of stoichiometry on the lifetime and doping concentration of polycrystalline CdTe, IEEE J. Photovoltaics 7 (5) (2017) 1450–1455, Sep, https://doi.org/10.1109/JPHOTOV.2017.2730865.
[188] V. Palekis, et al., Near infrared laser CdCl2heat treatment for CdTe solar cells," presented at the Conference Record of the, IEEE Photovoltaic Specialists Conference 2016-November (2016) 1498–1502, https://doi.org/10.1109/PVSC.2016.7749867.
[189] B.J. Simonds, et al., Near infrared laser annealing of CdTe and in-situ measurement of the evolution of structural and optical properties, J. Appl. Phys. 119 (16) (2016), https://doi.org/10.1063/1.4947186.
[190] B.J. Simonds, H.J. Meadows, S. Misra, C. Ferekides, P.J. Dale, M.A. Scarpulla, Laser processing for thin film chalcogenide photovoltaics: a review and prospectus, J. Photon. Energy 5 (1) (Jan. 2015), 050999, https://doi.org/10.1117/1.JPE.5.050999.
[191] S. Misra, M.I. Khan, V. Palekis, C. Ferekides, M.A. Scarpulla, Continuous-wave laser driven post deposition chlorine treatment of CdTe," presented at the 2015 IEEE 42nd Photovoltaic Specialist Conference, PVSC (2015), https://doi.org/10.1109/PVSC.2015.7356092, 2015.
[192] A. Abbas, The Microstructure of Thin Film Cadmium Telluride Photovoltaic Materials,, PhD Thesis, Loughbourough University, 2014 [Online]. Available: https://repository.lboro.ac.uk/articles/thesis/The_microstructure_of_thin_film_cadmium_telluride_photovoltaic_materials/9524558.
[193] J. Fritsche, A. Klein, W. Jaegermann, Thin film solar cells: materials science at interfaces, Adv. Eng. Mater. 7 (10) (Oct. 2005), https://doi.org/10.1002/adem.200500126. Art. no. 10.
[194] B.E. McCandless, L.V. Moulton, R.W. Birkmire, Recrystallization and sulfur diffusion in CdCl2-treated CdTe/CdS thin films, Prog. Photovoltaics Res. Appl. 5 (4) (1997) 4, https://doi.org/10.1002/(SICI)1099-159X(199707/08)5:4<249::AID-PIP178>3.0.CO, 2-S.
[195] A. Abbas, et al., Cadmium chloride assisted re-crystallization of CdTe: the effect of annealing over-treatment, IEEE 40th Photovolt. Special. Conf. (PVSC) (2014), https://doi.org/10.1109/PVSC.2014.6925018. Jun. 2014, pp. 0701–0706.
[196] P. Hatton, M. J. Watts, A. Abbas, J. M. Walls, R. Smith, and P. Goddard, "Chlorine activated stacking fault removal mechanism in thin film CdTe solar cells: the missing piece," Nat. Commun., vol. 12, no. 1, Art. no. 1, A\1, doi: 10.1038/s41467-021-25063-y.
[197] T. Paulauskas, et al., Atomic-resolution characterization of the effects of CdCl2 treatment on poly-crystalline CdTe thin films, Appl. Phys. Lett. 105 (7) (Aug. 2014), 071910, https://doi.org/10.1063/1.4893727.
[198] D. Mao, G. Blatz, C.E. Wickersham, M. Gloeckler, Correlative impurity distribution analysis in cadmium telluride (CdTe) thin-film solar cells by ToF-SIMS 2D imaging, Sol. Energy Mater. Sol. Cells 157 (Dec. 2016) 65–73, https://doi.org/10.1016/j.solmat.2016.05.019.
[199] D. Mao, C.E. Wickersham, M. Gloeckler, Measurement of chlorine concentrations at CdTe grain boundaries, IEEE J. Photovoltaics 4 (6) (Nov. 2014) 1655–1658, https://doi.org/10.1109/JPHOTOV.2014.2357258.
[200] S.P. Harvey, G. Teeter, H. Moutinho, M.M. Al-Jassim, Direct evidence of enhanced chlorine segregation at grain boundaries in polycrystalline CdTe thin films via three-dimensional TOF-SIMS imaging: chlorine segregation at grain boundaries in CdTe thin films, Prog. Photovoltaics Res. Appl. 23 (7) (Jul. 2015), https://doi.org/10.1002/pip.2498. Art. no. 7.
[201] A. Abbas, et al., The effect of cadmium chloride treatment on close spaced sublimated cadmium telluride thin film solar cells, IEEE 38th Photovolt. Special. Conf. (PVSC) PART 2 (2012) 1–6, https://doi.org/10.1109/PVSC-Vol2.2012.6656778. Jun. 2012.
[202] A. Abbas, et al., The effect of a post-activation annealing treatment on thin film cdte device performance, IEEE 42nd Photovoltaic Specialist Conference (PVSC) (2015) 1–6, https://doi.org/10.1109/PVSC.2015.7356441. New Orleans, LA, Jun. 2015.
[203] C. Li, et al., Grain-boundary-enhanced carrier collection in CdTe solar cells, Phys. Rev. Lett. 112 (15) (2014), 156103, https://doi.org/10.1103/physrevlett.112.156103.
[204] M. Gloeckler, J.R. Sites, W.K. Metzger, Grain-boundary recombination in Cu(In, Ga)Se2 solar cells, J. Appl. Phys. 98 (11) (Dec. 2005), 113704, https://doi.org/10.1063/1.2133906.
[205] W.K. Metzger, M. Gloeckler, The impact of charged grain boundaries on thin-film solar cells and characterization, J. Appl. Phys. 98 (6) (Sep. 2005), 063701, https://doi.org/10.1063/1.2042530.
[206] D. Bonnet, Manufacturing of CSS CdTe solar cells, Thin Solid Films 361–362 (Feb. 2000) 547–552, https://doi.org/10.1016/S0040-6090(99)00831-7.
[207] Y. Qu, P.V. Meyers, B.E. McCandless, HCl vapor post-deposition heat treatment of CdTe/CdS films, in: Conference Record of the Twenty Fifth IEEE Photovoltaic Specialists Conference, 1996, pp. 1013–1016, https://doi.org/10.1109/PVSC.1996.564303. May 1996.
[208] A. Salavei, I. Rimmaudo, F. Piccinelli, P. Zabierowski, A. Romeo, Study of difluorochloromethane activation treatment on low substrate temperature deposited CdTe solar cells, Sol. Energy Mater. Sol. Cells 112 (May 2013) 190–195, https://doi.org/10.1016/j.solmat.2013.01.019.
[209] A. Rios-Flores, O. Arés, J.M. Camacho, V. Rejon, J.L. Peña, Procedure to obtain higher than 14% efficient thin film CdS/CdTe solar cells activated with HCF2Cl gas, Sol. Energy 86 (2) (Feb. 2012), https://doi.org/10.1016/j.solener.2011.12.002. Art. no. 2.

[210] E. Regalado-Pérez, M.G. Reyes-Banda, X. Mathew, Influence of oxygen concentration in the CdCl 2 treatment process on the photovoltaic properties of CdTe/CdS solar cells, Thin Solid Films 582 (May 2015) 134–138, https://doi.org/10.1016/j.tsf.2014.11.005.

[211] B.I. MacDonald, A. Martucci, S. Rubanov, S.E. Watkins, P. Mulvaney, J. J. Jasieniak, Layer-by-Layer assembly of sintered CdSe *x* Te 1– *x* nanocrystal solar cells, ACS Nano 6 (7) (Jul. 2012) 7, https://doi.org/10.1021/nn3009189.

[212] X. Zheng, et al., Recombination and bandgap engineering in CdSeTe/CdTe solar cells, Apl. Mater. 7 (7) (Jul. 2019), 071112, https://doi.org/10.1063/1.5098459.

[213] J. Fritsche, et al., Surface analysis of CdTe thin film solar cells, Thin Solid Films 387 (1) (May 2001) 161–164, https://doi.org/10.1016/S0040-6090(00)01851-4.

[214] J.D. Major, Grain boundaries in CdTe thin film solar cells: a review, Semicond. Sci. Technol. 31 (9) (Sep. 2016) 9, https://doi.org/10.1088/0268-1242/31/9/093001.

[215] I.M. Dharmadasa, Review of the CdCl2 treatment used in CdS/CdTe thin film solar cell development and new evidence towards improved understanding, Coatings 4 (Jun. 2014) 2, https://doi.org/10.3390/coatings4020282. Art. no. 2.

[216] C.V. Thompson, Grain growth in thin films, Annu. Rev. Mater. Sci. 20 (1) (1990) 245–268, https://doi.org/10.1146/annurev.ms.20.080190.001333.

[217] N. Spalatu, et al., Effect of CdCl2 annealing treatment on structural and optoelectronic properties of close spaced sublimation CdTe/CdS thin film solar cells vs deposition conditions, Thin Solid Films 582 (May 2015) 128–133, https://doi.org/10.1016/j.tsf.2014.11.066.

[218] H. Tai and S. Hori, "Equilibrium Phase Diagrams of the CdTe-CdCl2 and CdTe-CdBr2 Systems," J. Jpn. Inst. Met. Mater., vol. 40, no. 7, pp. 722–725, doi: https://doi.org/10.2320/jinstmet1952.40.7_722.

[219] F.J. Keneshea, D.D. Cubicciotti, Vapor pressure of cadmium chloride and thermodynamic data for CdCl2 gas, J. Chem. Phys. 40 (6) (1964) 1778–1779, Mar, https://doi.org/10.1063/1.1725404.

[220] J. Hiie, CdTe:CdCl2:O2 annealing process, Thin Solid Films 431 (432) (May 2003) 90–93, https://doi.org/10.1016/S0040-6090(03)00205-0.

[221] D. Shaw, E. Watson, The diffusion of chlorine in CdTe, J. Phys. C Solid State Phys. 17 (28) (1984) 4945–4950, Oct, https://doi.org/10.1088/0022-3719/17/28/011.

[222] L. Verger, et al., Electronic properties of chlorine doped cadmium telluride used as high energy photoconductive detector, Nucl. Instrum. Methods Phys. Res. Sect. Accel. Spectrometers Detect. Assoc. Equip. 322 (3) (Nov. 1992) 357–362, https://doi.org/10.1016/0168-9002(92)91197-H.

[223] C. Li, et al., Electrical activity of defects in CdTe solar cells via aberration-corrected STEM, Microsc. Microanal. 19 (S2) (Aug. 2013) 334–335, https://doi.org/10.1017/S1431927613003668.

[224] E. Kučys, J. Jerhot, K. Bertulis, V. Bariss, Copper impurity behaviour in CdTe films, Phys. Status Solidi A 59 (1) (1980) 91–99, https://doi.org/10.1002/pssa.2210590112.

[225] D. Krasikov, A. Knizhnik, B. Potapkin, S. Selezneva, T. Sommerer, First-principles-based analysis of the influence of Cu on CdTe electronic properties, Thin Solid Films 535 (May 2013) 322–325, https://doi.org/10.1016/j.tsf.2012.10.027.

[226] D. Guo, et al., Numerical simulation of copper migration in single crystal CdTe, IEEE J. Photovoltaics 6 (5) (2016) 1286–1291, Sep, https://doi.org/10.1109/JPHOTOV.2016.2571626.

[227] C. Gretener, et al., New perspective on the performance stability of CdTe solar cells, Sol. Energy Mater. Sol. Cells 146 (Mar. 2016) 51–57, https://doi.org/10.1016/j.solmat.2015.11.017.

[228] I. Rimmaudo, et al., Improved stability of CdTe solar cells by absorber surface etching, Sol. Energy Mater. Sol. Cells 162 (Apr. 2017) 127–133, https://doi.org/10.1016/j.solmat.2016.12.044.

[229] H.R. Moutinho, M.M. Al-Jassim, D.H. Levi, P.C. Dippo, L.L. Kazmerski, Effects of CdCl2 treatment on the recrystallization and electro-optical properties of CdTe thin films, J. Vac. Sci. Technol., A 16 (3) (May 1998) 1251–1257, https://doi.org/10.1116/1.581269.

[230] J.-H. Yang, W.K. Metzger, S.-H. Wei, Carrier providers or killers: the case of Cu defects in CdTe, Appl. Phys. Lett. 111 (4) (Jul. 2017), 042106, https://doi.org/10.1063/1.4986077.

[231] M. Lingg, A. Spescha, S.G. Haass, R. Carron, S. Buecheler, A.N. Tiwari, Structural and electronic properties of CdTe1-xSex films and their application in solar cells, Sci. Technol. Adv. Mater. 19 (1) (Dec. 2018) 683–692, https://doi.org/10.1080/14686996.2018.1497403.

[232] A. Zunger, Practical doping principles, Appl. Phys. Lett. 83 (1) (Jul. 2003) 57–59, https://doi.org/10.1063/1.1584074.

[233] J. Yang, S.-H. Wei, First-principles study of the band gap tuning and doping control in CdSe x Te1-x alloy for high efficiency solar cell, Chin. Phys. B 28 (8) (Aug. 2019), 086106, https://doi.org/10.1088/1674-1056/28/8/086106.

[234] D. Krasikov, Selenium lowers bulk recombination, Nat. Energy 4 (6) (Jun. 2019) 442–443, https://doi.org/10.1038/s41560-019-0393-3.

[235] A.R. Shaik, et al., PVRD-FASP: a unified solver for modeling carrier and defect transport in photovoltaic devices, IEEE J. Photovoltaics 9 (6) (2019) 1602–1613, Nov, https://doi.org/10.1109/JPHOTOV.2019.2937238.

[236] J.P. Chamonal, E. Molva, J.L. Pautrat, L. Revoil, Complex behaviour of Ag in CdTe, J. Cryst. Growth 59 (1) (Sep. 1982) 297–300, https://doi.org/10.1016/0022-0248(82)90340-2.

[237] N.R. Paudel, D. Kwon, M. Young, K.A. Wieland, S. Asher, A.D. Compaan, Effects of Cu and CdCl2 treatment on the stability of sputtered CdS/CdTe solar cells, 35th IEEE Photovolt. Special. Conf. (2010), https://doi.org/10.1109/PVSC.2010.5614605. Jun. 2010, pp. 001009–001013.

[238] K.L. Barth, R.A. Enzenroth, W.S. Sampath, Consistent processing and long term stability of CdTe devices, in: Conference Record of the Thirty-First IEEE Photovoltaic Specialists Conference, 2005, pp. 323–326, https://doi.org/10.1109/PVSC.2005.1488134. Jan. 2005.

[239] M. Schweiger, J. Bonilla, W. Herrmann, A. Gerber, U. Rau, Performance stability of photovoltaic modules in different climates, Prog. Photovoltaics Res. Appl. 25 (12) (2017) 968–981, https://doi.org/10.1002/pip.2904.

[240] T.J. Silverman, M.G. Deceglie, B. Marion, S.R. Kurtz, Performance stabilization of CdTe PV modules using bias and light, IEEE 40th Photovolt. Special. Conf. (PVSC) (2014) 3676–3681, https://doi.org/10.1109/PVSC.2014.6924904. Jun. 2014.

[241] W. Orellana, E. Menéndez-Proupin, M.A. Flores, Self-compensation in chlorine-doped CdTe, Sci. Rep. 9 (1) (Jun. 2019), https://doi.org/10.1038/s41598-019-45625-x. Art. no. 1.

[242] L. Kranz, et al., Effect of sodium on recrystallization and photovoltaic properties of CdTe solar cells, Sol. Energy Mater. Sol. Cells 105 (Oct. 2012) 213–219, https://doi.org/10.1016/j.solmat.2012.06.019.

[243] E. Artegiani, D. Menossi, A. Salavei, S. di Mare, A. Romeo, Analysis of the influence on the performance degradation of CdTe solar cells by the front contact, Thin Solid Films 633 (Jul. 2017) 101–105, https://doi.org/10.1016/j.tsf.2016.09.052.

[244] N.R. Paudel, Y. Yan, Fabrication and characterization of high-efficiency CdTe-based thin-film solar cells on commercial SnO2:F-coated soda-lime glass substrates, Thin Solid Films 549 (Dec. 2013) 30–35, https://doi.org/10.1016/j.tsf.2013.07.020.

[245] Y. Yan, et al., SiO2 as Barrier Layer for Na Out-Diffusion from Soda-Lime Glass, *35th* IEEE Photovoltaic Specialists Conference, Honolulu, HI, USA, 2010, https://doi.org/10.1109/PVSC.2010.5614657. Jun. 2010, pp. 002519–002521.

[246] M.K. Jamarkattel, et al., Reduced recombination and improved performance of CdSe/CdTe solar cells due to Cu migration induced by light soaking, ACS Appl. Mater. Interfaces 14 (17) (May 2022) 19644–19651, https://doi.org/10.1021/acsami.1c23937.

[247] S. Demtsu, S. Bansal, D. Albin, Intrinsic Stability of Thin-Film CdS/CdTe Modules, *35th* IEEE Photovoltaic Specialists Conference, Honolulu, HI, USA, Jun, 2010, https://doi.org/10.1109/PVSC.2010.5614753, 2010, pp. 001161–001165.

[248] X. Wu, et al., Phase control of CuxTe film and its effects on CdS/CdTe solar cell, Thin Solid Films 515 (15) (May 2007), https://doi.org/10.1016/j.tsf.2006.12.151. Art. no. 15.

[249] A. Romeo, et al., Electrical characterization and aging of CdTe thin film solar cells with Bi2Te3 back contact, IEEE 39th Photovolt. Special. Conf. (PVSC) (2013) 1178–1182, https://doi.org/10.1109/PVSC.2013.6744350. Tampa, FL, USA, Jun. 2013.

[250] L. Kranz, et al., Doping of polycrystalline CdTe for high-efficiency solar cells on flexible metal foil, Nat. Commun. 4 (1) (Oct. 2013), https://doi.org/10.1038/ncomms3306. Art. no. 1.

[251] L. Zhang, J.L.F. Da Silva, J. Li, Y. Yan, T.A. Gessert, S.-H. Wei, Effect of copassivation of Cl and Cu on CdTe grain boundaries, Phys. Rev. Lett. 101 (15) (Oct. 2008), https://doi.org/10.1103/PhysRevLett.101.155501. Art. no. 15.

[252] J. Beach, F.H. Seymour, V.I. Kaydanov, T.R. Ohno, Studies of Basic Electronic Properties of CdTe-Based Solar Cells and Their Evolution during Processing and Stress, 1 November 2005 - 31 October 2006, in: Annual Technical Report, National Renewable Energy Laboratory (NREL), Golden, CO., US, 2007, https://doi.org/10.2172/898922. NREL/SR-520-41097, Jan.

[253] E. Artegiani, et al., Analysis of a novel CuCl2 back contact process for improved stability in CdTe solar cells, *Prog. Photovolt. Res. Appl.*, p. pip. 3148 (May 2019), https://doi.org/10.1002/pip.3148.

[254] M. Nardone, D.S. Albin, Degradation of CdTe solar cells: simulation and experiment, IEEE J. Photovoltaics 5 (3) (May 2015) 962–967, https://doi.org/10.1109/JPHOTOV.2015.2405763.

[255] D.H. Rose, et al., Fabrication procedures and process sensitivities for CdS/CdTe solar cells, Art. no. 5, Sep, Prog. Photovoltaics Res. Appl. 7 (5) (1999), https://doi.org/10.1002/(SICI)1099-159X(199909/10)7:5<331::AID-PIP257>3.0. CO;2-P.

[256] D.S. Albin, Accelerated Stress Testing and Diagnostic Analysis of Degradation in CdTe Solar Cells," Presented at the Solar Energy + Applications, Aug. 2008, p. 70480N, https://doi.org/10.1117/12.795360. San Diego, CA.

[257] P.V. Meyers, S. Asher, M.M. Al-Jassim, A search for degradation mechanisms of CdTe/CdS solar cells, MRS Proc 426 (1996) 317, https://doi.org/10.1557/PROC-426-317.

[258] S.S. Hegedus, B.E. McCandless, CdTe contacts for CdTe/CdS solar cells: effect of Cu thickness, surface preparation and recontacting on device performance and stability, Sol. Energy Mater. Sol. Cells 88 (1) (Jun. 2005), https://doi.org/10.1016/j.solmat.2004.10.010. Art. no. 1.

[259] J.F. Hiltner, J.R. Sites, Stability of CdTe Solar Cells at Elevated Temperatures: Bias, Temperature, and Cu Dependence, AIP Conference Proceedings, Denver, Colorado (USA), 1999, pp. 170–175, https://doi.org/10.1063/1.57895.

[260] R. Harju, V.G. Karpov, D. Grecu, G. Dorer, Electron-beam induced degradation in CdTe photovoltaics, J. Appl. Phys. 88 (4) (Aug. 2000), https://doi.org/10.1063/1.1305857. Art. no. 4.

[261] S. Johnston, et al., Imaging, microscopic analysis, and modeling of a CdTe module degraded by heat and light, Sol. Energy Mater. Sol. Cells 178 (May 2018) 46–51, https://doi.org/10.1016/j.solmat.2017.12.021.

[262] R.C. Powell, et al., Stability testing of CdTe/CdS thin-film photovoltaic modules, in: Conference Record of the Twenty Fifth IEEE Photovoltaic Specialists Conference - 1996, May 1996, pp. 785–788, https://doi.org/10.1109/PVSC.1996.564245.

[263] S.S. Hegedus, B.E. McCandless, R.W. Birkmire, Analysis of stress-induced degradation in CdS/CdTe solar cells, in: Conference Record of the Twenty-Eighth

IEEE Photovoltaic Specialists Conference - 2000, Sep. 2000, pp. 535–538, https://doi.org/10.1109/PVSC.2000.915891. *Cat. No.00CH37036)*.
[264] C. Corwine, Copper inclusion and migration from the back contact in CdTe solar cells, *Sol. Energy Mater. Sol. Cells*, Mar. (2004), https://doi.org/10.1016/j.solmat.2004.02.005.
[265] M. Nardone, Towards understanding junction degradation in cadmium telluride solar cells, J. Appl. Phys. 115 (23) (Jun. 2014), https://doi.org/10.1063/1.4883368. Art. no. 23.
[266] D. Redfield, R.H. Bube, Photo-induced Defects in Semiconductors, Cambridge University Press, 2006.
[267] M. Nardone, et al., Quantifying large lattice relaxations in photovoltaic devices, Phys Rev Appl 13 (2) (2020), 024025, https://doi.org/10.1103/physrevapplied.13.024025.
[268] C.-S. Jiang, et al., Electrical potential investigation of reversible metastability and irreversible degradation of CdTe solar cells, Sol. Energy Mater. Sol. Cells 238 (2022), 111610.
[269] T.D. Hill, Stability of Thin-Film CdTe Solar Cells with Various Back Contacts, MS Thesis, Colorado State University, 2020.
[270] V.G. Karpov, A.D. Compaan, D. Shvydka, Random diode arrays and mesoscale physics of large-area semiconductor devices, Phys. Rev. B 69 (4) (Jan. 2004), https://doi.org/10.1103/PhysRevB.69.045325. Art. no. 4.
[271] V.G. Karpov, D. Shvydka, Understanding and mitigating effects of nonuniformities on reliability of thin film photovoltaics, presented at the SPIE Solar Energy + Technology (Aug. 2009) 74120L, https://doi.org/10.1117/12.828937. San Diego, CA.
[272] V.G. Karpov, A.D. Compaan, D. Shvydka, Effects of nonuniformity in thin-film photovoltaics, Appl. Phys. Lett. 80 (22) (Jun. 2002), https://doi.org/10.1063/1.1483118. Art. no. 22.
[273] V.G. Karpov, Coupled electron–heat transport in nonuniform thin film semiconductor structures, Phys. Rev. B 86 (Oct. 2012) 16, https://doi.org/10.1103/PhysRevB.86.165317. Art. no. 16.
[274] A. Agency, For Toxic Substances and Disease Registry, "Toxicological Profile for Cadmium, Agency for toxic substances and disease registry, Atlanta, GA, 2012. Accessed: Nov. 08, 2022. [Online]. Available: https://www.atsdr.cdc.gov/toxprofiles/tp5.pdf.
[275] A. Taylor, Biochemistry of Tellurium," presented at the New perspectives in the research of hardly known trace elements and in element interaction, Budapest, Budapest, Hungary, Conference Proceedings (1994) 147.
[276] V. Fthenakis, C. Athias, A. Blumenthal, A. Kulur, J. Magliozzo, D. Ng, Sustainability evaluation of CdTe PV: an update, Renew. Sustain. Energy Rev. 123 (2020), https://doi.org/10.1016/j.rser.2020.109776.
[277] C. National, Renewable Energy Centre, "First Solar CdTe Photovoltaic Technology: Environmental, Health and Safety Assessment," Fundacion Chile, 2013. Chile.
[278] The Virginia Center for Coal and Energy Reasearch, Assessment of the Risks Associated with Thin Film Solar Panel Technology, Virginia Tech, Blacksburg, VA, 2019.
[279] P.D. Moskowitz, H. Steinberger, W. Thumm, Health and environmental hazards of CdTe photovoltaic module production, use and decommissioning, Proceedings of 1994 IEEE 1st World Conference on Photovoltaic Energy Conversion - WCPEC (A Joint Conference of PVSC, PVSEC and PSEC) 1 (Dec. 1994) 115–118, https://doi.org/10.1109/WCPEC.1994.519821, 1.
[280] V.M. Fthenakis, Life cycle impact analysis of cadmium in CdTe PV production, Renew. Sustain. Energy Rev. 8 (4) (Aug. 2004) 303–334, https://doi.org/10.1016/j.rser.2003.12.001.
[281] V. Fthenakis, "Environmental Life Cycle Assessment of Cadmium Telluride Solar Cells: Cd Emissions," Jan. 1AD.
[282] A. Rix, J. Steyl, J. Rudman, U. Terblanche, J. van Niekerk, First Solar's CdTe Module Technology- Performand, Lifecycle, Health and Safety Impact Assessment, Stellenbosch University, Centre for Renewable and Sustainable Energy Studies, South Africa, 2015.
[283] C. Zeng, A. Ramos-Ruiz, J.A. Field, R. Sierra-Alvarez, Cadmium telluride (CdTe) and cadmium selenide (CdSe) leaching behavior and surface chemistry in response to pH and O2, J. Environ. Manag. 154 (May 2015) 78–85, https://doi.org/10.1016/j.jenvman.2015.02.033.
[284] A. Ramos-Ruiz, J.V. Wilkening, J.A. Field, R. Sierra-Alvarez, Leaching of cadmium and tellurium from cadmium telluride (CdTe) thin-film solar panels under simulated landfill conditions, J. Hazard Mater. 336 (Aug. 2017) 57–64, https://doi.org/10.1016/j.jhazmat.2017.04.052.
[285] C.A. Poland, et al., Bioaccessibility as a determining factor in the bioavailability and toxicokinetics of cadmium compounds, Toxicology 463 (Nov. 2021), 152969, https://doi.org/10.1016/j.tox.2021.152969.
[286] USGS, "Mineral Commodity Summaries, Lead, US Geological Survey, Washington DC, 2022.
[287] U.N. Environment, Lead Acid Batteries, UNEP - UN Environment Programme, 2017. Oct. 05, http://www.unep.org/explore-topics/chemicals-waste/what-we-do/emerging-issues/lead-acid-batteries. (Accessed 5 January 2023).
[288] J.M. Turner, Charged: A History of Batteries and Lessons for a Clean Energy Future, University of Washington Press, 2022.
[289] Assessing Fire Risks in Photovoltaic Systems and Developing Safety Concepts for Risk Minimization," Energy.gov. https://www.energy.gov/eere/solar/downloads/assessing-fire-risks-photovoltaic-systems-and-developing-safety-concepts-risk (accessed January. 05, 2023).
[290] U. Environmental Protection Agency, Wood Smoke and Your Health, 2013. May 28, https://www.epa.gov/burnwise/wood-smoke-and-your-health. (Accessed 5 January 2023).
[291] USGS, "Minneral Commodity Summary, Cadmium, US Geological Survey, Wsahington, DC, 2022.
[292] USGS, "Mineral Commodity Summaries, Tellurium, US Geological Survey, Washington, DC, 2022.
[293] K. Cha, M. Son, Y. Matsuno, V. Fthenakis, T. Hur, Substance flow analysis of cadmium in Korea, Resour. Conserv. Recycl. 71 (Feb. 2013) 31–39, https://doi.org/10.1016/j.resconrec.2012.11.005.
[294] Y. Matsuno, T. Hur, V. Fthenakis, Dynamic modeling of cadmium substance flow with zinc and steel demand in Japan, Resour. Conserv. Recycl. 61 (Apr. 2012) 83–90, https://doi.org/10.1016/j.resconrec.2012.01.002.
[295] B. Voigt, J. Bradley, Boliden Summary Report: Resources and Reserves 2020 Kankberg- Akulla Ostra, Dec. 2020. Accessed: Jul. 19, 2021. [Online]. Available: https://www.boliden.com/globalassets/operations/exploration/mineral-resources-and-mineral-reserves-pdf/2020/resources-and-reserves-kankberg-2020-12-31.pdf.
[296] R. Tinto, Rio Tinto starts tellurium production at Kennecott, accessed Nov. 05, 2022), https://www.riotinto.com/news/releases/2022/Rio-Tinto-starts-tellurium-production-at-Kennecott, May 11, 2022.
[297] S.M. Hayes, E. McCullough, Critical minerals: a review of elemental trends in comprehensive criticality studies, Resour. Pol. 59 (2018) 192–199, https://doi.org/10.1016/j.resourpol.2018.06.015.
[298] N.T. Nassar, H. Kim, M. Frenzel, M.S. Moats, S.M. Hayes, Global tellurium supply potential from electrolytic copper refining, Resour. Conserv. Recycl. 184 (2022), https://doi.org/10.1016/j.resconrec.2022.106434.
[299] B.A. McNulty, S.M. Jowitt, Byproduct critical metal supply and demand and implications for the energy transition: a case study of tellurium supply and CdTe PV demand, Renew. Sustain. Energy Rev. 168 (2022), https://doi.org/10.1016/j.rser.2022.112838.
[300] N.T. Nassar, S.M. Fortier, Methodology and Technical Input for the 2021 Review and Revision of the U.S. Critical Minerals List, 2021, https://doi.org/10.3133/ofr20211045. Reston, VA, Report 2021–1045.
[301] K.J. Spaleta, Finding Solutions to the World's Pending Critical Minerals Supply Crisis: Developing New Geochemical Analytical Methods and Evaluating the Potential for Te and Bi Extraction from Existing Au Mines, University of Alaska Fairbanks, Fairbanks, AK, 2022.
[302] G. Kavlak, T.E. Graedel, Global anthropogenic tellurium cycles for 1940-2010, Resour. Conserv. Recycl. 76 (Jul. 2013) 21–26, https://doi.org/10.1016/j.resconrec.2013.04.007.
[303] F. Ojebuoboh, Selenium and tellurium from copper refinery slimes and their changing applications, World Metall. 61 (1) (2008) 33–39.
[304] A. Skidmore, The Behavior of Tellurium during Cupper Ore Processing at the American Smelting and Refining Company (Tucson, AZ), University of Alaska Fairbanks, Alaska, Fairbanks, 2016.
[305] C. Fountain, The Whys and Wherefores of Penalty Elements in Copper Concentrates," Presented at the Metallurgical Plant Design and Operating Strategies, Jul. 2013, pp. 502–518. Perth, WA.
[306] M. Moats, L. Alagha, K. Awuah-Offei, Towards resilient and sustainable supply of critical elements from the copper supply chain: a review, J. Clean. Prod. 307 (2021), https://doi.org/10.1016/j.jclepro.2021.127207.
[307] S.M. Jowitt, Can Critical Metal Supply Problems Be Solved Using Existing but Hidden Materials Flows? Tellurium and the USA-Canadian Mining Value Chain, vol. 54, Geological Society of America Abstracts with Programs, Denver, CO, 2022, https://doi.org/10.1130/abs/2022AM-378325 presented at the.
[308] S. Hayes, N.M. Piatak, R. McAleer, Environmental Behavior of Tellurium in Mine Tailings, vol. 54, Geological Society of America Abstracts with Programs, Denver, CO, 2022, https://doi.org/10.1130/abs/2022AM-381806 presented at the.
[309] I. Behre, Dolbear Asia, "Independent Technical Review of the Dashuigou and Majiagou Tellurium Projects in Sichuan Province, the People's Republic of China, 2009. https://www.sec.gov/Archives/edgar/data/726435/000140677409000056/exhibit992.htm. (Accessed 22 July 2021).
[310] R.J. Goldfarb, B.R. Berger, M.W. George, R.R. Seal, Tellurium, in: R.K.J. Schulz, J.J.H. DeYoung, R.R. Seal, D.C. Bradley (Eds.), Critical Mineral Resources of the United States- Economic and Environmental Geology and Prospects for Future Supply, Department of Interior: Department of Interior, USGS, 2017, pp. R1–R27, https://doi.org/10.3133/pp1802.
[311] M.E. Schlesinger, M.J. King, W.G. Davenport, Extractive Metallurgy of Copper, fifth ed., Elsevier, New York, 2011.
[312] Getting More Gold from Slimes: Higher Productivity in Wet Chlorination | E & MJ." https://www.e-mj.com/features/getting-more-gold-from-slimes-higher-productivity-in-wet-chlorination/(accessed January. 19, 2023).
[313] M.L. Bustamante, G. Gaustad, The evolving copper-tellurium byproduct system: a review of changing production techniques & their implications, in: Rare Metal Technology 2014, TMS (The Minerals, Metals & Materials Society), 2014.